Title
Effects of pore fluids in the subsurface on ultrasonic wave propagation

Author
Seifert, Patricia Katharina

Publication Date
1998-05-01

LBNL-41781

ERNEST ORLANDO LAWRENCE
BERKELEY NATIONAL LABORATORY

Effects of Pore Fluids in the Subsurface on Ultrasonic Wave Propagation

Patricia K. Seifert

Earth Sciences Division

May 1998

Ph.D. Thesis

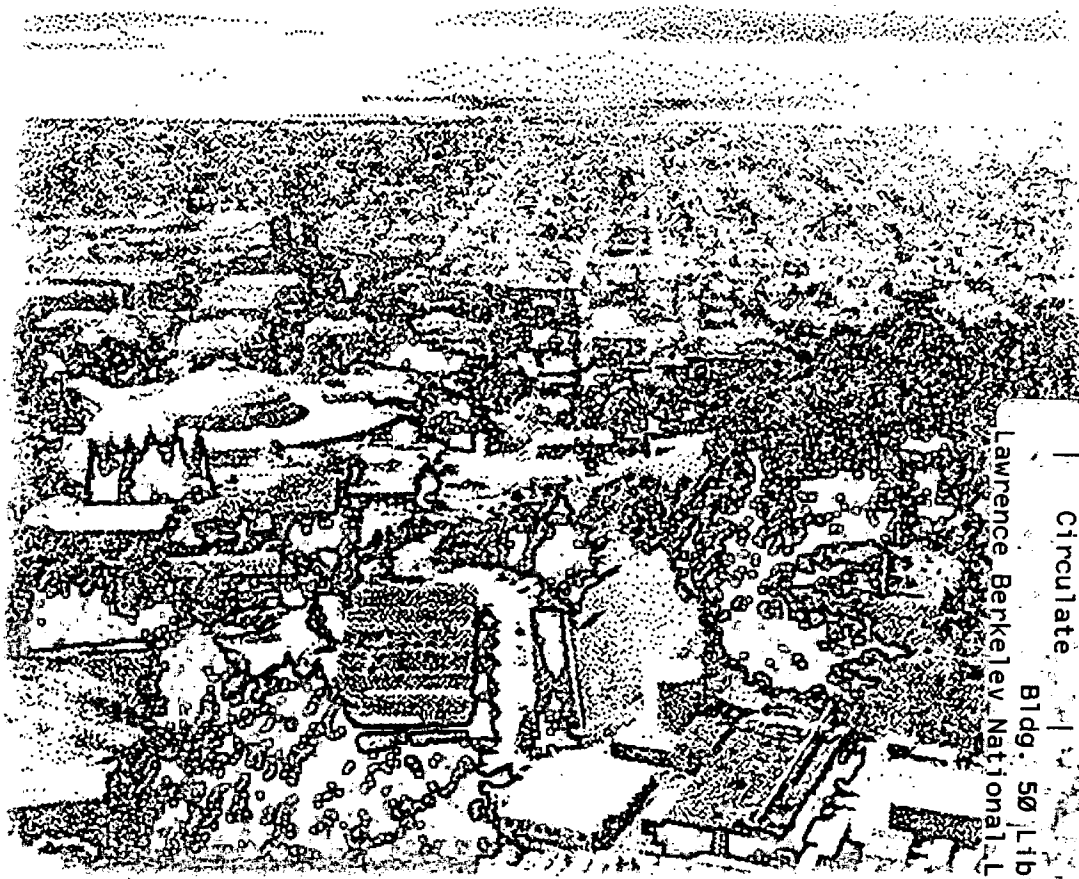

DISCLAIMER

LBNL-41781

Effects of Pore fluids in the subsurface on Ultrasonic Wave Propagation

Patricia Katharina Seifert

Ph.D.Thesis

Department of Geology and Geophysics
University of California, Berkeley

and

Earth Sciences Division
Ernest Orlando Lawrence Berkeley National Laboratory
University of California
Berkeley, CA 94720

May 1998

This work was done at the Center for Computational Seismology supported by the Director, Office of Energy Research, Office of Basic Energy Sciences, Geosciences Program, through U.S. Department of Energy under contract No. DE-AC03-76F00098, the U.S. Environmental Protection Agency Geophysics Program, Las Vegas, Nevada and by the Air Force Office of Scientific Research contract AFOSR-960010.

Abstract

Effects of Pore Fluids in the Subsurface

on Ultrasonic Wave Propagation

by

Patricia Katharina Seifert

Doctor of Philosophy in Geophysics

University of California at Berkeley

Professor Lane R. Johnson, Chair

This thesis investigates ultrasonic wave propagation in unconsolidated sands in the presence of different pore fluids. Laboratory experiments have been conducted in the sub-MHz range using quartz sand fully saturated with one or two liquids. Elastic wave propagation in unconsolidated granular material is computed with different numerical models: In one-dimension a scattering model based on an analytical propagator solution, in two dimensions a numerical approach using the boundary integral equation method, in three dimensions the local flow model (LFM), the combined Biot and squirt flow theory (BISQ) and the dynamic composite elastic medium theory (DYCEM).

The combination of theoretical and experimental analysis yields a better understanding of how wave propagation in unconsolidated sand is affected by

a) homogeneous phase distribution

b) inhomogeneous phase distribution, (fingering, gas inclusions)

c) pore fluids of different viscosity

d) wettabilities of a porous medium.

The first study reveals that the main ultrasonic P-wave signatures, as a function of the fraction of nonaqueous-phase liquids (NAPL) in initally water-saturated sand samples, can be explained by a one-dimensional scattering model. Wave attenuation and velocity dispersion increase with increasing NAPL saturation. Velocity is sensitive to NAPL fraction only, whereas, the amplitude behavior is more complicated. A two-dimensional model shows that inhomogeneous fluid distribution, e.g., fingering and gas inclusions, can cause additional attenuation. Hence, amplitudes reflect the fraction of NAPL present in the sample as well as its distribution.

The next study investigates effects of pore fluid viscosity on elastic wave propagation, in laboratory experiments conducted with sand samples saturated with fluids of different viscosities. P-wave attenuation always shows a frequency squared dependence, independent of the pore fluid viscosity. The LFM and BISQ theory can not explain the laboratory observations for all the viscosities. Only the DYCEM model gives the correct frequency dependence and the calculations fit the measurements within the uncertainty.

The last study concentrates on the wettability of the grains and its effect on

elastic wave propagation and electrical resistivity. Experiments have been performed in both initally water-saturated and initally n-dodecane-saturated media, for water-wetting and n-dodecane-wetting sand, as a function of n-dodecane saturation. Changes in the wettability of a n-dodecane-water-mineral system affect the effective amplitude of the P-wave, the capability of measuring S-waves and the electrical resistivity.

To Sara Wong,

and in memory of my father,

Frederick Seifert.

Contents

List of Figures

List of Tables

Acknowledgments

My sincere thanks are given foremost to my advisor, Professor Lane Johnson. He has been a constant source of inspiration to me and an outstanding mentor. It has been a privilege to be part of his research group. Dr. Jil Geller also deserves my most earnest thanks for her continuous support and guidance throughout my years in Berkeley. She introduced me to the laboratory and was a true mentor and friend. I was very fortunate to work with these two remarkable investigators.

I am grateful to Professor James Kirchner and Professor James Rector for serving on my thesis commitee. Their attentive reviews have improved this material. Also, I wish to thank Bruno Kaelin, Dr. Stefan Finsterle, Dr. Kurt Nihei and Tom Daley, who were very generous with their time in discussing my ideas and reviewing this material.

Furthermore I like to thank the lab 'gang' Grace Su, Seiji Nakagawa, Michael Kowalsky, Jil Geller, Kurt Nihei, Galen Hesler, Tim Kneafsey, Sharon Borglin, Brad Bessinger and Roberto Suarez-Rivera for giving our dark, cluttered, sometimes cold and flooded laboratory a cooperative atmosphere and creating a setting for learning experimental research. Sometimes the lab rats went really wild, leaving their safe stomping grounds and celebrated birthdays, awards and had lots of fun. Thanks again, I really enjoyed working in the laboratory. For the windows of recreation and humanity in a strongly scientific and digital

environment (once a day around noon), I want to thank Julie Najita, Bruno Kaelin, Stefan Finsterle, Henk Keers, April James, Roland Gritto, Paul Parker and Valerie Korneev.

My Berkeley friends outside the department reminded me of life away from Lawrence Berkeley National Laboratory. Sara Wong, Chaincy Kuo, Augie Kuo, Frederike Schilter (also known as little giant), Jeff Dodge, Hermann Kim, Romy Choi, Emily Zedler, Pierre Korzilius, Matthias Luthi, Keary Hildenbrand, Sybilla Lob, Susan Riggle, John McWhorter, Christine Clements, Rakhi Rao and Charles Ford, are great friends. Thank you for the many dinner parties, skiing weekends, hiking adventures (I will just say mama bear and three cubs), surf trips, racquet ball tournaments, coffees, high teas, wine tastings, cooking and sewing lessons we shared.

I owe deepest appreciation to Renate Scheidegger, who has taught me to appreciate and value knowledge. She and Rita Sadak have been enthusiatic supporters of my studies. I want to thank my mother and my sister for the many postcards and letters they have sent me throughout my time in Berkeley and their love.

I gratefully acknowledge the financial support from Office of Energy Research, Office of Basic Energy Sciences, Geosciences Program, through U.S. Department of Energy and by the Air Force Office of Scientific Research.

Chapter 1

Introduction

The book "A Civil Action" (Harr, 1995), a work of nonfiction, is a good example to show that contaminated aquifers and their effect on daily life is a real problem and not just an academic one. The story narrates how TCE and other organic liquids used in tanneries for cleaning leather were dumped onto the ground or burried in barrels, which started to leak due to corrosion. Once the contaminants were released to the subsurface, they started to migrate and eventually invaded the aquifers. The organic liquids then got transported with the groundwater and reached the individual households. A statistically significant percentage of the population, which were exposed to the contaminated tap water for years, suffered from leukaemia.

Organic liquids were not only used in tanneries, but they were also commonly used for dry cleaning purposes, in the metal cleaning industry, as heat transfer fluids and to remove oil and paints. This group of liquids, containing chlorinated solvents and hydrocarbon fuels, are also known as non-aqueous phase liquids

(NAPLs) and are nowadays one of the major organic groundwater contaminants.

A major challenge in remediating subsurface contamination by organic liquids is to detect and delineate their distribution. NAPLs can attain highly irregular distributions, extending from residual liquid segments held in pore spaces to pools over regions of low permeability. If the subsurface is fully saturated, i.e., below the water table, modern seismic systems (1 to 15 kHz) could provide field resolution on the scale necessary to characterize organic liquid distributions, on the order of centimeters. Development of high-frequency seismic tomography to map NAPL distributions between boreholes and to monitor changes during remediation requires a physical understanding of seismic wave propagation through unconsolidated porous media with immiscible liquid phases. Hence, laboratory and numerical studies were conducted of wave transmission through NAPL-water-sand systems.

1.1 Background

The velocity and attenuation of seismic waves can be used to determine elastic material properties. In porous media, seismic wave transmission is also affected by the physical and chemical characteristics of the pore fluid and its interaction with the solid phase (e.g., Tutuncu and Sharma, 1992). Geller and Myer (1995) showed in laboratory studies that ultrasonic P-wave propagation in unconsolidated fully saturated media is sensitive to the presence of NAPL. The

differences in acoustic velocity, density and viscosity between water and NAPL contaminants strongly affect the seismic wave transmission. With increasing fraction of NAPL in the pore space the travel time of the first arrival is delayed and the amplitude decreases. Velocity reflects the difference in bulk moduli between the water and NAPL and the fraction of NAPL present, but is insensitive to its distribution. In contrast, the amount of energy attenuated is a function of the NAPL fraction in the pore space as well as its distribution. Despite extensive research, there is still considerable uncertainty about the relationships between rock properties and seismic behavior and the mechanisms which cause these effects.

I have conducted laboratory experiments to observe how different pore fluids in unconsolidated sand effect ultrasonic wave propagation. Three independent sets of experiments gave better understanding of how ultrasonic waves are affected by

a) inhomogeneous phase distribution such as fingering or gas inclusions

a) pore fluids of different viscosity

a) wettabilities of a porous media, such as water- and NAPL-wetting sand.

Measurements were made in a specially designed triaxial test cell (Geller and Myer, 1995) shown in Figure 1.1. The apparatus contains four piezoelectric elements with a resonant frequency of 1 MHz to generate and detect elastic

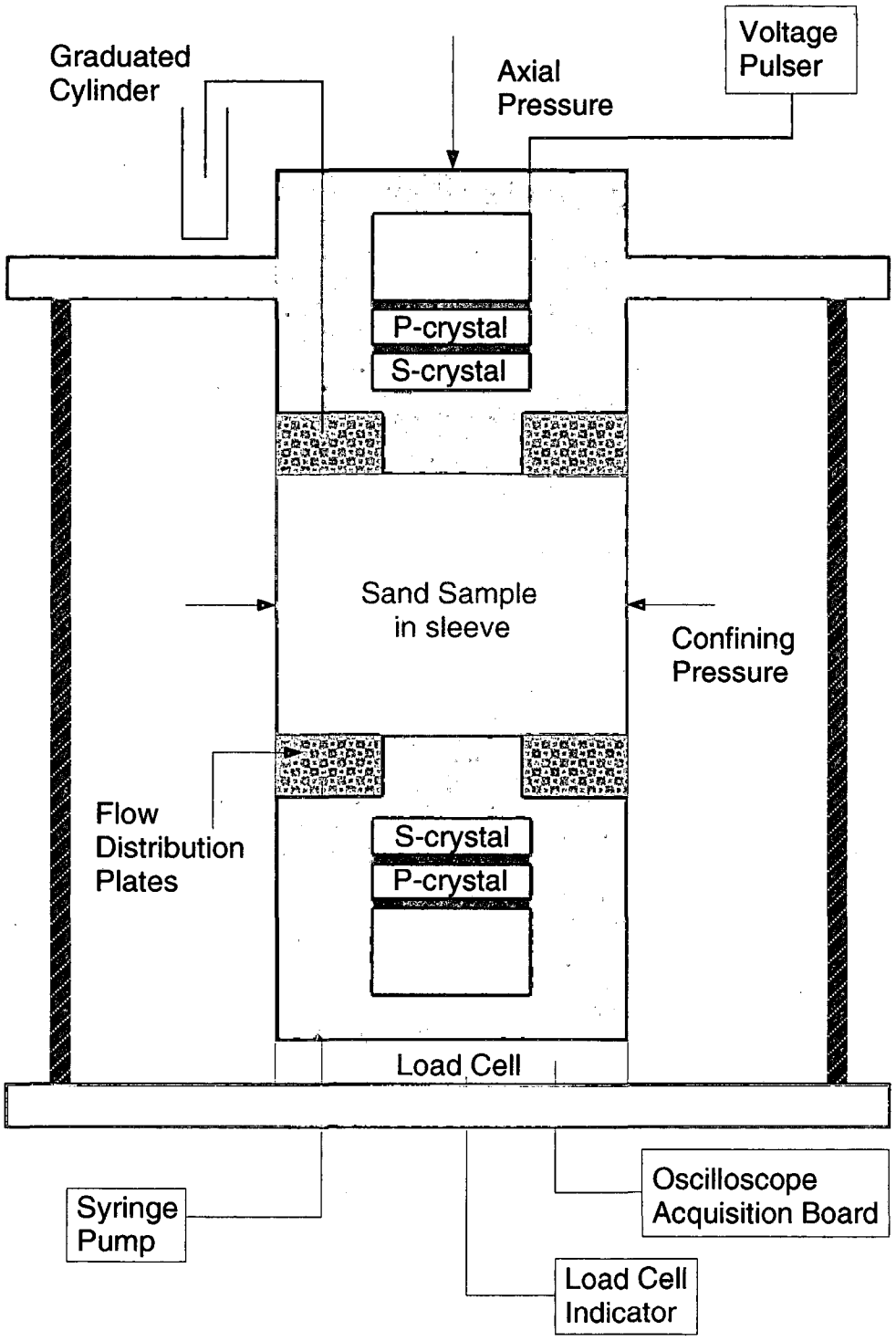

Figure 1.1: Apparatus setup for measuring ultrasonic wave transmission as a function of NAPL saturation in fully saturated sand samples.

P-waves and S-waves. The sand samples are placed between the transducers and held in place by a flexible shrink tube sleeve, which is cut to fit over the end-caps. On each transducer lies a donut-shaped ceramic flow distribution plate, which assures that the injected fluid is evenly distributed over the column cross-section. Confining and axial stresses on the sample were maintained at approximately 60 and 140 kPa, respectively, characteritic of the shallow subsurface ($\sim$ 10 m depth). The change in travel time and amplitude with increasing NAPL-saturation was measured by first saturating the sample fully with water and then displacing the water by injecting the NAPL in small increments into the sample with a syring pump.

1.2 Outline of work performed

The first study (Chapter 2) contains numerical computations to simulate the laboratory measurements by Geller and Myer 1995. The measurements show a significant change in traveltime and amplitude of the primary P-wave arrival as a function of NAPL saturation. The main trends in this behavior can be simulated with a one-dimensional scattering model.

Since the one-dimensional scattering model gives good velocity estimates but underestimates the magnitude of attenuation in some cases, we obtained a qualitative understanding how energy losses are affected by the pore fluid distribution (Chapter 3). A two-dimensional numerical approach was used to

simulate laboratory experiments, which showed that fluid distribution can be heterogeneous due to unstable displacement mechanisms. If the pore fluids are very volatile, small changes in pressure or temperature can also produce gas inclusions. With the numerical model we illustrate how waves are scattered by heterogeneous fluid distributions and cause attenuation additional to that due to scattering from the pores and grains.

Chapter 4 combines theoretical and experimental analysis to evaluate the main loss mechanisms caused by different viscosities of the pore fluid ranging from 0.001 to 1 Pa/sec. The laboratory measurements were compared with three theoretical models, the Local Flow Model (LFM), the unified Biot and Squirt flow theory (BISQ) and the Dynamic Composite Elastic Medium theory (DYCEM).

The overall object of the last study in Chapter 5 was to determine if wettability affects wave propagation and electric resistivity measurements. Hence laboratory measurements of sand columns saturated with water and n-dodecane were taken as a function of n-dodecane saturation for drainage and imbibition of water. The experiments were performed in both initally water-saturated and initally NAPL-saturated media and for water-wetting and NAPL-wetting sand.

Chapter 2

Effect of P-Wave Scattering on Velocity and Attenuation in Unconsolidated Sand Saturated with Immiscible Liquids

2.1 Abstract

Seismic wave tomography is a potentially powerful tool to detect and delineate non-aqueous phase liquid (NAPL) contaminants in the shallow subsurface. To develop this application we are conducting laboratory and numerical studies to understand the mechanisms of P-wave transmission through NAPL-water-sand systems.

Measurements of travel time and amplitude through saturated sand with variable NAPL content were taken. For our experiments piezoelectric elements were used to transmit and receive P-waves in the 100-900 kHz range. To simulate

the stress conditions of the shallow surface, low confining and axial pressure of 60 and 140 kPa, respectively, were applied. The measurements show a significant change in the travel time and amplitude of the primary arrival as a function of NAPL saturation.

To simulate the laboratory measurements, we performed numerical calculations of P-wave propagation through a one-dimensional medium. The results show that the main behavior of traveltime and amplitude variation can be explained by P-wave scattering. This represents an alternative explanation to the theories that describe local fluid flow as the dominant mechanism for seismic wave attenuation and velocity dispersion.

2.2 Introduction

A major challenge in remediating subsurface contamination by nonaqueous phase liquids (NAPLs) is to detect and delineate their distribution. Seismic methods have been applied in the petroleum industry to detect oil-bearing formations (Clark, 1992). A variety of laboratory experiments have been performed on sedimentary rocks to study the effect of pore fluid distribution on attenuation and velocity for different fluids under high pressure (Endres and Knight, 1989; Knight and Nolen-Hoeksema, 1990). However, the same mechanisms are not directly applicable to NAPL in groundwater aquifers, since the in-situ stresses at depths where oil and contaminating NAPL can be found are orders of magnitude

lower. In addition, there is also a difference in rock type and porosity between formations in the shallow subsurface and at depth of hundreds or thousands of meters.

On the basis of the available literature, it appears that the problem of seismic wave propagation in unconsolidated media containing NAPLs has received little attention. One laboratory study measured the response of ultrasonic wave propagation to the presence of NAPLs in unconsolidated media (Geller and Myer, 1995). Another set of field experiments monitored DNAPL (dense NAPL) migration in a naturally sandy aquifer using methods such as radar, electromagnetic induction, and electric resistivity (Greenhouse et al., 1993).

Different mechanisms have been proposed to describe the change in seismic wave attenuation and velocity with the type and extent of saturation of the pore fluids. For liquid-saturated rocks, these include grain sliding (Mavko, 1979), fluid flow as described by Biot (1956a; 1956b) and Johnston and Toksöz (1979) and local fluid flow (Biot, 1962; Akbar et al., 1994). Using a stratified medium of steel and plastic discs, Marion et al. (1994) conducted a joint experimental and theoretical study of the effect of multiple impedance contrasts on P- and S-wave velocities. They suggested that the change in velocity is a function of the ratio of wavelength to layer spacing (λ/d) in accordance with scattering theory. When λ/d is large, velocity is well described by effective medium theory, and when λ/d is small, by ray theory. For the entire range from effective medium

low-frequency results to the high-frequency prediction of ray theory, a complete theory for one-dimensional scattering can be found in Shapiro and Zien (1993) and Shapiro et. al (1994).

The main purpose of the present work is to obtain a better mechanistic understanding of the the changes in velocity and amplitude as a function of NAPL saturation which were observed in the laboratory by Geller and Myer (1995). We simulated P-wave propagation with a one-dimensional model and compared the amplitude and the traveltime of the first arrival for different NAPL-saturations with the laboratory data.

2.3 Experimental Method

Geller and Myer (1995) measured significant changes in P-wave velocity and attenuation as a function of NAPL saturation in initially water-saturated quartz sand packs. The properties of the NAPLs used, n-dodecane, iso-octane and freon 113, are listed in Table 1. Following the injection of incremental volumes of NAPL, ultrasonic P-wave measurements were taken by the pulse-transmission method. Traveltime, amplitude, and the shape of the waveform were recorded as a function of the volume of NAPL in the medium. P- wave measurements were also taken through sand samples initially saturated with NAPL.

The P-wave measurements were performed as follows. The sample was placed between transmitter and receiver in a triaxial cell, jacketed by a flexible teflon

sleeve. To obtain a homogeneous distribution of NAPL over the sample cross section, lexan plates with grooves were placed between the transducers and the sample. Confining and axial stresses on the sample were maintained at 60 and 140 kPa, respectively, which corresponds to the pressure conditions in the shallow subsurface. The sand columns were 73 mm in diameter and 39 mm in length. The sand consisted of washed, sub-rounded quartz grains sieved between 60 and 70 mesh (0.212 and 0.250 mm openings) packed to a porosity of 42%. The excitation signal was a pulse with frequencies ranging from 0.1 to 1.9 MHz, with a central frequency of approximately 0.5 MHz. Further details can be found in Geller and Myer (1995).

2.4 Experimental Results

P-wave velocity and normalized amplitude as a function of NAPL-saturation are plotted in Figure 2.1 and 2.2 for n-dodecane, iso-octane and freon 113. NAPL saturation is the fraction of pore space occupied by the NAPL; the remaining fraction is filled with water. The traveltime of the primary wave is picked at the first break from the amplitude baseline. The amplitude of the primary wave is the vertical difference between the first peak and trough and is normalized by the amplitude for the initially water-saturated sample.

It can be seen that the seismic wave transmission is strongly affected by the physical properties of the pore-filling fluids. The overall behavior is that the sig-

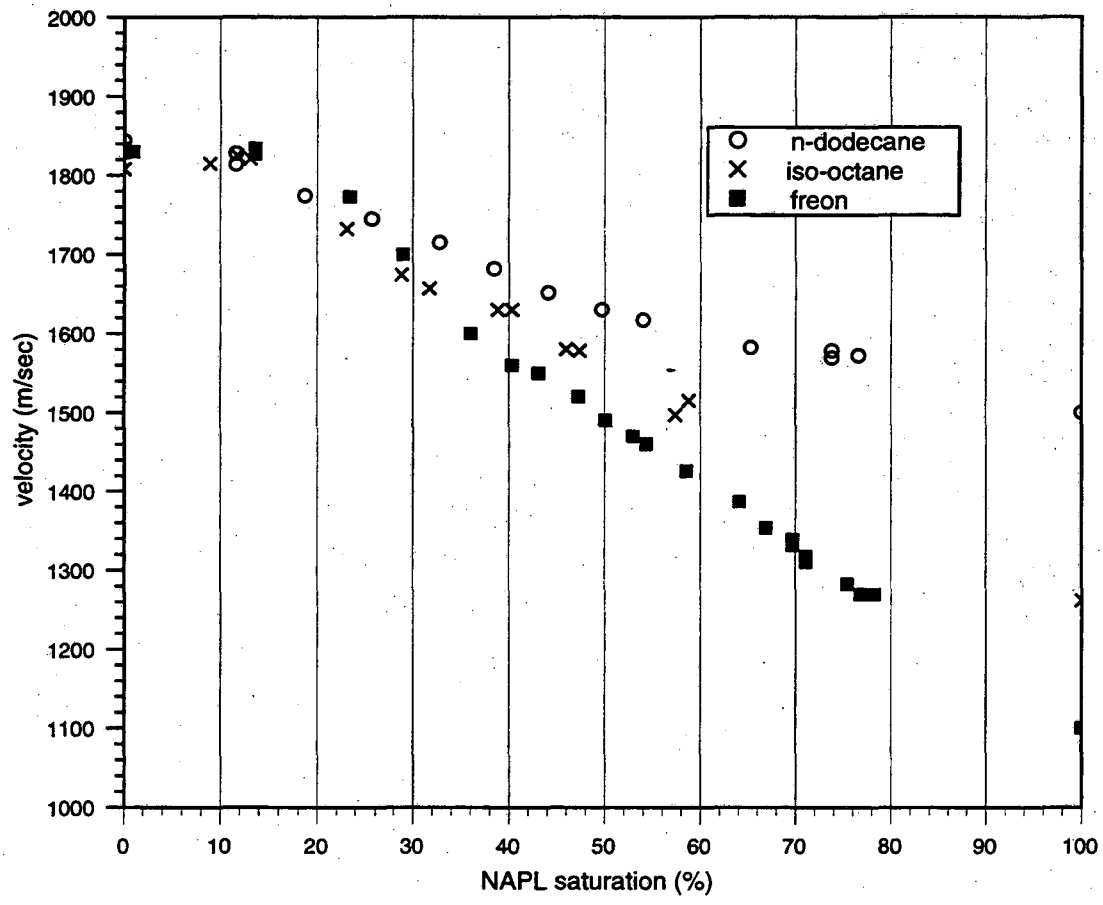

Figure 2.1: P-wave velocity as a function of NAPL (non-aqueous phase liquid) saturation for n-dodecane, iso-octane and freon where the remaining pore space is filled with water (Geller and Myer, 1995).

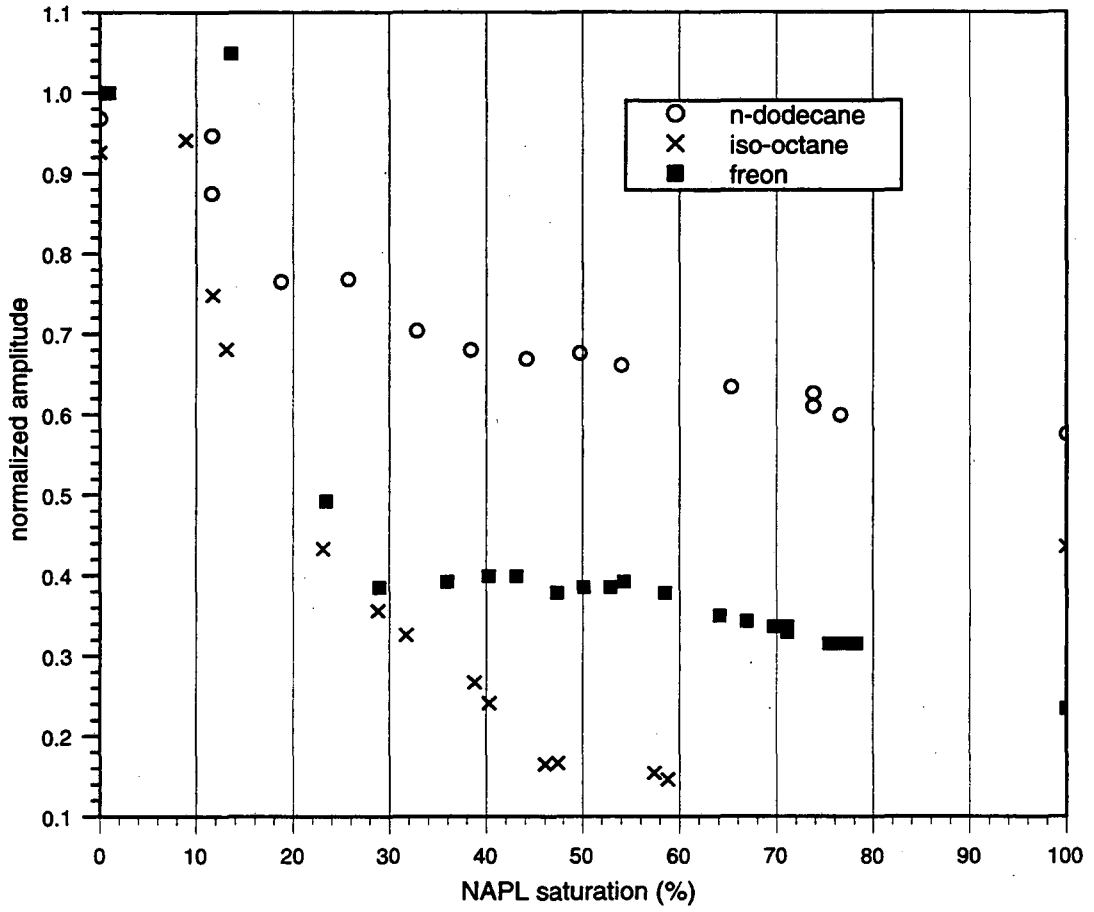

Figure 2.2: Normalized amplitude as a function of NAPL (non-aqueous phase liquid) saturation for n-dodecane, iso-octane and freon where the remaining pore space is filled with water (Geller and Myer, 1995).

nal is attenuated and the velocity decreases with increasing NAPL saturation. It should be pointed out that the minimum value for the amplitude for iso-octane at a NAPL saturation of 60% is much lower than for the other two NAPLs. Geller and Myer (1995) hypothesized that the low viscosity of iso-octane relative to water produced fingering of iso-octane throughout the sample. The injection of n-dodecane produced a stable injection front, because of its higher viscosity relative to the displaced water. Homsey (1987) provides an extensive review of mechanisms of flow instability and viscous fingering produced by the displacement of a more viscous fluid by a less viscous one in homogeneous porous media. To support this idea of viscous fingering, we photographed the displacement of water by NAPL in a thin, glass-walled sand box, 13 cm long by 7 cm wide by 0.2 cm deep. The box was packed with the same sand used by Geller and Myer (1995) and mounted vertically in front of a light box. The sand was fully saturated with deaired water with blue dye (white in Figure 2.3). In the next step, a red-dyed NAPL was injected (black in Figure 2.3), to displace the water. To minimize gravity-driven instabilities in the displacement of water, the lighter-than-water NAPLs (n-dodecane and iso-octane) were introduced from the top as in Geller and Myer (1995). In Figure 2.3 we can see the flow path for different injected volumes of n-dodecane and iso-octane, respectively. n-Dodecane shows a stable NAPL-front propagating downward with increasing saturation, whereas the iso-octane distribution shows fingering and large residual pockets

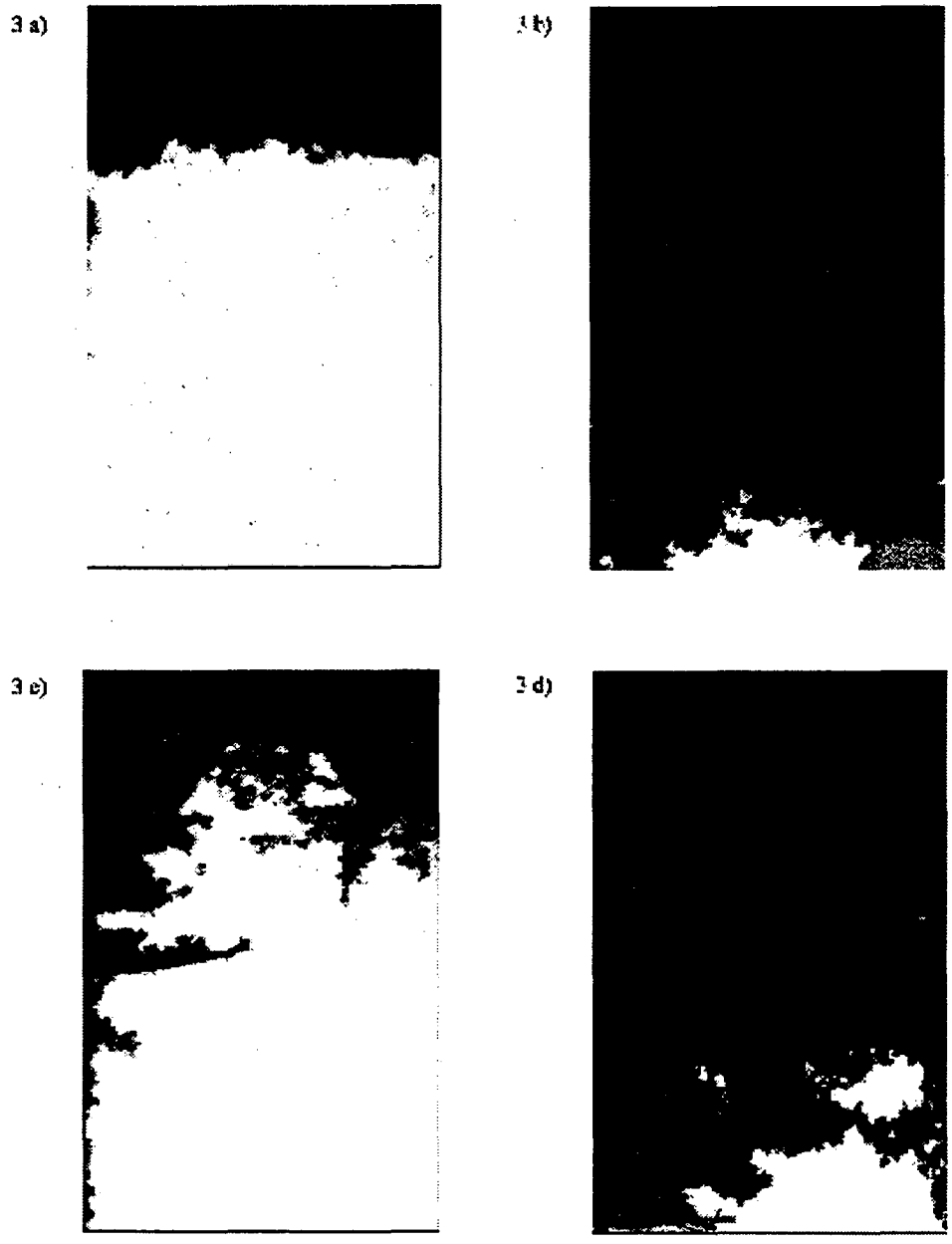

Figure 2.3: Sand fully saturated with deaired water (white), which is displaced by a NAPL (black). n-Dodecane shows a stable NAPL-front propagating downward with increasing saturation (Figure 2.3a and 2.3b), whereas the iso-octane distribution shows fingering and large residual pockets of water (Figure 2.3c and 2.3d).

of water. This experiment shows that it is very likely that the distribution of iso-octane is much more irregular than n-dodecane and may explain the larger P-wave attenuation measured for iso-octane.

These results demonstrate that the wave signature is sensitive to the NAPL-fraction in the pore space as well as its distribution. All the experiments used the same kind of sand and only the saturation and NAPL were changed. Thus any change in seismic signature results from a change in the liquid and not in the solid phase nor the pore structure.

2.5 Numerical Study

The use of numerical calculations to simulate laboratory results can often help in their interpretation. The case of sand grains surrounded by water and NAPLs presents a difficult elastic wave propagation problem, as there is no complete analytic solution available for the multiple scattering that occurs. Van de Hulst (1957) showed that in a three-dimensional medium only the scattered wave parallel to the incident wave is important, if only forward scattering is considered. In this case, the three-dimensional problem can be approximated by a one-dimensional model. In analogy with this assumption, we used a one-dimensional model with normal incidence for our calculations. The computation of elastic P-waves through a layered medium was performed with a propagator method, (Kennett, 1983). This method gives the complete solution for an inci-

dent plane wave through a layered medium between two half-spaces. Each layer has its own quality factor, velocity, density and thickness.

The saturated sample was represented by a series of layers having different sequences of solid matrix and pore fluid. The initially water-saturated sand pack was modelled with a simple two-layer sequence of water and quartz. When the wetting phase, water, is displaced by the non-wetting NAPL, residual water remains in contact with the sand. This situation was simulated by a four-layer sequence of matrix, water, NAPL and water. The different saturations of NAPL in the sample were modeled by a composite of two- and four-layer sequences (Figure 2.4). Typically 116 sequences composed of these two types were used to model the total sample length of about 39 mm. The layer thicknesses were Gauss-distributed and not correlated, with their mean and standard deviation based on the laboratory measurements.

The layer thickness of the matrix was determined by the average grain size of 0.23mm diameter with a standard deviation of 18%. The layer representing the pore space was determined by the porosity of 32% with a standard deviation of 18%. Figure 2.1 and 2.2 show that the residual water saturation for iso-octane displacing water is about 40%, which is almost twice as large as for n-dodecane and freon 113. This was accounted for by changing the thickness of the residual water layer for each NAPL. The matrix is composed of quartz with a velocity of 5750 m/sec and a density of 2650 kg/m^3 (Selfridge, 1985). The properties

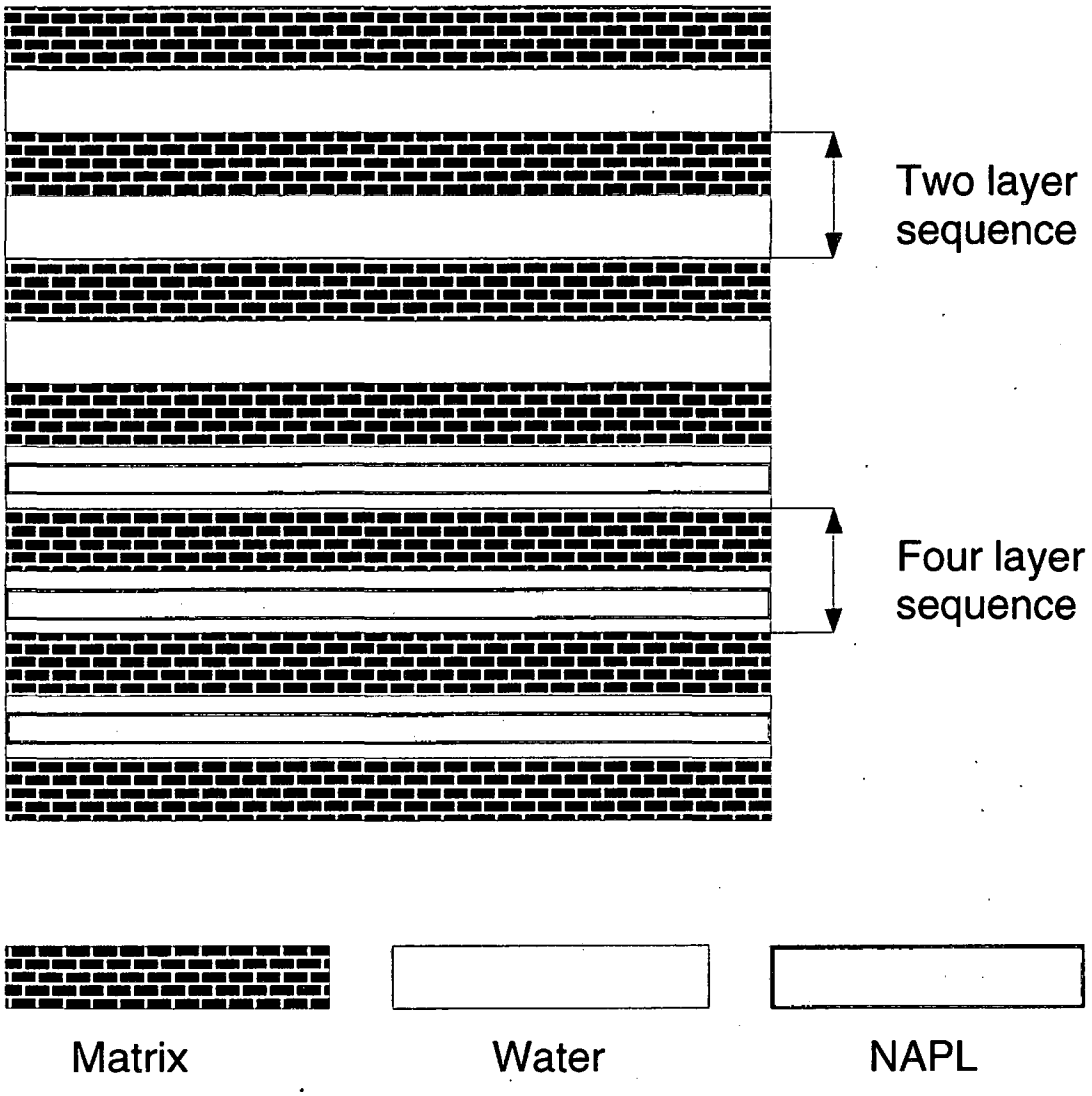

Figure 2.4: Model for NAPL (non-aqueous phase liquid) which has displaced some of the water layers. At the top we have the undisturbed case, quartz sand layers saturated with water. At the bottom, the water is replaced by a NAPL. A residual layer stays in each sequence, representing the wetting phase.

Table 2.1: Material properties (values are at 25° C and atmospheric pressure unless otherwise noted).

	Density[a] (kg/m^3)	**P-wave velocity**[b] (m/s)	**Viscosity** (mPa/s)	**Reflection Coefficient with water**[f] (kPa s/m)
freon 113 (1,1,2-Trichloro-1,2,2-trifluoroethan)	1560[d]	716	0.711 (20°)	-0.137
n-dodecane (2,2,4-Trimethyl pentane)	745	1290[c]	1.378	-0.212
iso-octane	690 (20°)	1120[e]	0.504 (20°)	-0.314
water	997	1497	0.890	N/A

a) Riddick and Bunger (1970), b) Selfridge (1985), c) Wang and Nur (1991), 22° C, d) CHRIS (U.S. Coast Guard, 1984), e) Geller and Myer (1995), f) $R = \frac{(\rho_2 v_2 - \rho_1 v_1)}{(\rho_2 v_2 + \rho_1 v_1)}$, using values in table

of the pore-filling liquids are listed in Table 2.1. The quality factor, Q, was set to infinity for the matrix, to 10,000 for water (Toksöz and Johnston, 1981) and to 1,000 for the NAPL. The Q value for the NAPL was calculated with the spectral ratio method by using the direct and the reflected wave traveling through a column of freon as suggested by Feustel and Young (1994). As in the laboratory experiments, we placed the series of layers between two lexan plates with a thickness of 10 mm, density of 1200 kg/m^3 (Selfridge, 1985), P-wave velocity of 2300 m/sec (Selfridge, 1985) and a Q value equal to infinity.

Calculation for this stack of layers was based on a white source spectrum.

For comparison of the numerical data and the laboratory measurements, we convolved the obtained Green function with a measured reference signal. The amplitude spectrum used as a reference was obtained from the Fourier transform of the first arriving pulse through a column of water with lexan plates attached to the transducers.

2.6 Numerical Results and Interpretation

To constrain our computational model, we varied porosity, grain size and their standard deviation to match the velocity and normalized amplitude of our synthetic data with the measured data. The mean grain size was the same as in the experiments (0.23mm). The standard deviation for our model was taken as 18%, instead of about 10% from the difference in 60 to 70 mesh sizes, due to the fact that grains are not perfect spheres. The value of the porosity was adjusted by fitting the calculated velocities to the measured data. The fitted porosity is 32%, which is less than the actual value of 42%. To explain this discrepancy, Figure 2.5 compares the layer sequence with an equivalent cross section of randomly packed spheres in terms of sample length and porosity where the sphere diameter equals the thickness of the matrix layer. This sketch shows how a straight ray traveling through spheres encounters more interfaces and therefore can be reflected more often than when traveling through layers. As a result, if the number of reflections were to be the same, the porosity of the random

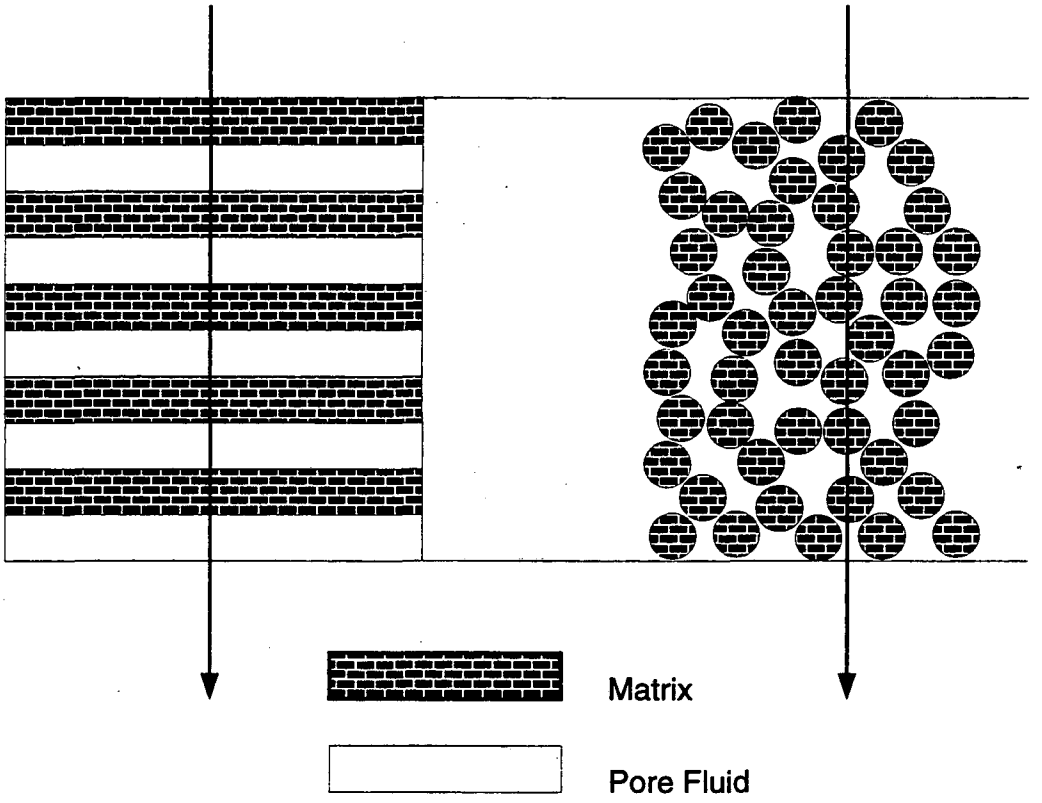

Figure 2.5: This sketch shows how a straight ray traveling through an idealized sandpack encounters more interfaces than through a series of layers.

sphere pack would be greater than the one-dimensional model. Therefore in a one-dimensional model, a smaller porosity fits the data best. Amplitude and traveltime of a seismic wave through a series of layers were calculated in increments of 5% NAPL saturation. For each saturation, ten realizations were performed with a random number generator which chooses the thickness of the layers according to a Gaussian distribution with a mean of 0.23 mm and a standard deviation of 0.04 mm (Press et al., 1992). From the ten realizations, the mean velocity, the mean normalized amplitude, and their standard deviation

were calculated. The mean amplitude of the transmitted wave was normalized by the mean amplitude for the initially water-saturated sample.

In Figure 2.6 and 2.7 the dashed lines connect the theoretically calculated data points and the filled boxes are the experimentally observed ones. The error bars show the standard deviation of the ten realizations. It should be noticed that a single realization can still lie outside this range and fit the data almost perfectly (Figure 2.8). Figure 2.6 and 2.7 show that the numerical and the measured data decrease monotonically as a function of NAPL saturation.

Mechanisms for velocity dispersion and seismic wave attenuation are usually a combined effect of scattering and intrinsic attenuation. Intrinsic attenuation is caused by energy transformation into heat and is described by the quality factor Q. By using a Q of 10,000 for water, 1,000 for NAPL, and infinity for the matrix, the intrinsic attenuation is very small. Figure 2.8 shows a comparison of the change in velocity and amplitude as a function of NAPL saturation for two different models, one with the quality factors listed above, which are generally used in all the models for our computations, and the second with all quality factors equal to infinity. These figures show that intrinsic attenuation has an insignificant effect on amplitude and on traveltime. In our case, scattering within the layered medium produces the velocity dispersion and attenuation. For the case of uncorrelated layers, the scattering mechanism depends upon the ratio of wavelength (λ) to layer thickness (d) (Marion et al., 1994), otherwise it is

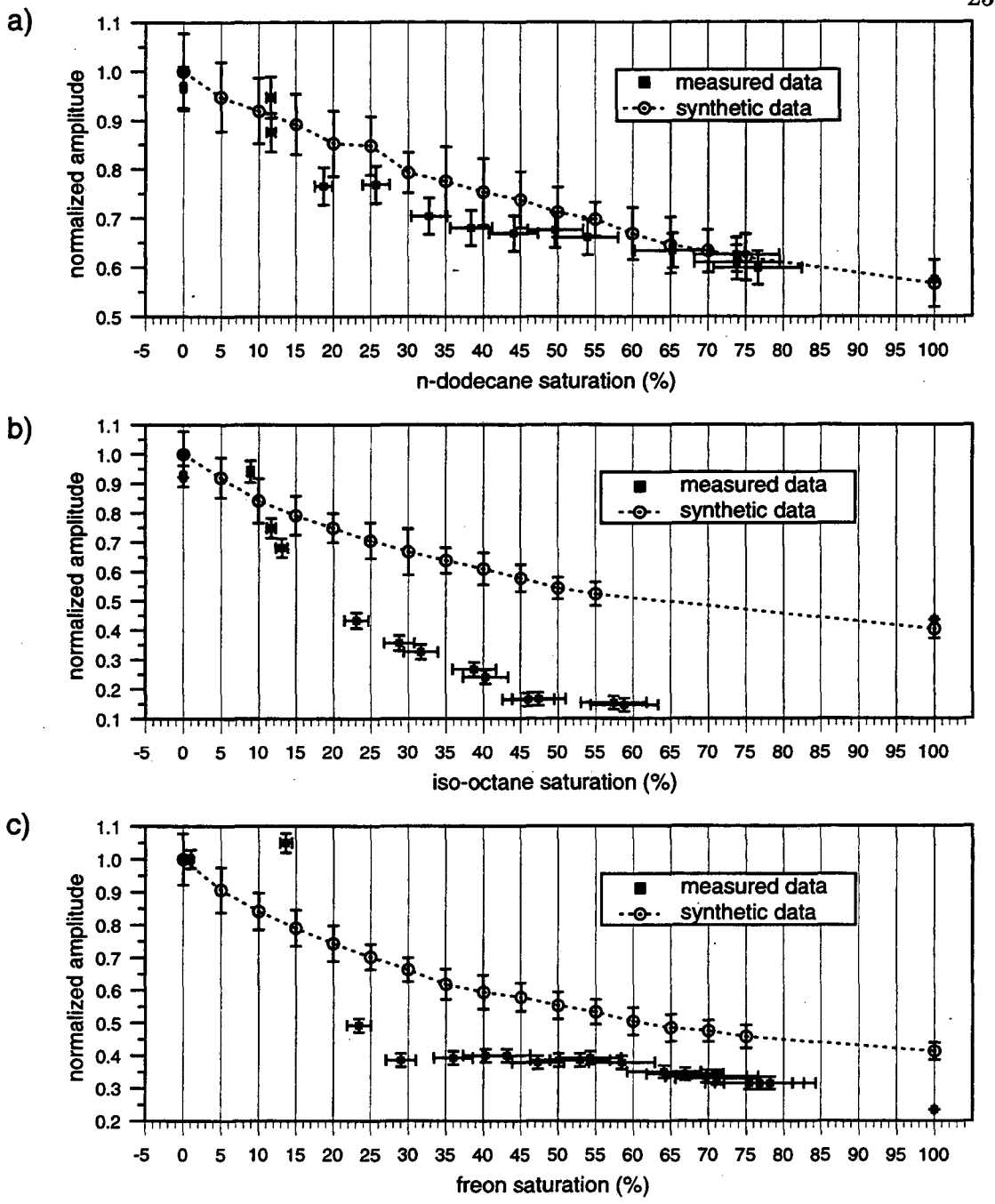

Figure 2.6: Normalized amplitude as a function of NAPL (non-aqueous phase liquid) saturation for a) n-dodecane, b) iso-octane and c) freon. Error bars of the synthetic data show standard deviation of ten realizations, which were performed with a random number generator which changed the layer thickness within 0.23mm + 0.04mm. Error bars for the measured data show the estimated experimental error.

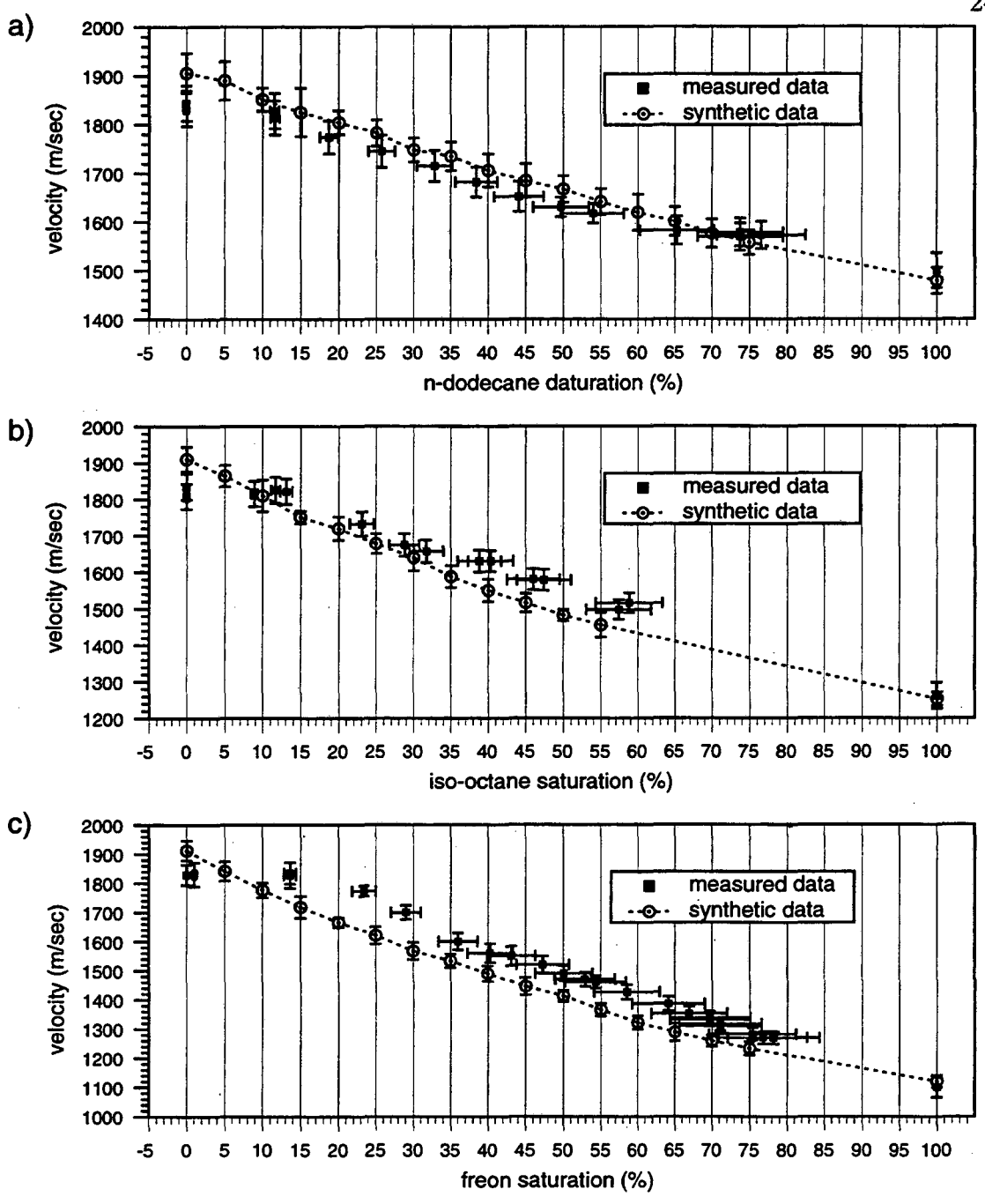

Figure 2.7: P-wave velocity as a function of NAPL (non-aqueous phase liquid) saturation for a) n-dodecane, b) iso-octane and c) freon. Error bars for the synthetic data show standard deviation of ten realizations, which were performed with a random number generator which changed the layer thickness within 0.23mm + 0.04mm. Error bars for the measured data show the estimated experimental error.

a function of the ratio of wavelength to correlation length (a). To find the correlation distance of our model we performed autocorrelations for different stacks of two-layer and four-layer sequences. These results showed that there was no correlation between the layering and therefore the correlation length is equal to the layer thicknesses. Shapiro et al. (1994) derived an analytical solution for a one-dimensional medium which is valid for all frequencies, i.e., from effective medium to ray theory, and therefore includes Rayleigh as well as Mie scattering regimes. For a transmitted wave with a normal incidence, their theory shows that the Rayleigh scattering assumption is a good approximation, if $k \cdot d < 0.1$, where k is the wave number. The critical frequency where Rayleigh scattering is dominant is therefore

$$f_c < \frac{0.1 \cdot v}{2 \cdot \pi \cdot d} \tag{2.1}$$

Taking the velocities listed in Table 1 for the pore fluids, a velocity of 5750 m/sec for quartz and average layer thicknesses of 0.23 mm for the matrix, 0.108 mm for the pores, 0.0866 mm for the non-wetting phase and 0.0108 mm for the wetting phase, results in critical frequencies between 105 kHz and 390 kHz. Since we have used a frequency range from 100-900 kHz, we encounter some Rayleigh scattering, but mostly Mie scattering.

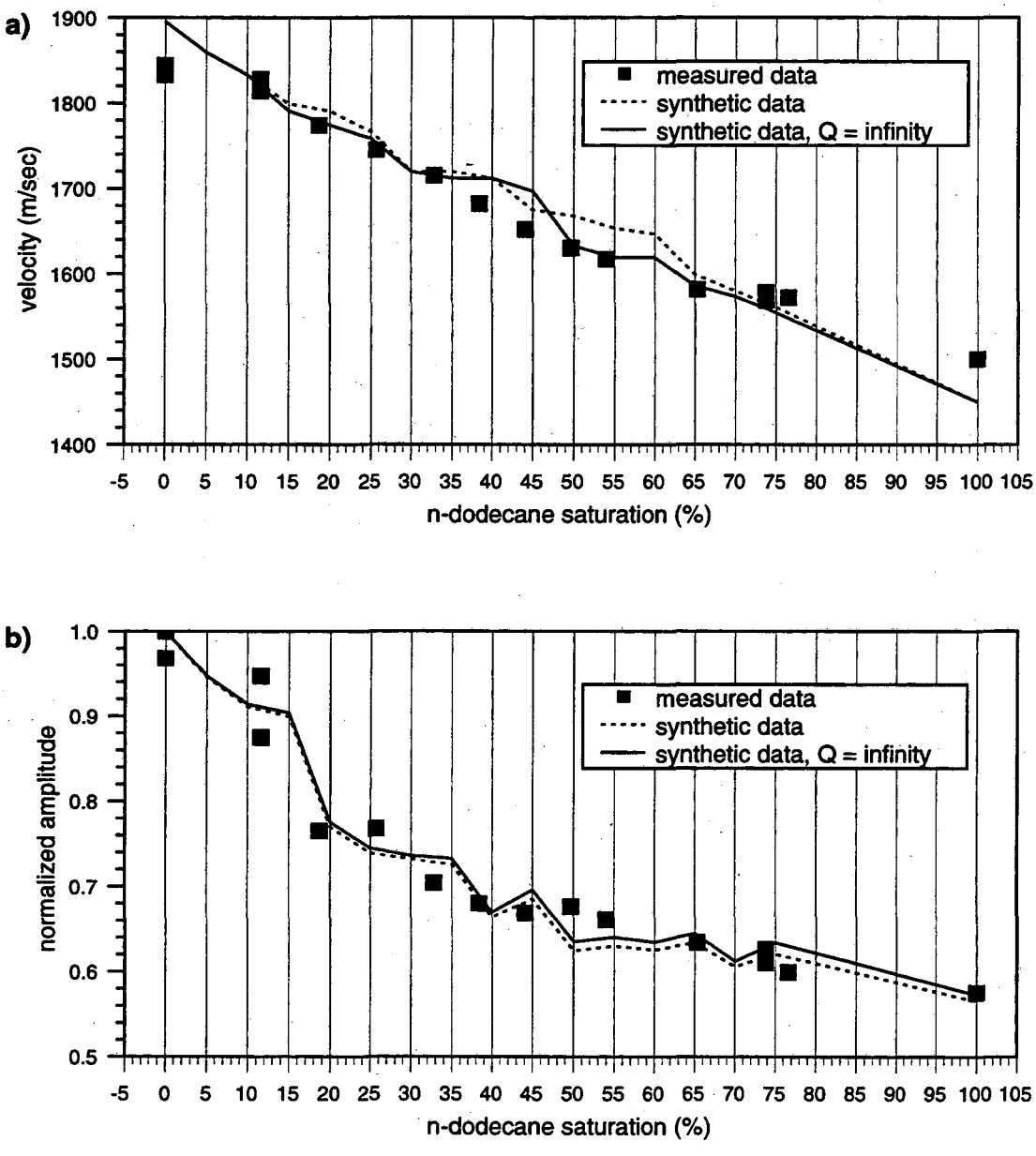

Figure 2.8: One realization of a) velocity and b) normalized amplitude as a function of n-dodecane saturation. Comparison between two different models one with quality factors Q_{water} = 10,000, Q_{NAPL} = 1,000, Q_{matrix} = infinity, the other one with quality factors equal to infinity.

2.7 Comparison of Numerical Results with Laboratory Measurments

Measured and calculated velocities and amplitudes correlate well for n-dodecane (Figure 2.5 a and 2.6 a), indicating that for this specific NAPL, scattering mechanisms are sufficient to explain the observed seismic wave attenuation and velocity dispersion. The small deviation between the measured and simulated data is most likely based on either differences in the distribution of the NAPL between the experiment and the model or other intrinsic attenuation effects, such as local fluid flow.

For the normalized amplitude and velocity of iso-octane, the calculated data match the measured data at the endpoints (Figure 2.6 b, 2.7 b). The mismatch between the intermediate measured and modeled points may be caused by the irregular NAPL distribution created by fingering as mentioned earlier. This is a three dimensional effect and which cannot be simulated with our model.

For freon 113 our computations underestimate the attenuation and the velocity change with NAPL saturation. The amplitude data deviate from the model more than the velocity data do. This could occure if the freon produces gas inclusions that cause strong reflections and increase attenuation. To show the effect of gas bubbles, we placed one small layer (0.05 mm - 0.16 mm) of air in our modeled NAPL-water-sand sequences. The computations were done to match the experimental data for freon 113 saturations of 30%, 50%, 70% and

100%. The results are plotted in Figure 2.9. Even though bubbles are again a three dimensional problem, our model tells us that a very small amount of gas produces a significant change in attenuation, but hardly affects the velocity. Therefore, a small amount of gas trapped in the sample could have caused the attenuation effects observed for freon.

2.8 Conclusions

A one-dimensional model was used to simulate measured data of ultrasonic wave propagation through sand samples of different NAPL saturations. The main trend observed in the laboratory of amplitude and velocity change as a function on NAPL saturation could be simulated with our model. Small differences between the experimental and the synthetic data are most likely caused either by heterogeneous distributions of the immiscible liquids or by intrinsic attenuation effects, such as local fluid flow. Loss mechanisms caused by liquid fingering or inclusions of gas-bubbles are not represented in our model, because these are three-dimensional effects. Our results show that most of the seismic wave attenuation and velocity dispersion observed in the laboratory can be explained by scattering in the Mie regime. This represents an alternative explanation to the theories which describe the observed behaviors by local fluid flow. Nevertheless it is possible that several loss mechanisms are acting simultaneously.

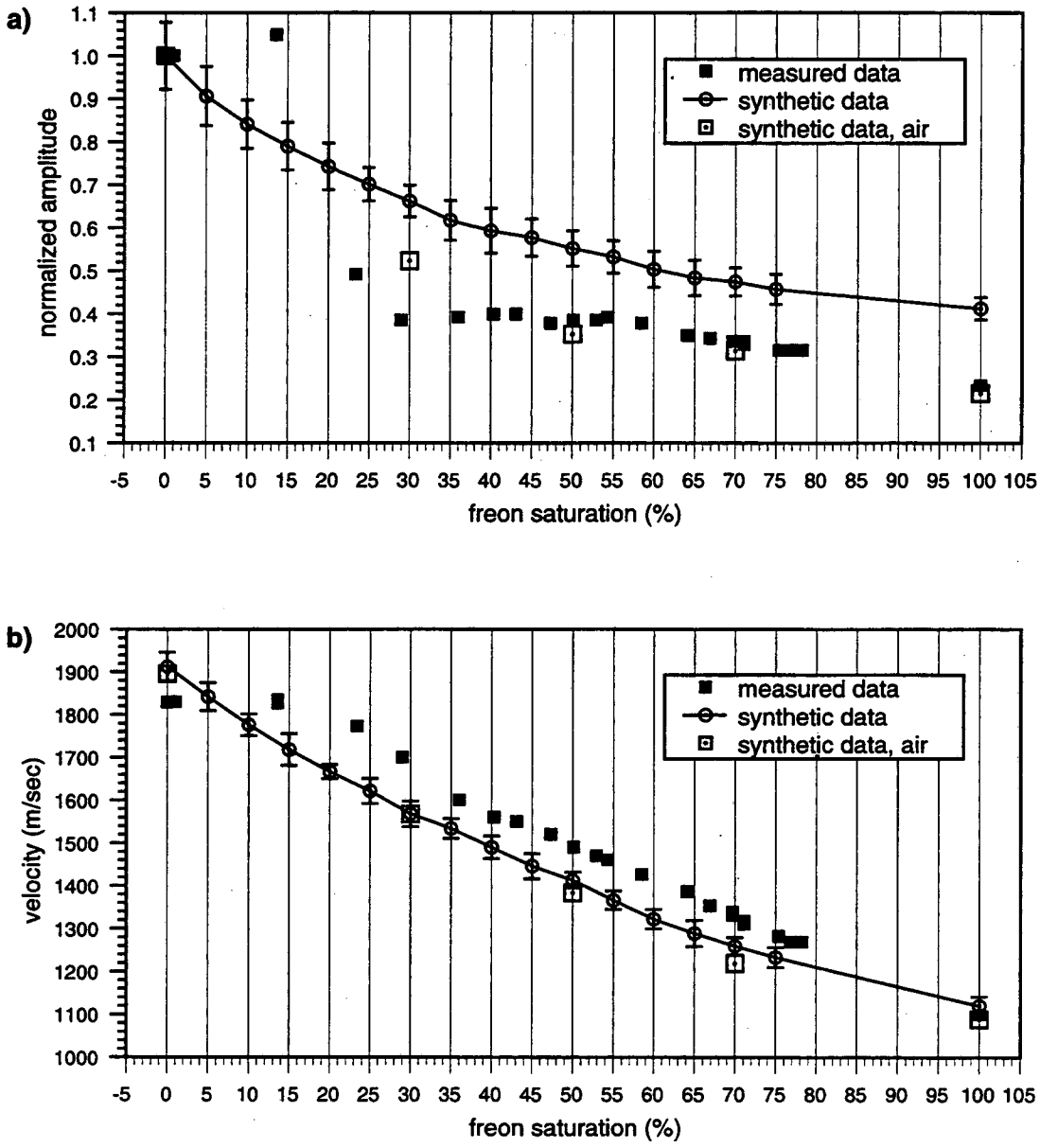

Figure 2.9: Normalized amplitude and b) P-wave velocity as a function freon saturation. The same calculations were done with small layers of air included in our model. The thickness (d) of the air layer was for different saturations (s), s=30%, d=0.05mm / s=50%, d=0.07mm / for s=70%, d=0.16mm.

The agreement found in this study between laboratory measurements and numerical calculations suggests several topics for additional research. The use of one-dimensional calculations to help explain effects in three-dimensional media needs further justification. Similar experiments with S-waves would help constrain the interpretation, and such studies are currently in progress. Furthermore the importance of scattering in partially saturated media should be investigated.

Chapter 3

Qualitative Explanation of Attenuation Effects Observed in Unconsolidated Saturated Sand

3.1 Abstract

The velocity and attenuation of seismic waves in liquid-saturated unconsolidated sand are strongly affected by the pore-filling fluids. Displacing water in a fully water saturated sand sample by a non-aqueous phase liquid (NAPL) can be an unstable process, leading to heterogeneous phase distributions. Experiments were performed to determine how the physical and chemical properties of NAPL may give rise to heterogeneities, such as fingering at the water-NAPL displacement front or gas inclusions.

Using two-dimensional numerical simulations we illustrate how ultrasonic P-waves are scattered by these heterogeneous fluid distributions to cause attenuation in addition to the scattering from the pores and grains. We model

the situation in our laboratory tests where spatial resolution is limited by the receiver size. This prevents us from resolving heterogeneities that are smaller than the receiver, but even in this case the mean seismic amplitude over the width of the receiver is affected by such heterogeneities and it is possible to obtain qualitative agreement between measured and modeled data for the cases of fingering and gas inclusions.

3.2 Introduction

In recent years, seismic measurements have become increasingly important as a means of studying the shallow subsurface. Majer et al. (1997) used high frequency seismic waves to detect fractures at depths between 15 and 30 m; Yamamoto et al. (1994) performed crosswell acoustic tomography experiments down to 60 m below the surface using high carrier frequencies of 1 to 10 kHz; Dvorking and Nur (1996) conducted seismic laboratory and theoretical studies on poorly-cemented and un-cemented grains; Bryant and Raikes (1995) made predictions of elastic-wave velocities using models for certain depositional and diagenetic processes. These techniques potentially may be applied to the detection and delineation of organic liquid contamination in groundwater aquifers. These contaminants are minimally soluble in water and persist in the subsurface as non-aqueous phase liquids (NAPLs). NAPLs that have densities greater than water (DNAPLs) can migrate below the water table (McKee et al., 1972;

Schwille, 1967; Schwille, 1984). Lighter than water NAPLs (LNAPLs) spread along the capillary fringe and may, however, occur below the water table as a result of fluctuations of the water table (Schwille, 1981; Mercer and Cohen, 1990). Therefore, NAPLs entrapped in soils and aquifers can attain highly irregular distributions.

The objective of this study is to investigate, how inhomogeneous contaminant distribution affects the amplitude of ultrasonic waves. Previous laboratory measurements showed that velocity and attenuation of seismic waves in liquid-saturated unconsolidated sand are strongly affected by the pore-filling fluids. In sand pores saturated with varying fractions of NAPL and water, Geller and Myer (1995) showed that P-wave velocity reflects the difference in bulk moduli between water and NAPL and the fraction of NAPL present, but is insensitive to its distribution, whereas the amplitude is sensitive to both the fraction of NAPL and its distribution. Seifert et al. (1998) showed that if the amplitude decreases monotonically with increasing NAPL saturation, and if a stable propagation of the NAPL-water front can be assumed, the amplitude and velocity change can be explained with a one-dimensional scattering model. However, if the fluid distribution is heterogeneous due to unstable displacement mechanisms or the pore fluid is very volatile and small changes in pressure or temperature produce gas inclusions, the one-dimensional scattering model still gives good velocity estimates but underestimates the magnitude of attenuation. Since these

effects are two- or three-dimensional, the amplitude (which is sensitive to the distribution of the pore-filling fluid) cannot be explained with a one-dimensional model, which accounts only for the NAPL fraction. To obtain a qualitative understanding of these additional attenuation effects caused by either gas inclusion or NAPL fingering, we apply a two-dimensional numerical approach in this paper. It should be noted that in this study the word attenuation refers to the non-geometrical decrease in the amplitude of elastic waves as they propagate and includes the effects of both intrinsic attenuation and scattering.

3.3 Previous Laboratory Results and Numerical Simulation

Geller and Myer (1995) measured significant changes in P-wave velocity and attenuation as a function of NAPL saturation in initially water-saturated quartz sand packs. The three NAPLs used for their measurements were physical and chemical analogs of NAPL contaminants: n-dodecane (an analog of diesel), isooctane (an analog of gasoline) which are lighter than water and Freon 113, which has a higher density than water (a common contaminant and an analog of dense halogenated hydrocarbons such as TCE).

Following the injection of incremental volumes of NAPL, ultrasonic P-wave measurements were made with the pulse transmission method. Traveltime, amplitude and shape of the waveform were recorded as a function of the volume

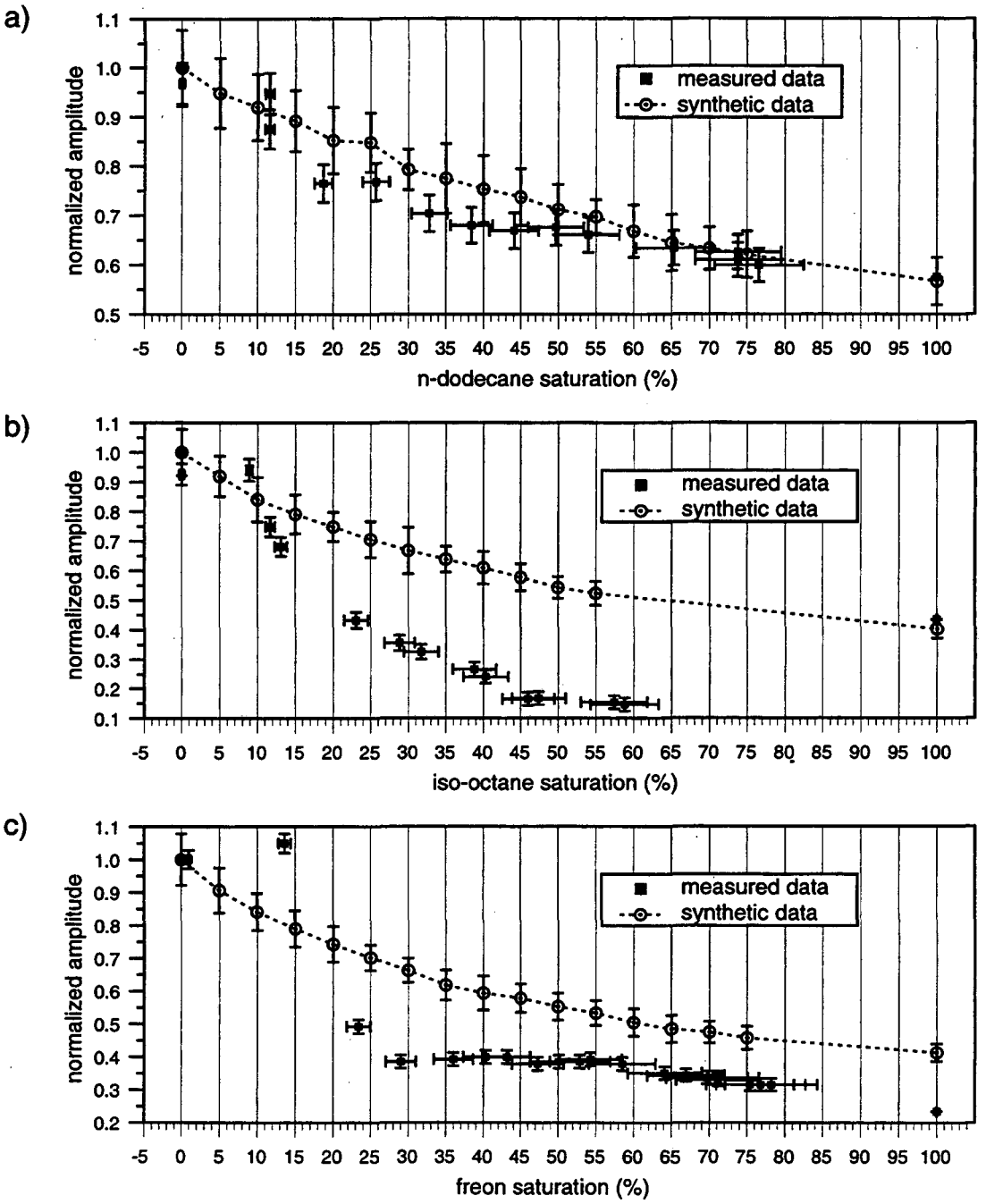

Figure 3.1: Normalized P-wave amplitude as a function of NAPL (non-aqueous phase liquid) saturation for a) n-dodecane, b) iso-octane and c) freon.

of NAPL in the medium. P-wave measurements were also taken through sand samples fully saturated with NAPL. Figure 3.1 shows the measured amplitude of the transmitted wave as a function of NAPL saturation, normalized by the amplitude for the initially water-saturated sample. Error bars for the synthetic data show standard deviation of 10 realizations and the ones for the measured data show the estimated experimental error. The saturation, or fraction of pore space occupied by the NAPL, is determined from a mass balance of the volume of NAPL injected and the volume of liquids (water and NAPL) displaced in the initially water-saturated sand pack. In general the amplitudes decrease monotonically with increasing NAPL-saturation, except for the case of iso-octane, where the amplitude at residual water saturation is less than the amplitude at 100% iso-octane saturation. The data show that the seismic wave is strongly affected by the NAPL saturation and the physical properties of the pore-filling fluids. Figure 3.1 also shows synthetic data (Seifert et al., 1998), which were computed with a one-dimensional model based on the propagator method (Kennett, 1983). The significant differences between the calculated and measured amplitudes for iso-octane and freon experiments may be caused by the model assumption of a sharp NAPL-water front during displacement. This hypothesis will be scrutinized by looking at the stability of the displacement process and the uniformity of the resulting saturation distribution. Measured and calculated velocities agree well for all three NAPLs and are, therefore, not

further considered in this study (Seifert et al., 1998).

When displacing the water by NAPL in the initially water-saturated sample, different fluid distributions can occur depending on the NAPL's physical properties. The NAPL-water front may remain uniform during displacement (Figure 3.2a), or fingering may occur which may result in bypassing patches of water-saturated media (Figure 3.2b). Once a finger extends over the entire length of the sample, the NAPL has found a fast path through the sample, and further increase in NAPL saturation is difficult to achieve. Hence the residual water saturation is usually higher than in the case of an unstable water-NAPL displacement front. Thermal, viscous and gravitational factors can give rise to unstable displacement. Fingering can also be initiated by heterogeneities in the porous medium (Homsey, 1987). Since our sample is made of clean quartz sand, with grains varying only within one mesh size, we assume a homogeneous porous medium. The samples were isothermal and the temperature in the laboratory was held constant, therefore we assume that the instabilities are driven by differences between either densities or viscosites of the fluids.

For n-dodecane (Figure 3.1a), the amplitude of the synthetic and the measured data match well, indicating that fingering of NAPL-water front is not needed to explain the measurements. For the normalized amplitude of iso-octane (Figure 3.1b), the calculated data match the measured data at the endpoints. The difference between the intermediate measured and modeled data may be

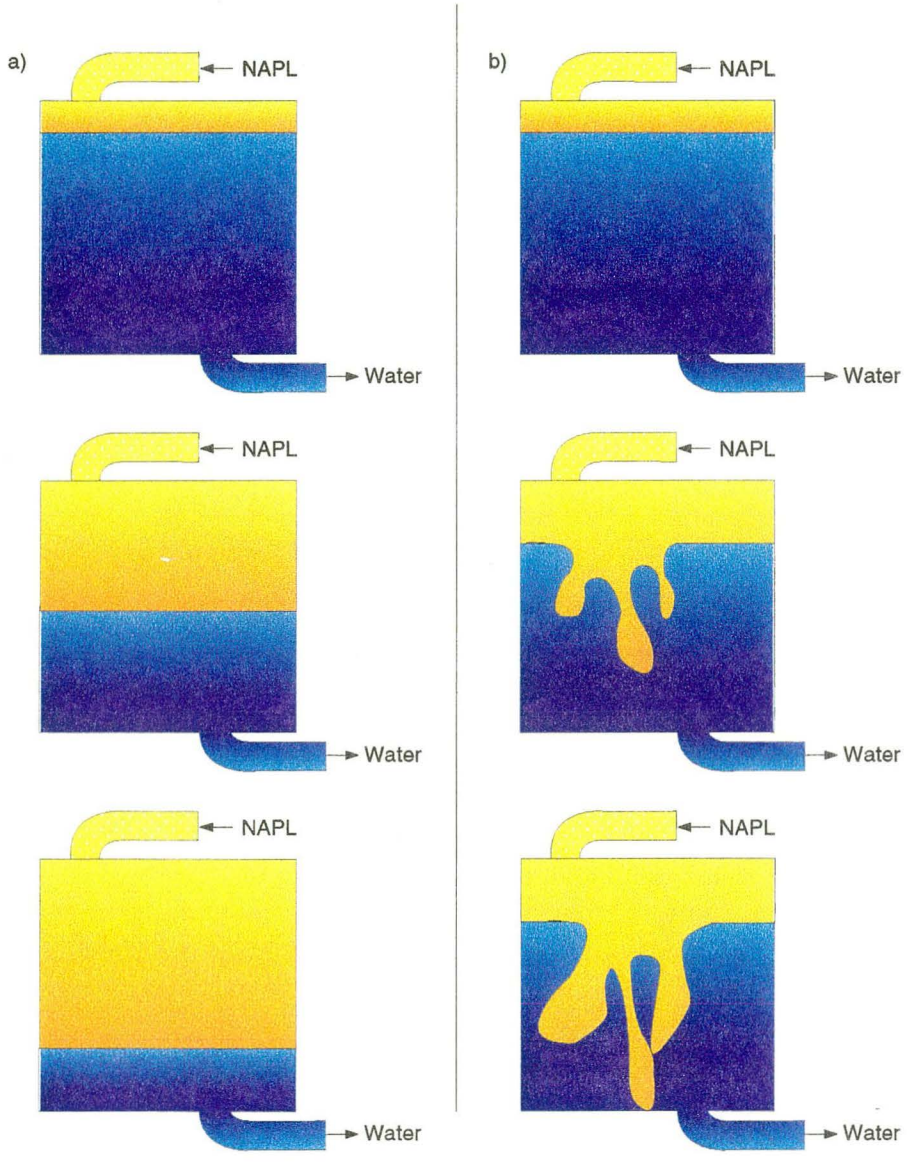

Figure 3.2: Different fluid distributions can occur depending on the physical properties of the NAPL. a) shows a stable NAPL-water front that is propagating through the sample. In b) the front starts out uniformly but then breaks up into fingers.

caused by irregular NAPL distribution. Another indication of inhomogeneous fluid distribution is the fact that the residual saturation of water in the experiment with iso-octane (ca. 40%), is considerably greater than the 20% residual saturation achieved for n-dodecane and freon. Since iso-octane is less viscous than water, it may finger when displacing water.

Pictures of the displacement of water by NAPL in sand packed between parallel glass plates support the differences in displacement (Seifert et al., 1998). Figure 3.3 shows the displacements using n-dodecane (Figure 3.3a), iso-octane (Figure 3.3b) and freon (Figure 3.3c), respectively. To avoid the gravity-driven instabilities in the displacement of water (white), the NAPLs (black) were introduced from the top or the bottom such that the denser liquid was on the bottom. n-Dodecane shows a stable NAPL-water front propagating downward, whereas the iso-octane distribution shows significant fingering and this fingering can even lead to bypassing of large water saturated regions (upper right side of Figure 3.3b). Freon, which was injected from the bottom, also shows a stable front propagating upward. These experiments show that it is very likely that the distribution of iso-octane is much more irregular than of the other two NAPLs, which may explain the larger attenuation measured for iso-octane.

Our computations for freon also underestimate the attenuation change with NAPL saturation (Figure 3.1c). Note that, unlike the case of iso-octane, the discrepancy occurs for both partial and 100% NAPL saturation. The deviation

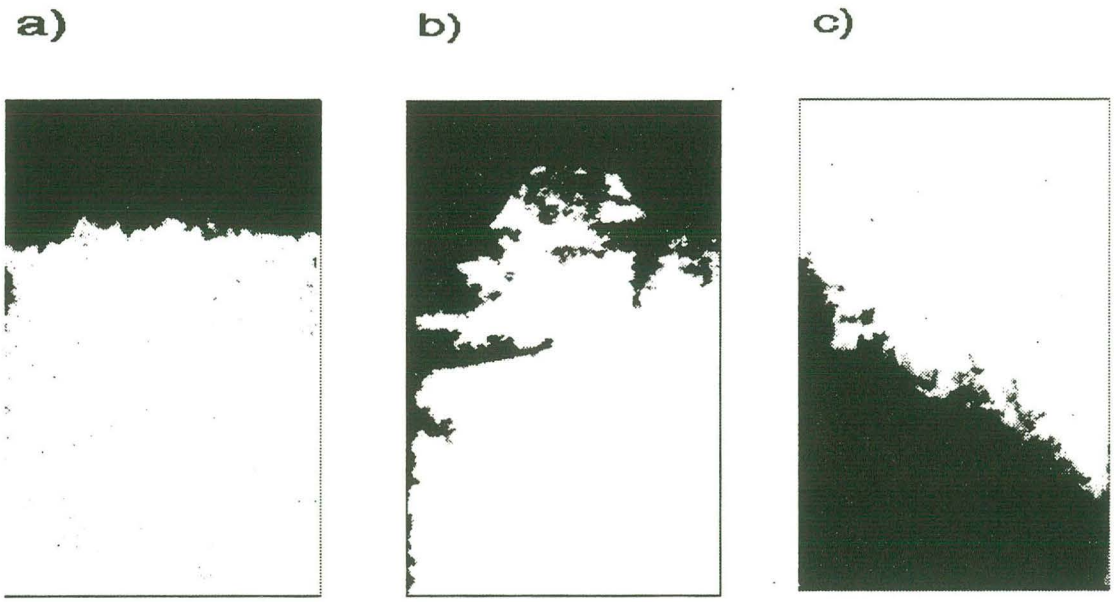

Figure 3.3: Sand initally fully saturated with deaired water (white), which is displaced by a NAPL (black). a) n-Dodecane: stable NAPL-water front propagating downward; b) iso-octane: fingering and bypassing of water saturated regions; c) freon (injected from the bottom): stable front propagating upward (the angle of the front was caused by clogging in an injection tube).

Table 3.1: Physical and chemical properties of NAPL contaminants

Liquid	Density[a)] (kg m^{-3})	Viscosity[a)] (mPa s)	vapor pressure[b)] (kPa)	Reflection Coefficent[a]
water	997	0.890	3.17	—
n-dodecane	745	1.378	0.016	-0.212
iso-octane	690	0.504	6.5	-0.314
freon 113	1560	0.711	44.8	-0.137

a) Geller and Myer (1995) b) Lide (1995)

in amplitude may be due to the high vapor pressure of freon (see Table 3.1) which produces gas inclusions that cause scattering and further attenuation. Since a NAPL-water displacement experiment takes about two to three days, it is most likely that the temperature in the laboratory and pressures in the load cell may change and small freon vapor inclusions are produced.

3.3.1 Numerical simulations of fingering and gas inclusions in sand samples and comparison with experiments

As discussed in the previous section, the results in Seifert et al. (1998) show that the dominant loss mechanism in granular media can be explained by P-wave scattering. Reflections from heterogeneities remove energy from the direct seismic wave and redistribute this energy into scattered waves. In granular me-

dia these heterogeneities can range in scale from pores and grain contacts to fractures, faults, and sedimentary layers. Seifert et al.'s (1998) numerical calculations simulated wave propagation through a one-dimensional medium and computed scattering caused by the granular medium and the different pore fluids, but did not account for the two- and three-dimensional effects of the irregular pore fluid distribution. In real porous media, irregular liquid distribution and gas inclusions can occur, causing further loss in energy.

Wave attenuation caused by fingering and gas inclusions can be simulated in a two dimensional model. The numerical approach used employs the boundary integral equation method as developed by Nihei et al. (1995). Figure 3.4 shows the different input models used to represent:

a) n-dodecane propagating downward as a stable NAPL-front

b) fingering caused by the viscosity difference between iso-octane and water

c) a gas inclusion in a freon saturated sand.

The blue area in Figure 3.4a and 3.4b represents a fully water-saturated sand. The orange area is a NAPL saturated sand with residual water. For n-dodecane the residual water in the NAPL region is 20% according to the measurements. For iso-octane the residual saturation is more difficult to determine, since water exists as residual water in the iso-octane region and as entrapped water patches. Because the interfacial tension and dielectric constants for the different NAPLs

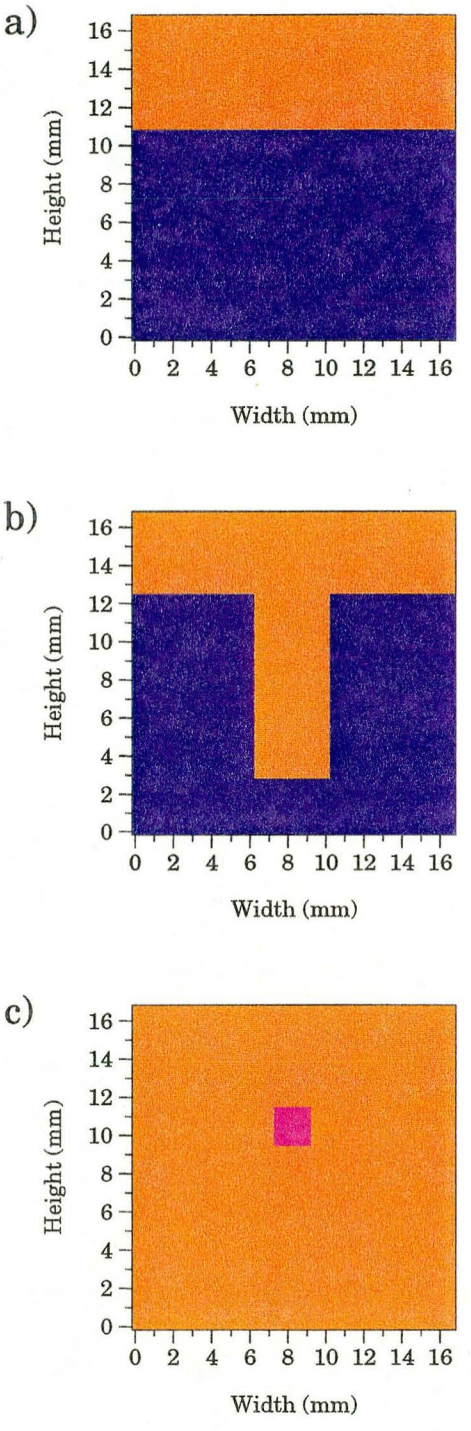

Figure 3.4: Models used for distribution of pore-fluid pairs in a unconsolidated sand. a) Flat interface as observed in the case of n-dodecane and water; b) fingering as in the case of iso-octane and water; c) gas inclusion which could be produced from the high volatility of freon. The material properties are listed in Table 3.1

Table 3.2: Physical and chemical properties of NAPL contaminants

Liquid	Interfacial Tension[a)] (dyne cm^{-1})	Dielectric Constant[a)] (mg L^{-1})	Solubility in water[a)]
water	—	78.3	—
n-dodecane	52.8	2.014	0.0037
iso-octane	50.1	1.948	2.4
freon 113	37	2.41	200

a) Geller and Myer (1995)

are similar (Table 3.1), we conclude that without entrapped water regions the residual water saturation for iso-octane would be similar to freon and n-dodecane and reach 20%. The difference of 20% is attributed to entrapped regions of water in iso-octane with residual water. The orange region in Figure 3.4b was therefore calculated with the properties of a sand which is 80% saturated with iso-octane and 20% saturated with water. For the velocity we have chosen the mean value between the 60% and fully iso-octane saturated sample. The dimensions of the finger shown in Figure 3.4b (9 mm long and 4 mm wide) were chosen to represent the scale of the heterogeneities observed in Figure 3.3b.

We have used air to model the gas inclusion, whereas in the experiment freon vapor was present. Since the compressibilities of gases are comparable and about four orders of magnitude larger than those of liquids, the effect of this approximation is minimal. We observed that vapor bubbles of the size of 1

Table 3.3: Material properties used for the different computations

Sample	bulk P-velocity (m/s)	bulk modulus (MPa)
Sand fully saturated with water	1830	6554
Sand with residual saturation of n-dodecane/water (80%)	1572	2567
Sand with residual saturation of iso-octane/water (80%)	1588	2361
Sand saturated with freon	1080	2557
Sand saturated with air	663	675

to 3 mm can evolve in a freon-saturated sand when the temperature increases a few degrees. Hence, the gas inclusion was modelled as a square of dry sand with a diameter of 2 mm in an otherwise fully freon saturated sample (Figure 3.4c).

The bulk velocity and bulk density of the liquid saturated sand used for our computations were measured in the laboratory and are listed in Table 3.3. A line of nine sources at the upper boundary and a line of 33 receivers at the bottom of the model produced the synthetic data. The source time function used in the numerical simulations was a symmetric, three-lobe wavelet with a center frequency of 0.5 MHz, which is based on the characteristic frequency of the transducers used for the laboratory measurements.

Figure 3.5 illustrates the traces observed at the 33 receivers for the three models shown in Figures 3.4. As the wave progresses through the sample, it experiences scattering caused by the fluid interfacial heterogeneities. Figures 3.6

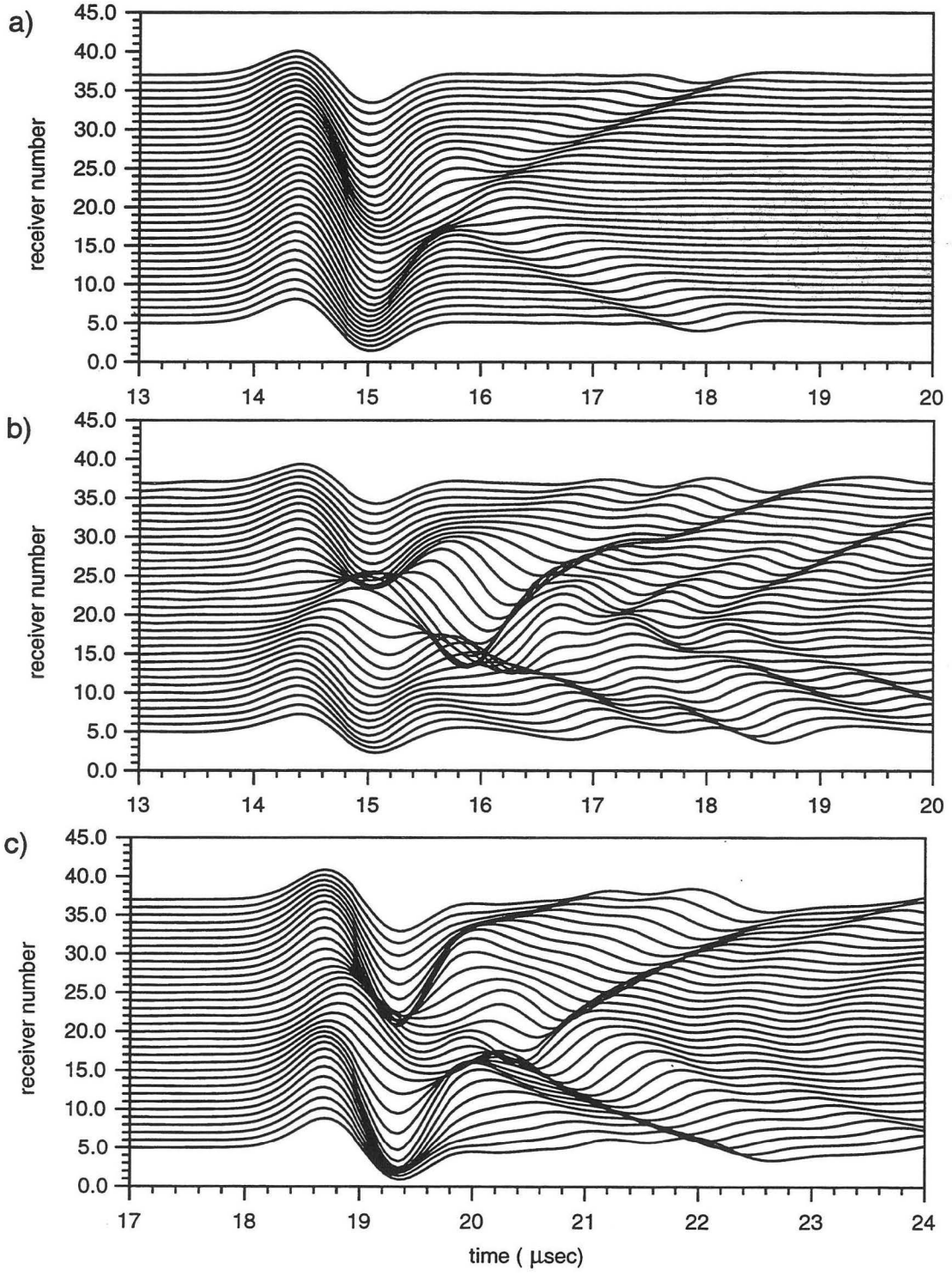

Figure 3.5: Synthetic waveforms for the three models with a) a flat interface with water and n-dodecane, b) a fingered interface with water and iso-octane and c) a gas inclusion surrounded by liquid freon.

Table 3.3: Material properties used for the different computations

Sample	bulk P-velocity (m/s)	bulk modulus (MPa)
Sand fully saturated with water	1830	6554
Sand with residual saturation of n-dodecane/water (80%)	1572	2567
Sand with residual saturation of iso-octane/water (80%)	1588	2361
Sand saturated with freon	1080	2557
Sand saturated with air	663	675

to 3 mm can evolve in a freon-saturated sand when the temperature increases a few degrees. Hence, the gas inclusion was modelled as a square of dry sand with a diameter of 2 mm in an otherwise fully freon saturated sample (Figure 3.4c).

The bulk velocity and bulk density of the liquid saturated sand used for our computations were measured in the laboratory and are listed in Table 3.3. A line of nine sources at the upper boundary and a line of 33 receivers at the bottom of the model produced the synthetic data. The source time function used in the numerical simulations was a symmetric, three-lobe wavelet with a center frequency of 0.5 MHz, which is based on the characteristic frequency of the transducers used for the laboratory measurements.

Figure 3.5 illustrates the traces observed at the 33 receivers for the three models shown in Figures 3.4. As the wave progresses through the sample, it experiences scattering caused by the fluid interfacial heterogeneities. Figures 3.6

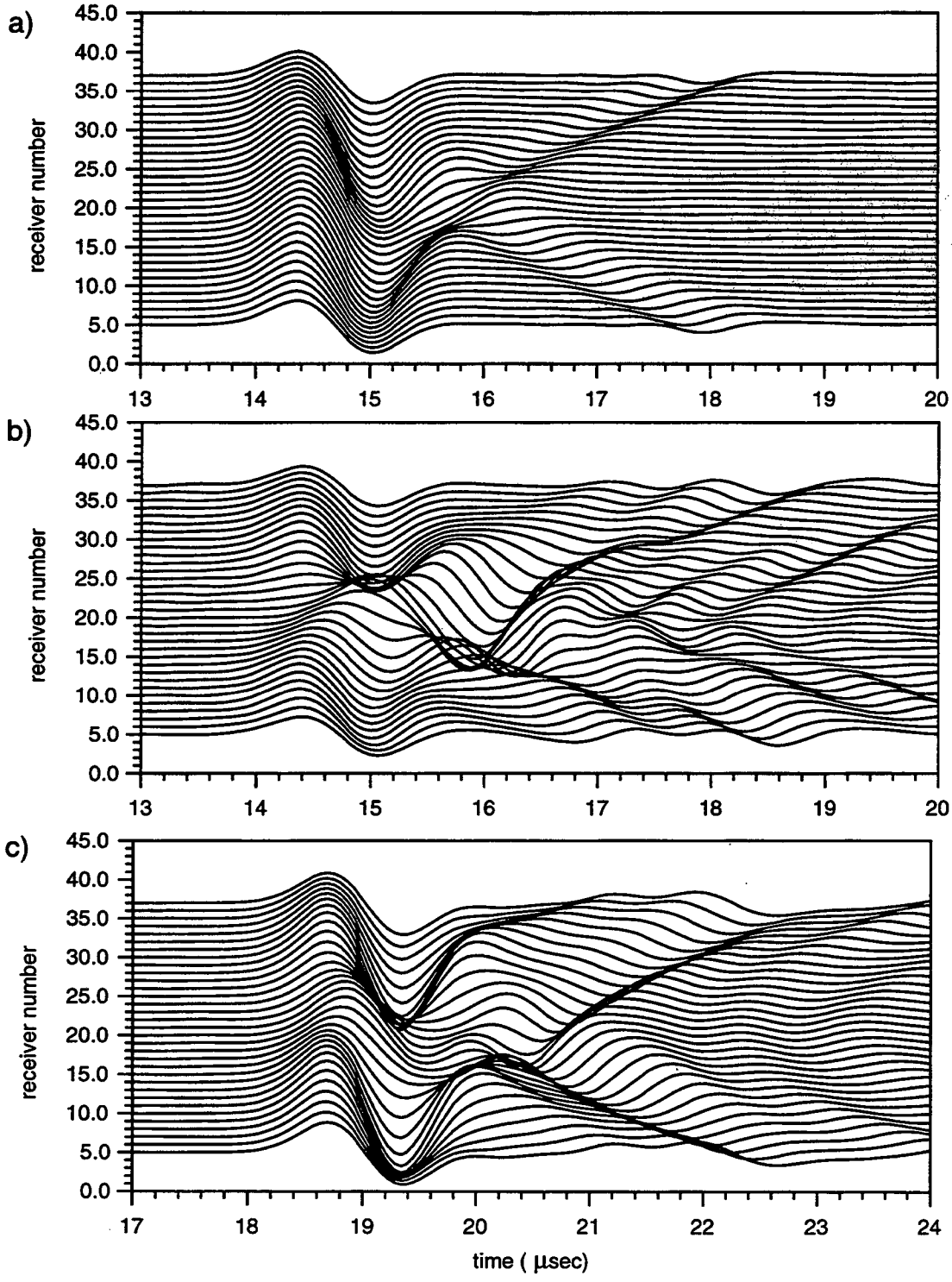

Figure 3.5: Synthetic waveforms for the three models with a) a flat interface with water and n-dodecane, b) a fingered interface with water and iso-octane and c) a gas inclusion surrounded by liquid freon.

and 3.7 show the wave field in a sand sample at different times for the irregular distribution of iso-octane in water (Figures 3.4b) and for an air inclusion surrounded by liquid freon (Figures 3.4c), respectively. The animation shows how the wavefront starts out as a plane wave and experiences considerable distortion when interacting with the inhomogeneities. This leads to an irregular wavefront at the receivers.

The piezoelectric elements used in the laboratory to transmit and receive the seismic signals are approximately 20 mm in diameter. Hence, the measured signal represents the mean seismic waveform over this distance. To simulate the averaging of the piezoelectric crystals, we stack the 33 traces which extend over a total lateral distance of 16 mm. Figure 3.8 shows the stacked traces at the receivers for the different models shown in Figure 3.4. To allow an easier comparison of the amplitudes, the traces of the model with a finger and with a gas inclusion have been shifted to match the arrival time of the model with the flat interface. Relative to the flat interface, fingering and gas inclusions lead to smaller amplitudes. This result is in general agreement with the laboratory observations. The normalized amplitude at the points where the residual water saturation is reached (Figure 3.1) is largest for n-dodecane at approximately 0.6, followed by freon with a value of about 0.3, and iso-octane at approximately 0.15. The synthetic waveforms in Figure 3.5 also help explain why a heterogeneous fluid distribution has a greater effect on estimates of attenuation than upon es-

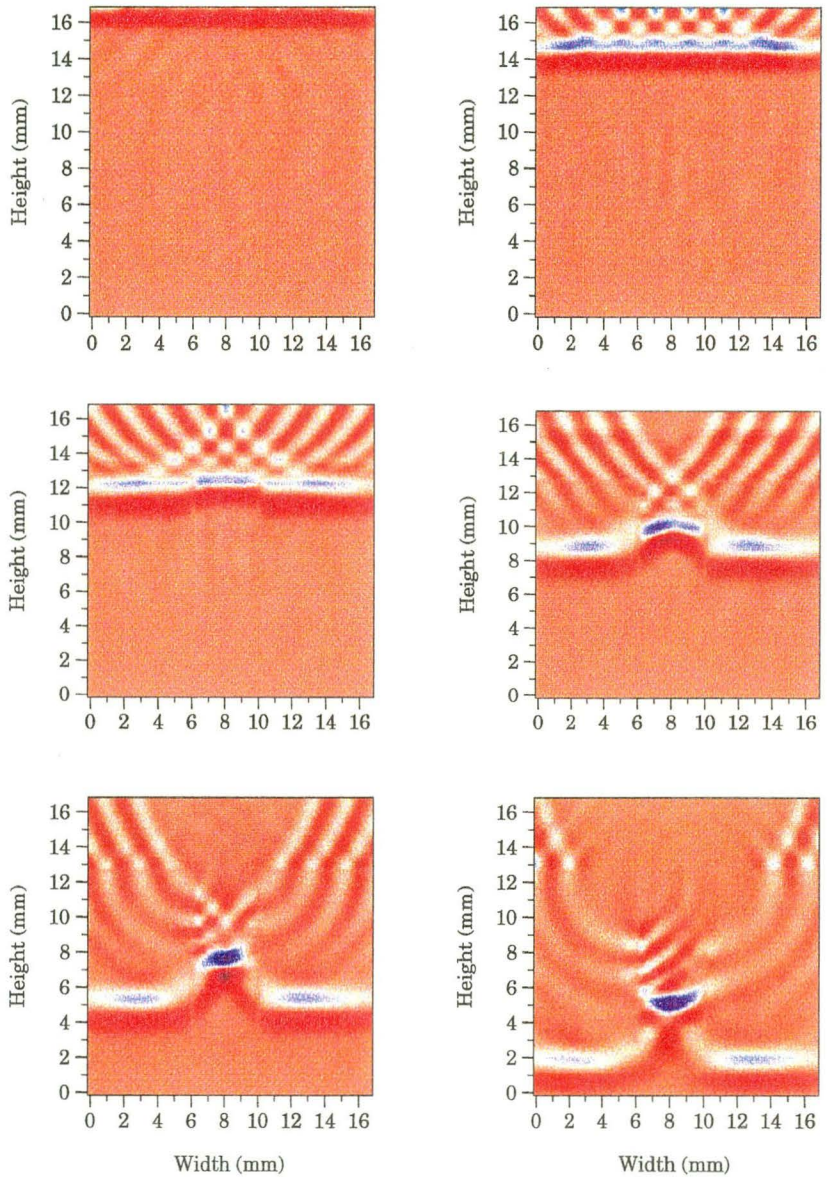

Figure 3.6: Sequence showing scattering of a wave propagating though a sand saturated with water and iso-octane with a NAPL-water finger in pure water. Time increases in the panels as they progress from upper left to lower right. (Red represent positive amplitudes and blue negative amplitudes in the wave front.)

timates of velocity. After averaging these waveforms to simulate the effect of the finite dimension of the receiver, it is clear that the first arrival time will be only slightly affected by the distortions in waveform caused by the heterogeneities. However, as shown in Figure 3.8 the effect upon the peak amplitude of the first arrival can be significant.

3.3.2 Dependence of attenuation on pore scale fluid distribution for identical pore-fluids

In order to allow a meaningful comparison between observations and calculations, consideration must be given to the fact that the models in Figure 3.4 and results in Figures 3.5 and 3.8 involve different pore-fluids for the three different models. Thus in these models the attenuation is not only caused by the irregular fluid distribution but is also partly caused by the different reflection coefficients of water-n-dodecane, water-iso-octane and freon-air. A direct comparison is therefore not possible without taking two attenuation mechanisms into account: the different reflection coefficient of the liquid pairs as well as the distribution of the pore filling fluids. To obtain the attenuation effect of the phase distribution only, we have to compare different spatial distributions for identical pore-fluid pairs.

In comparison to a stable NAPL-water front, a heterogeneous fluid distribution causes additional scattering and therefore further attenuation. As discussed

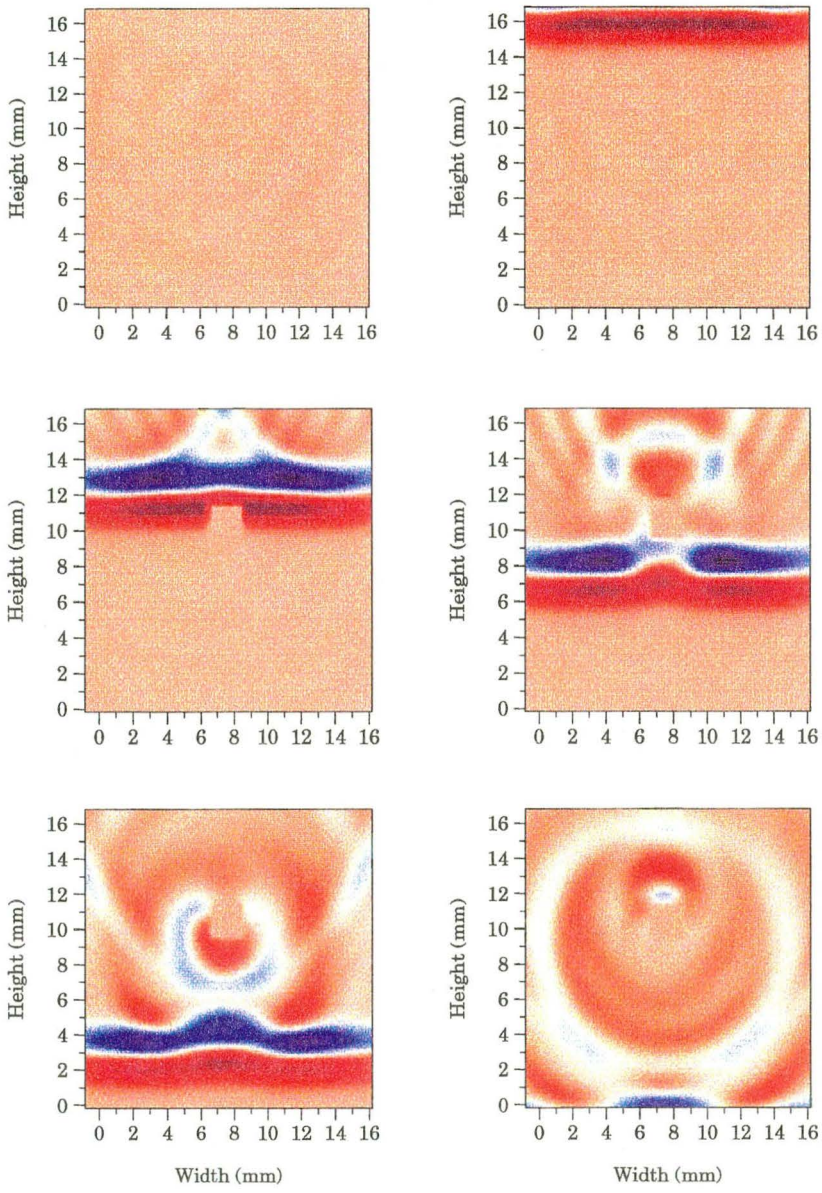

Figure 3.7: Similar to Figure 3.6 for the case of a wave propagating though a saturated sand with an air inclusion.

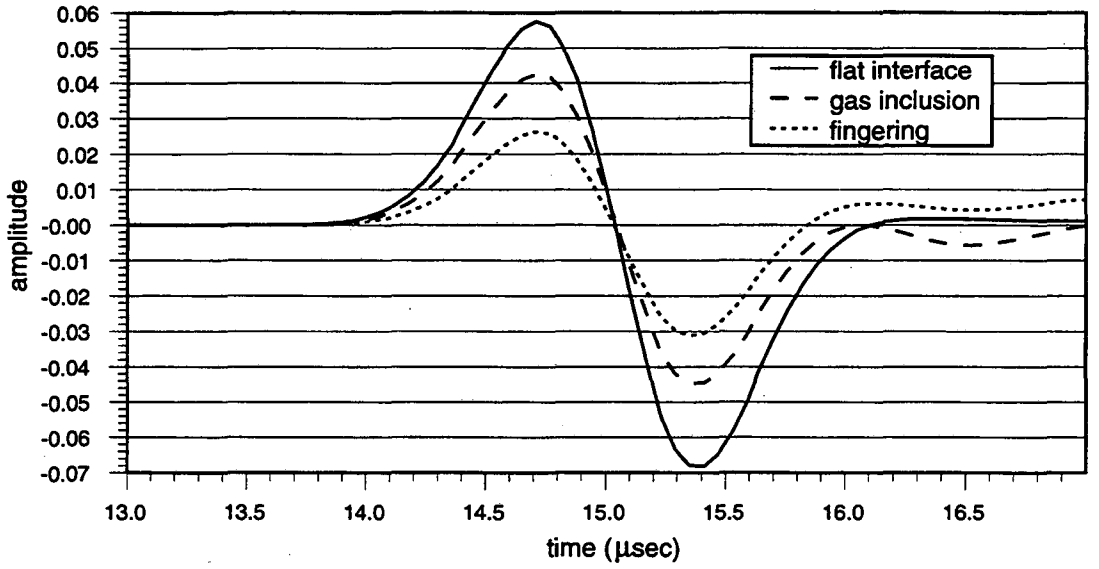

Figure 3.8: Average simulated waveforms for the three models shown in Figure 3.4. The 33 synthetic traces shown in Figure 3.5 for each model were stacked to obtain these waveforms. To allow for an easier comparison between the different models, the arrival times have been normalized, relative to the flat interface.

before, fingering most likely occurs for iso-octane displacing water due to a viscous instability. To focus only on the attenuation mechanism caused by the fluid heterogeneities, we compare the previous calculation of a finger of iso-octane in an otherwise water-saturated sand with the results obtained for a flat interface of water and iso-octane. The change in amplitude caused by the presence of a finger can be seen in Figure 3.9a, where the solid line represents the flat interface and the dotted line the uneven interface. The reduction in amplitude is 40% and is caused by the fluid distribution only. We also calculated the amplitude in a freon-saturated sand with and without an enclosed air bubble. The single gas inclusion results in an amplitude change of approximately 15% (Figure 3.9b). The result suggest that a very small amount of gas in an unconsolidated media,

significantly attenuates the elastic wave. The change in amplitude of approximately 40% for fingering and 15% for a gas inclusion are comparable to the differences between the measured and the synthetic data computed from a one-dimensional model in Figure 3.1b and c. In real media, it is most likely that multiple fingers and gas inclusions develop, which would further enhance attenuation resulting from scattering.

These simulations demonstrate that scattering from inhomogeneous pore-fluid distributions or from gas inclusions are important attenuation mechanisms for immiscible liquids in porous media. Attenuation effects are therefore dependent on the properties of the pore-fluids as well as their distributions.

3.4 Conclusion

This study shows that the amplitude of P-waves propagating through saturated sands is a function of NAPL fraction as well as its distribution. Because spatial resolution is limited to the size of the receiver, the resolution of heterogeneities smaller than the piezoelectric crystal is not possible, but the difference between the measured and the modeled data suggests that the fluid is not propagating through the sample as a stable NAPL-water front. Thus the measurement of both velocity and amplitude and comparison with model calculations may serve as a diagnostic tool for heterogeneous fluid distribution. If the velocity data fit the one-dimensional model but the amplitudes deviate from

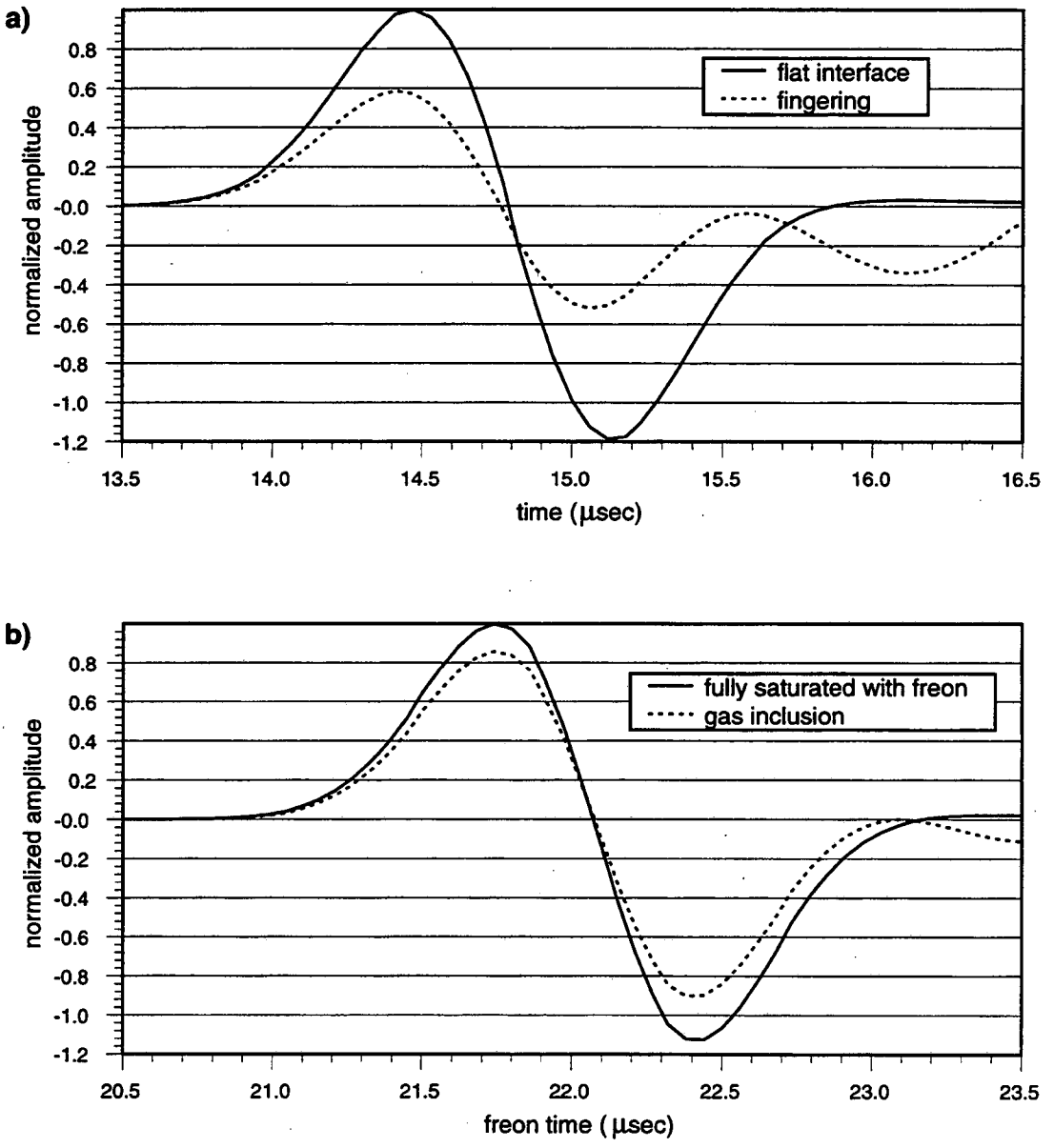

Figure 3.9: The normalized stacked amplitude of a wave propagating through a sandpack a) fully saturated with iso-octane and water. The solid line represents a flat and the dotted line a fingering interface between the two fluids. b) Similar results for a sandpack fully saturated with freon except for a single gas inclusion.

the data with increasing NAPL saturation, this may indicate that fingering or gas inclusions are present. In the real world inhomogeneous fluid distribution is most likely the norm, therefore ultrasonic attenuation measurements which are sensitive to the NAPL distribution, could be potential tool to delineate contaminants.

Chapter 4

Effects of Viscous Pore Fluids on Ultrasonic Waves in Unconsolidated Sand

4.1 Abstract

Ultrasonic attenuation measurements in unconsolidated sand with pore fluids of different viscosities were compared with three theoretical models. The comparison allows an evaluation of the main loss mechanisms, caused by the different pore fluids ranging in viscosity from 0.001 to 1 Pa/sec. In the laboratory, P-wave measurements were taken through sand samples saturated with water, castor oil and two different silicone oils. The attenuation shows a frequency squared dependence for all measurements regardless of viscosity. The results show that for unconsolidated sand the Local Flow Model (LFM) and the unified Biot and Squirt model (BISQ), which imply significant effects of the viscous pore fluids on ultrasonic waves, cannot explain the laboratory measure-

ments. The main attenuation effect observed in the laboratory can be simulated with a three-dimensional generalized Dynamic Composite Elastic Medium model (DYCEM), which includes scattering from the pores and grains as well as intrinsic attenuation caused by the viscous pore fluids. For the studied sand samples, scattering is the main attenuation effect for ultrasonic P-waves.

4.2 Introduction

The change of wave attenuation from dry to fluid-saturated rocks shows that the fluid content is crucial to understanding the loss mechanisms (e.g.,Vo-Thanh, 1991; Winkler and Murphy III, 1995; Murphy et al., 1986). Hence, the dependence of attenuation on material properties of different fluids and their interaction with the matrix have been the topic of various studies (Biot, 1956a; Biot, 1956b; Burridge and Keller, 1981; Mavko, 1979; Murphy et al., 1986; Gist, 1997).

In this study we focus on the importance of pore fluids in determining attenuation at ultrasonic frequencies by comparing experimental laboratory data with different theories. Three different attenuation mechanisms were examined to predict compressional wave attenuation in a quartz sand saturated with fluids of different viscosities. The first theory is the Local Flow Model (LFM) by O'Connell and Budiansky (1977), which is based on local flow losses due to fluid movement between pores and cracks and within cracks. The second model

by Dvorkin and Nur (1993) combines Biot's theory and squirt flow (BISQ). The third theory examined is the three-dimensional dynamic composite elastic medium theory by Kaelin and Johnson (1998), which combines the scattering attenuation of pores and grains and the intrinsic attenuation of the viscous fluids.

4.3 Experimental Procedure and Results

We have measured the P-wave attenuation of ultrasonic waves through an unconsolidated quartz sand in order to calculate the effect of different fluid viscosities. For the laboratory measurements, a sub-rounded quartz sand[1] sieved between 60 and 70 mesh (212 μm and 250 μm openings, respectively) was chosen.

The different pore fluids were water, two different silicone oils and castor oil, which had a three-decade variation in viscosity ranging from 0.001 to 1 Pa/s (Table 4.1). To saturate the specimens, the fluids were poured onto the transducer, which was jacketed by a flexible sleeve. A vacuum was applied to the fluids so that no air was retained. Then, the washed and dried sand was carefully poured into the fluid to avoid traped air in the sample. The specimens were packed to a porosity of about 35%. The sand samples were cylindrical with a diameter of 50.5 mm and an average length of 36.5 mm. During the measurements an axial pressure of 0.69 MPa was maintained. We used the

[1]Silica 60, Pyrominerals, Oakland, California, U.S.A.

and Toksöz, 1974). The obtained phase velocities in the low frequency limit for different samples are listed in Table 4.2.

At low frequencies, the attenuation shows a frequency squared dependence, regardless of the pore filling fluids (Figure 4.1b). At higher frequencies, the signals are highly attenuated, and we found that the signal-to-noise ratio becomes too small for reliable amplitude measurements if the amplitudes are smaller than about 5% of the reference signal. With an average sample length of 36.5 mm, the measured attenuations are therefore significant only if $\alpha < 0.08\ mm^{-1}$ (Figure 4.1b).

4.4 Evaluation of different theories of attenuation caused by pore fluids

4.4.1 Local Flow Model (LFM)

O'Connell and Budiansky (1977) identified two different mechanisms which cause attenuation of seismic waves in fluid saturated porous media. The first mechanism is the relaxation of shear stresses in individual cracks and becomes important only for frequencies greater than about 10 MHz. The critical angular frequency is

$$\omega_1 = \frac{\mu}{\eta}\frac{c}{a}, \tag{4.7}$$

where μ is the shear modulus of the matrix, η is the fluid viscosity and (c/a) is the aspect ratio of the cracks. Between 10 and 1000 kHz, the dominant

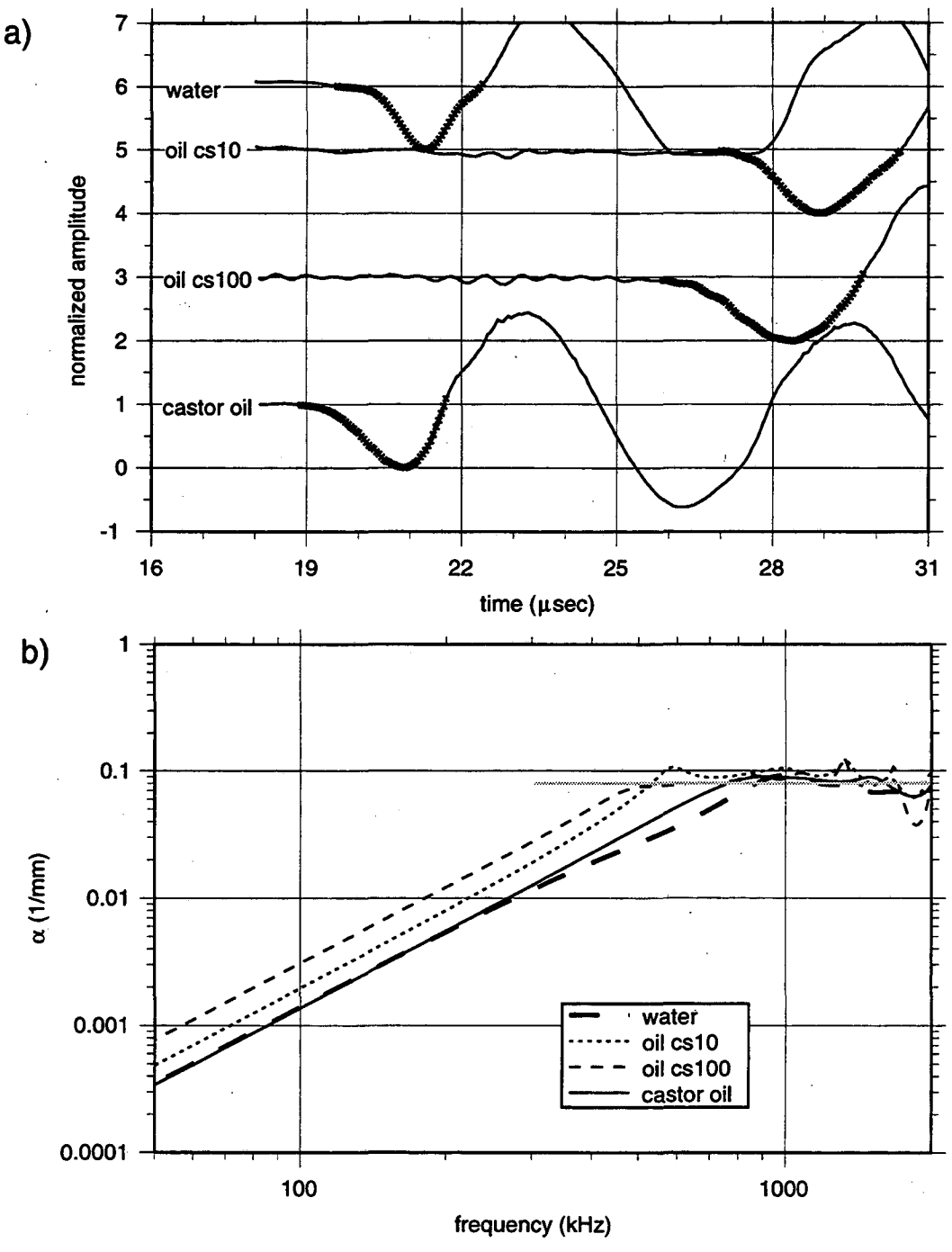

Figure 4.1: a) shows the measured P-wave traces for sand samples saturated with the pore fluids water, cs10, cs100 and castor oil. The time windows used to calculate the frequency dependent attenuation in b) have been marked. Attenuation are significant only if $\alpha < 0.08$ mm^{-1}, which is shown as a grey line.

dissipation mechanism is caused by fluid flow between cracks. In this case, the maximum attenuation occurs at

$$\omega_2 = \frac{K}{\eta}\left(\frac{c}{a}\right)^3, \tag{4.8}$$

where K is the bulk modulus of the matrix. O'Connell and Budiansky (1977) have shown that their model is applicable for solids containing fluid phases distributed as thin films and that the Local Flow Model (LFM) is applicable to laboratory data for water saturated rocks.

We calculated the frequency dependent attenuation by applying the LFM with the bulk and shear modulus of quartz (37.9 GPa and 44.3 GPa), respectively, Carmichael (1989), and the viscosity for the different fluids (Table 4.1). The only two unknowns are the aspect ratio and the crack density ϵ,

$$\epsilon = \frac{2N}{\pi}\frac{A^2}{P}, \tag{4.9}$$

where A is the area, P the perimeter and N the number of cracks per unit volume. We have varied the aspect ratio and the crack density to obtain the best fit to the measured water-saturated sample. With $\epsilon = 0.33$ and $c/a = 0.01$, the LFM fits the attenuation of the water-saturated sample very well (Figure 4.2a). Figure 4.2b, 4.2c and 4.2d show the P-wave attenuation as a function of frequency for the pore fluids silicone oil cs10, cs100 and castor oil, respectively. Each fluid has a viscosity ten times larger than the previous one. Equation (4.7) shows that the critical frequency is inversely proportional to the fluid viscosity.

Hence, the critical frequency is shifted by three orders of magnitude from water to castor oil. This feature is not observed in the measurements and, therefore, the misfit between measurements and LFM becomes large for the more viscous fluids.

4.4.2 Biot's theory and squirt flow (BISQ)

Dvorkin and Nur (1993) presented an unified dynamic poroelasticity model for the propagation of P-waves in poroelastic solids containing compressible viscous fluids. Their model takes into account two mechanisms of fluid-solid interaction:

1. The Biot mechanism, where the fluid is forced to participate in the solid's motion by viscous friction and inertial coupling.

2. The squirt mechanism, where the fluid is squeezed out of thin pores or cracks due to the solid's compressibility.

To compute the attenuation with the BISQ model, we have used the same fluid and solid properties as for the LFM model. The additional parameters needed are 35% porosity, $9.5 \cdot 10^{-12} m^2$ permeability and 0.25 Poisson's ratio of the water saturated sample, which were all obtained from laboratory measurements. The characteristic squirt flow length was set to 0.25 mm and the additional coupling density is zero, according to Berryman's (1980a) formula.

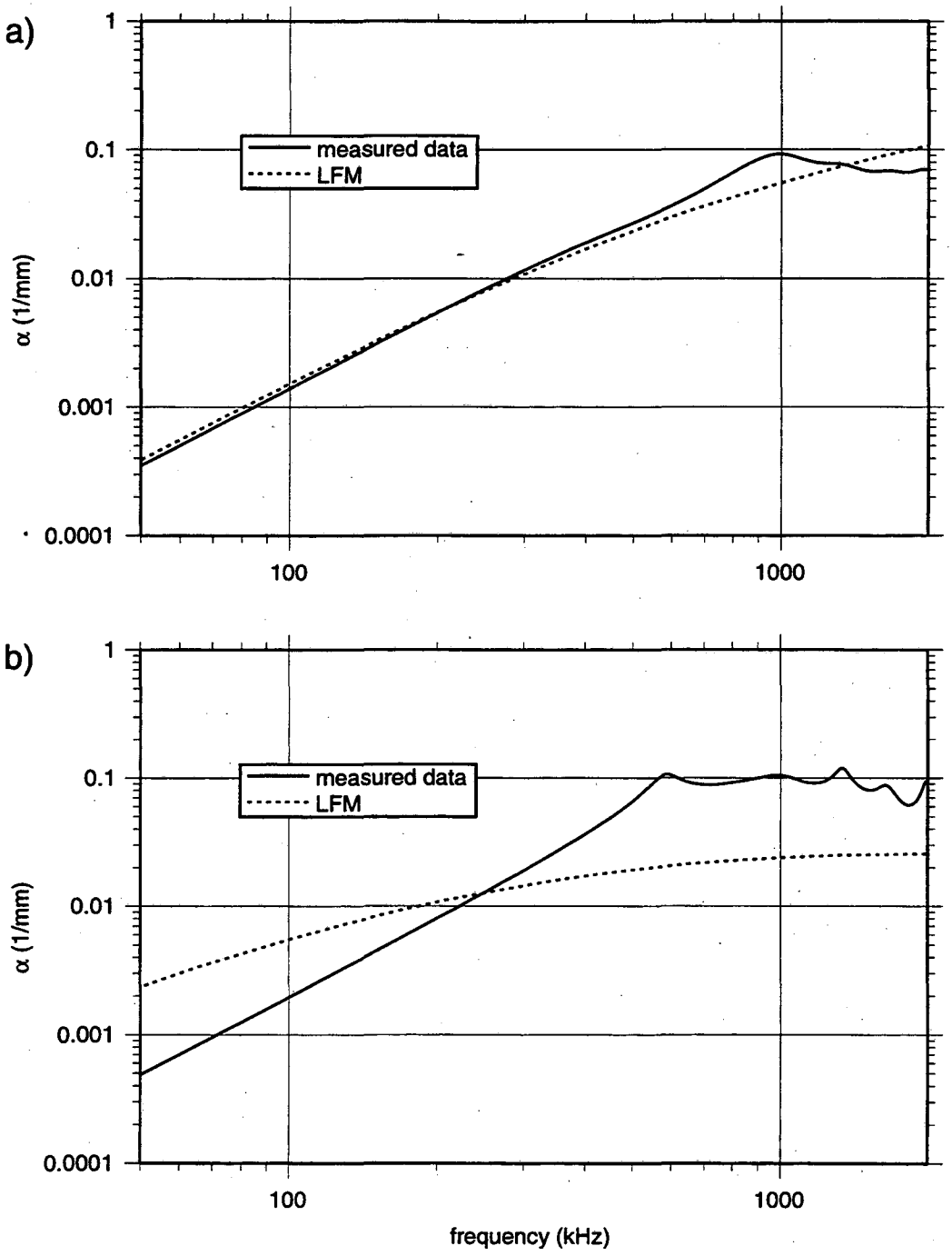

Figure 4.2: Frequency dependent attenuation for measured and synthetic data for a) water and b) 10cs silicone oil. For calculating attenuation with the Local Flow Model (LFM) by O'Connell and Budiansky (1997), we have used an aspect ratio 0.01 and a crack density of 0.35.

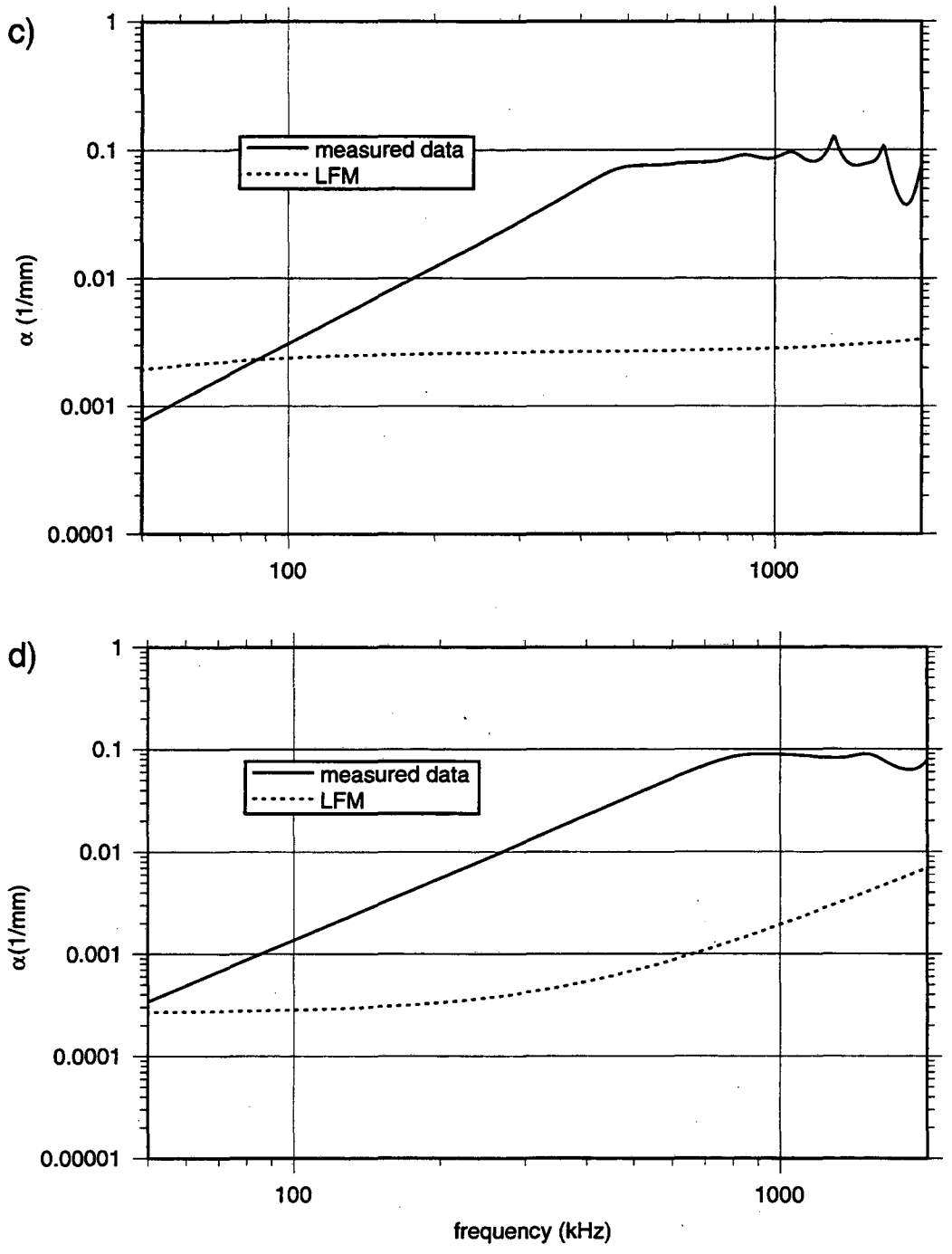

Figure 4.2: Attenuation as a function of frequency for measured and synthetic data for c) 100cs silicone oil and d) castor oil. For calculating the attenuation with the Local Flow Model (LFM) by O'Connell and Budiansky (1997), we have used an aspect ratio 0.01 and a crack density of 0.35.

Figure 4.3a shows the attenuation calculated with the BISQ model and the parameters above. Comparing the measurements in Figure 4.3b with the synthetic results in Figure 4.3a, we find that the measured attenuation is about one order of magnitude smaller than predicted by the BISQ model. Furthermore, the BISQ model shows the frequency squared dependance only for the case of the silicone oil cs100. Similar to the LFM, the BISQ model predicts a much stronger dependence on fluid viscosity, than is not observed in the measurements.

4.4.3 Dynamic composite elastic medium theory

The dynamic composite elastic medium theory includes multiple forward scattering from spherical pores and grains as well as intrinsic attenuation of viscous fluids (Kaelin and Johnson, 1998). The elastic P-waves and S-waves experience multiple scattering from grains and pores. Depending on the ratio of wavelength to grain size, different scattering regimes can be observed. Hence, it is important to know grain size and pore size distributions. Before the waveforms for the different samples can be calculated, we have to first determine the P-velocities and S-velocities of the matrix. In unconsolidated porous media, the velocities of elastic waves are generally smaller than those of the single crystals (e.g.,Gassmann, 1951; White, 1965). It has been generally accepted that this effect is caused by cracks within the grains and grain contacts.

In the low frequency limit, the dynamic composite elastic medium theory is

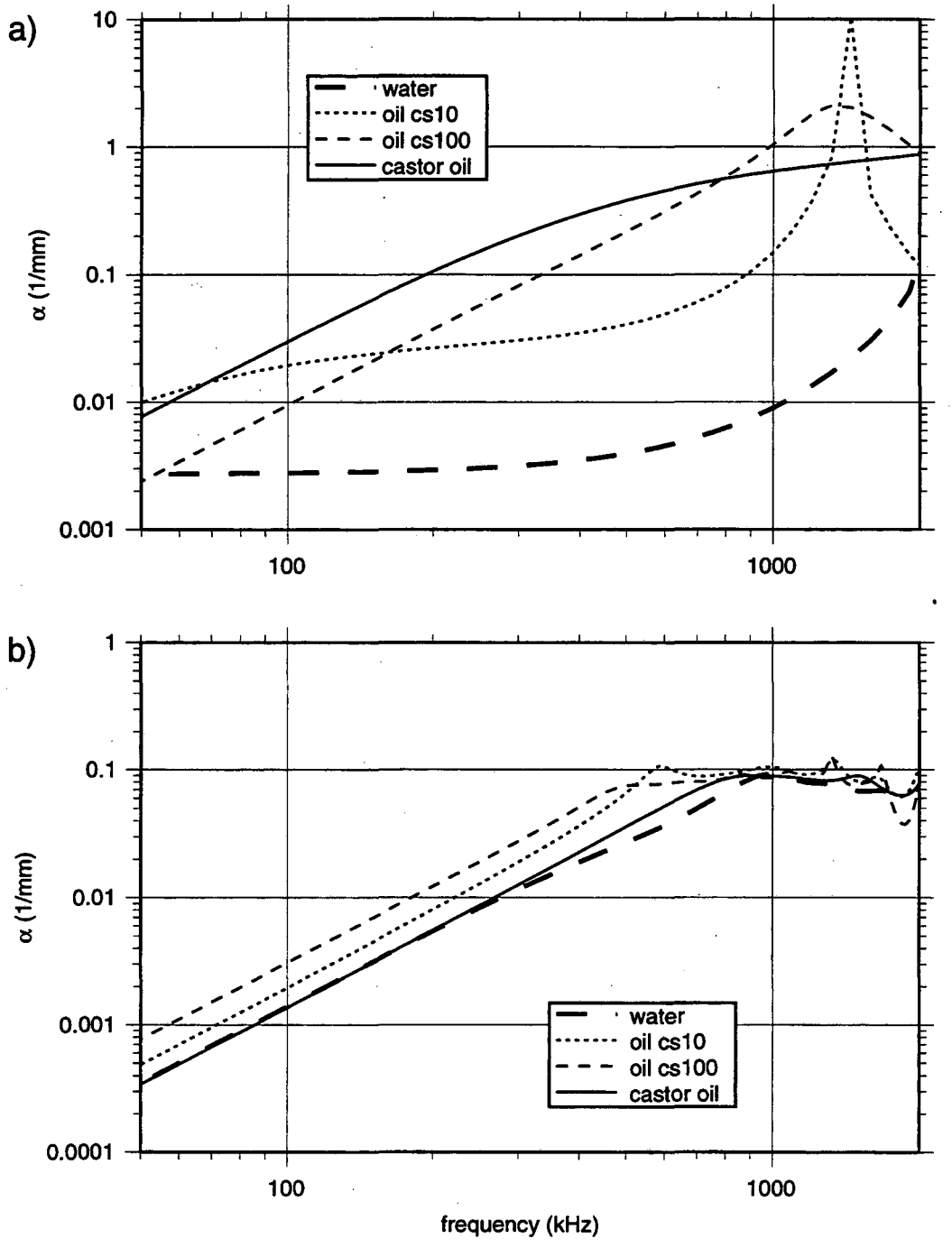

Figure 4.3: Frequency dependent attenuation for for a) synthetic data and b) measured data for different fluid viscosities. The synthetic data have been calculated with Biot's theory and the squirt flow model (BISQ) (Dvorkin and Nur, 1993) for the different pore fluids.

equivalent to Berryman's theory (Berryman, 1980b). Thus, with the porosities and phase velocities in Table 4.2 and the fluid properties in Table 4.1, the P- and S-velocities of the matrix can be calculated after Berryman (Berryman, 1980b).

$$\begin{aligned} K_{Ma} &= (1-\phi)\left[\frac{1}{K+4\mu/3}-\frac{\phi}{K_f+4\mu/3}\right]^{-1}-4\mu/3 \\ \mu_{Ma} &= (1-\phi)\left[\frac{1}{\mu+F}-\frac{\phi}{F}\right]^{-1}-F \\ F &= \frac{\mu}{6}\,\frac{9K+8\mu}{K+2\mu} \\ \rho &= (1-\phi)\rho_{Ma}+\phi\rho_f \\ \mu &= \rho v_s^2 \\ K &= \rho v_p^2-4\mu/3 \end{aligned} \tag{4.10}$$

where K_f is the bulk modulus and ρ_f the density of the fluid. K_{Ma}, μ_{Ma}, ρ_{Ma} and K, μ, ρ are the bulk modulus, shear modulus and density of the matrix and the saturated sample, respectively. The calculated matrix velocities in Table 4.3 vary significantly for the different samples, even though we have used the same quartz sand. We suspect that differences in the physical fluid properties have caused changes in the elastic matrix properties.

Table 4.3 also shows that the variation correlates strongly with the adhesion tension between the different fluids and the quartz grains. Adhesion tension was calculated for the different fluids from the measured surface tension and the capillary rise in a glass tube of 1 mm diameter. We suspect that during the sample preparation fluids remain as thin films between the quartz grains and

Table 4.2: Saturated sand: sample length, porosity and measured low frequency P- and S-wave velocities of the different samples. All samples were 50.5 mm in diameter.

Saturated Sand	length (mm)	porosity (%)	v_P (m/s)	v_S (m/s)
water	37.0	36	1810	1029
cs10 oil	36.5	35	1289	742
cs100 oil	36.5	35	1326	725
castor oil	35.5	34	1747	1012

fluids with high adhesion tension provide better contact between the grains. However, a detailed study of the adhesion tension effect on the ultrasonic waves is beyond the scope of this study.

The pore size distribution was determined from a fully water-saturated sand sample by progressively desaturating it by increasing the capillary pressure. By using the capillary bundle model (Childs and Collis-George, 1950), we can relate the pore radius to the cummulative relative frequency (Figure 4.4). Since the capillary bundle model is an idealization of the pore geometry represented by a collection of capillary tubes of different radii, we have used the obtained pore size distribution only and left the mean pore radius as an adjustable parameter. We found that the sum of two log-normal distributions can explain the measured pore size distribution reasonably well (Figure 4.5). Both log-normal distributions had a mean of 26.3 μm and standard deviations of 2.63 μm and 38.2 μm, respectively. The weight of the distributions was 47% and 53%. The grain size was determined from the sieve openings between 212 μm and 250 μm,

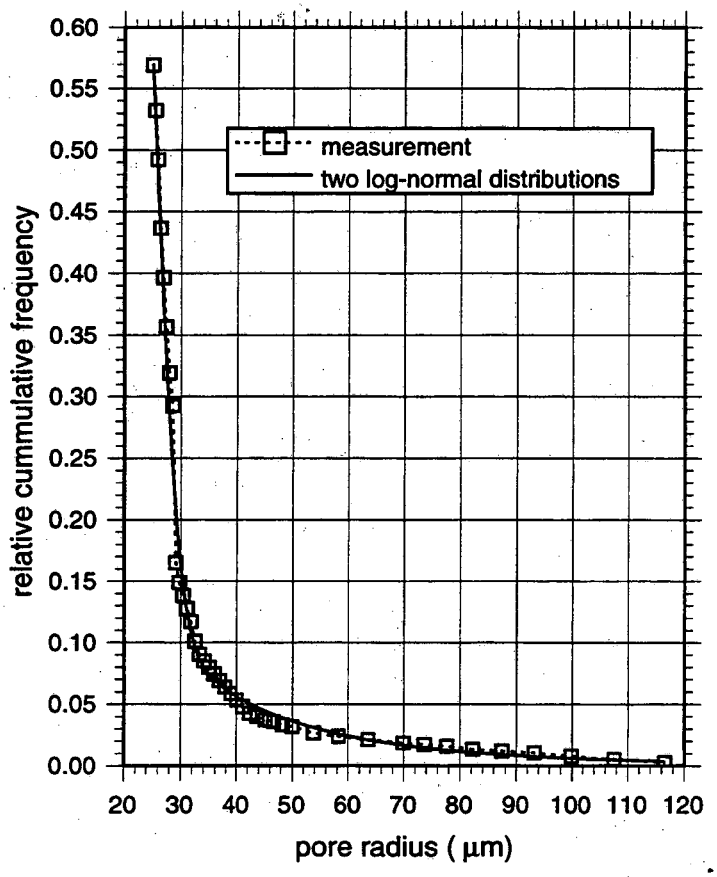

Figure 4.4: Pore size distribution from capillary pressure measurements on the primary drainage curve, assuming the pores can be represented by the capillary bundle model. To fit the measurements, we have used two log-normal distributions with a mean pore radius of 26.3 μm and standard deviations of 2.63 μm and 38.2 μm, respectively.

which corresponds to 230$\pm$20 μm grain diameter or 115$\pm$10 μm grain radius.

To obtain the mean pore radius of spherical pores, we have computed the frequency dependent attenuation with the dynamic composite elastic medium theory and the material properties in Table 4.1, the matrix velocities in Table 4.3 and the pore size distribution in Figure 4.5. By minimizing the difference between the calculated and the measured attenuation (Figure 4.1b), the mean pore

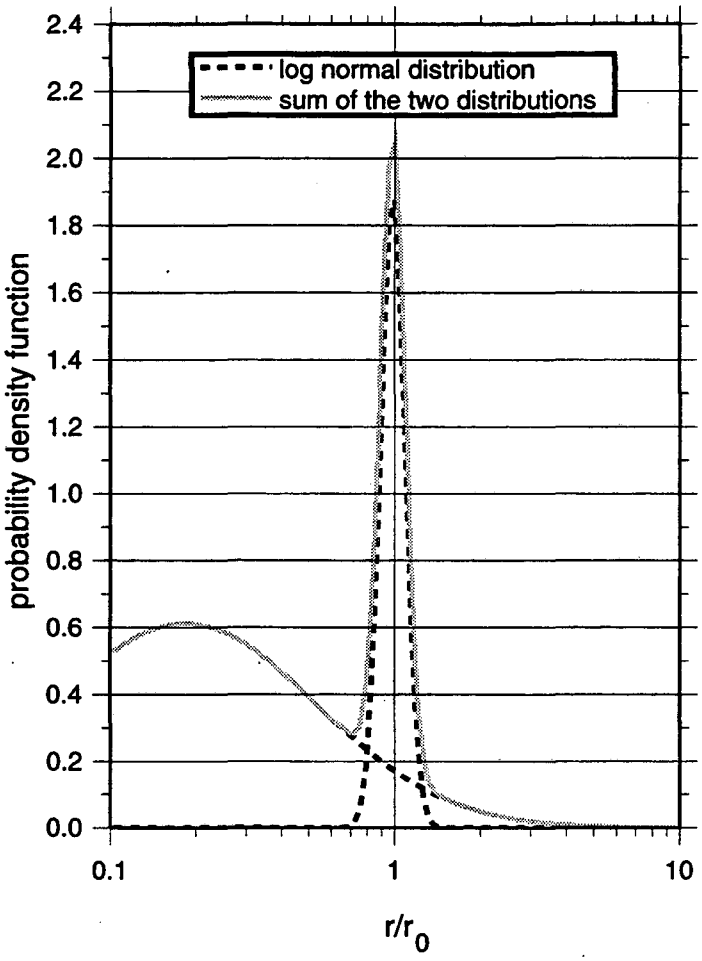

Figure 4.5: Two log-normal distributions representing the measured pore radii distribution (Figure 4.4). The first distribution takes up 47% and the second of 53% of the summed distribution.

radius for each sample was obtained (Table 4.3). Since each sample represents one realization of the grain and pore size distribution only, we have computed the average pore radius and its standard deviation of the four samples, which is $136 \pm 29\ \mu m$.

For comparison of the synthetic data and the laboratory measurements we convolved the obtained Green's functions with the reference spectrum. Fig-

Table 4.3: Calculated P- and S-wave velocities of the matrix after Berryman (1980), for different samples. The adhesion tension between pore fluids and quartz grains has been calculated with the measured surface tension and the capillary rise in a glass tube with 1 mm diameter. The mean spherical pore radius has been calculated with the dynamic composite elastic medium theory.

Saturated Sand	Matrix v_P* (m/s)	Matrix v_S* (m/s)	Spherical Pore Radius* (μm)	Surface Tension** (dyne/cm)	Capillary Rise** (mm)	Adhesion Tension* (dyne/cm)
Water	2390	1670	140	70.5	13	33.1
cs10 oil	1720	1180	94	23.1	6	14.5
cs100 oil	1750	1130	155	23.8	6	14.5
Castor oil	2150	1480	155	40.7	13	31

* calculated properties, ** measured properties

ure 4.6a shows the calculated and Figure 4.6b the measured P-waves which propagated through sand samples saturated with fluids of different viscosity. The amplitudes have been normalized by the first arrival. The frequency dependent attenuation has been computed with half a cycle of the first arrival, analogous to the measured traces. Figure 4.7 shows the attenuation as a function of frequency for calculated and measured data for a) water, b) 10cs silicone oil, c) 100cs silicone oil and d) castor oil. The mean synthetic attenuation and the limits shown in Figure 4.7 were obtained from the average pore radius of 136 μm and two standard deviations of 58 μm, respectively.

The measurements lie within the limits for all fluids and the attenuation always shows a frequency squared dependence with an insignificant dependence on viscosity. The differences between the different samples are mainly caused

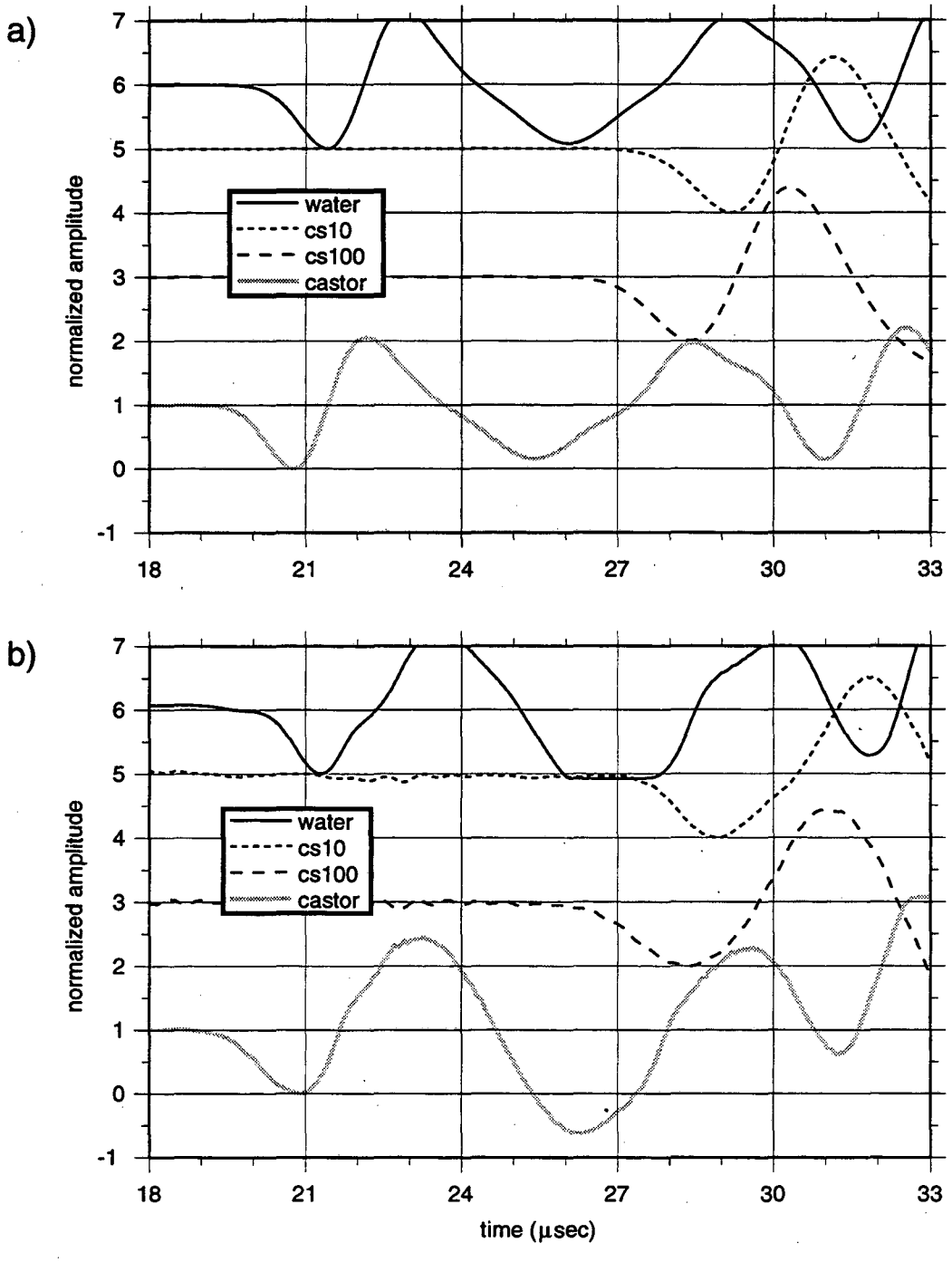

Figure 4.6: a) Synthetic and b) measured ultrasonic waves through a sand sample fully saturated with fluids of different viscosity. The synthetic traces have been calculated with the dynamic composite elastic medium theory.

by weaker or stronger scattering due to the velocity differences between matrix and fluids. Geometric spreading effects due to the velocity differences are much smaller and do not significantly add to the attenuation. Since the dynamic composite elastic medium theory accounts for scattering and viscous intrinsic attenuation, we can conclude that the viscous attenuation is much weaker than the scattering attenuation at the studied ultrasonic frequencies. Hence, the viscosity effect is negligible for unconsolidated sand with grain diameters of 230 μm or larger in the ultrasonic frequency range.

4.5 Conclusions

The P-wave attenuation of an unconsolidated sand with different viscous fluids shows a frequency squared dependence for frequencies between 100 and 1000 kHz. We have examined three different theories to explain the laboratory measurements. The Local Flow Model (LFM) is based on fluid movement between and within cracks. This model can explain the measurements for the water saturated sand well, but fails for fluids with larger viscosities. The combination of Biot's theory and squirt flow (BISQ) fails to adequately simulate the experimental data for all viscous fluids tested. The calculated P-wave attenuation is unrealistically high and only in the case of silicone oil cs100 does the attenuation show the correct frequency dependence. The last theory examined is the dynamic composite elastic medium theory, which is based on scattering

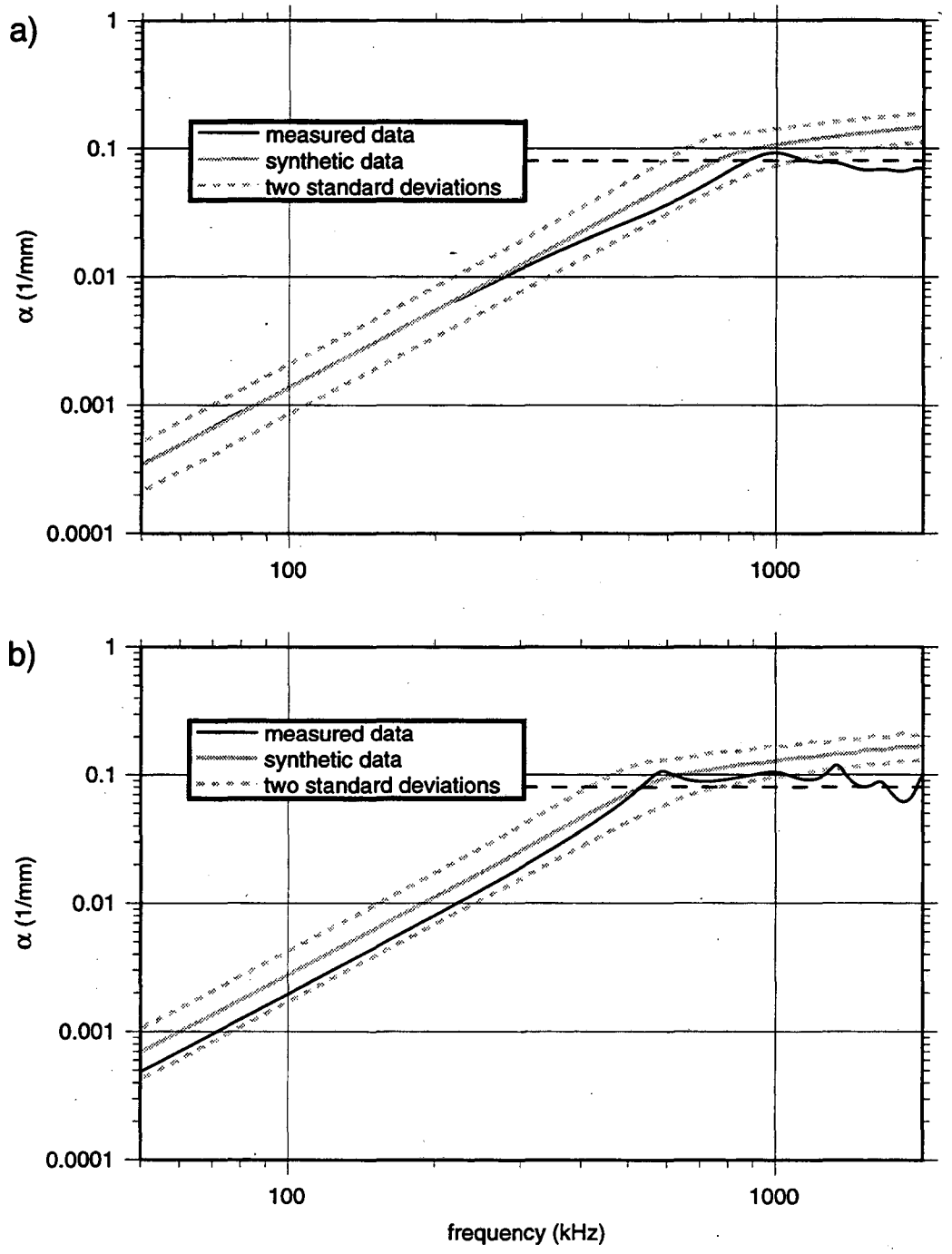

Figure 4.7: Attenuation as a function of frequency for measured data (Figure 4.6b) and synthetic data (Figure 4.6a) for a) water and b) 10cs silicone oil. Significant attenuation values are smaller then 0.08mm^{-1}, marked by the dashed lines.

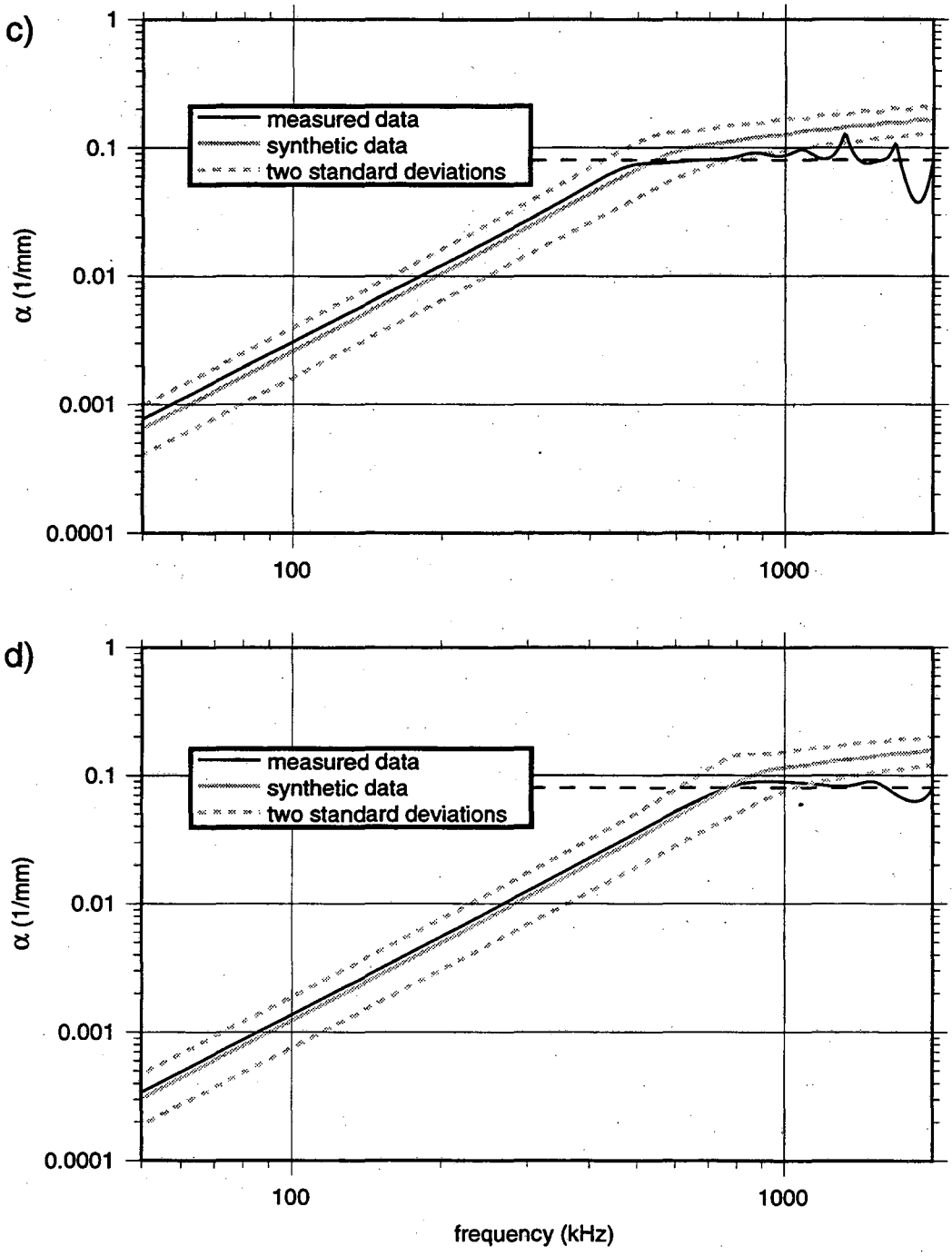

Figure 4.7: Attenuation as a function of frequency for measured and synthetical data for c) 100cs oil and d) castor oil. Significant attenuation values are smaller then 0.08mm^{-1}, marked by the dashed lines.

and intrinsic attenuation. This theory yields the correct frequency dependence and the measurements lie within the uncertainty due to the different sample realizations. After examining the laboratory data and three different physical models, we conclude that for grain diameters larger than 230 μm the P-wave attenuation in the studied ultrasonic frequency range is mainly caused by scattering attenuation. The viscosity of the pore fluid causes only a small amount of attenuation in the examined frequency range. At lower frequencies, scattering attenuation becomes weaker and viscous fluids may become important, which could explain some of the differences observed when comparing laboratory and field measurements.

4.6 Appendix: Measurement of capillary rise and surface tension to calculate adhesion tension

Adhesion tension is the quantity that determines how strongly a liquid will be drawn into spaces of small cross-section in the solid. Adhesion tension A_T can not be measured directly, but can be calculated from the capillary rise h_c and the surface tension σ_{fa}, both of which can be easily measured (Adam, 1941; Feather and Shoenberg, 1949).

$$A_T = \sigma_{fa}\, cos\theta, \tag{4.11}$$

Here f refers to the liquid and a to the air. The contact angle θ is given by

$$\cos\theta = \frac{r\ \rho_f\ g\ h_c}{2\ \sigma_{fa}}, \tag{4.12}$$

where r is the radius of the capillary tube, ρ_f is the density of the fluid and g is standard gravity.

The surface tension is commonly determined by the ring method. A ring made of a combination of platinum and iridium is immersed in the liquid whose surface tension is to be measured. The tension of the wire is increased by pulling the ring upward until the breaking point of the film is reached. The force of the pull exerted on the ring is the apparent surface tension. This value has to be modified with certain correction factors depending upon the density of the fluid, the maximum pull on the ring and the dimensions of the ring. For our measurements (Table 4.3), a DuNouy Tensiometer was used with ring #1 (r=9.5366mm).

Knowing the capillary rise, equation (4.12) allows the calculation of the contact angle. The rise of a liquid in a capillary tube is simply caused by adhesive forces between the water and tube. The height to which the meniscus rises depends upon the radius of the tube and its material. For our measurements (Table 4.3), a clean glass tube of 1 mm diameter was used.

Chapter 5

Wettability Effects on Ultrasonic and Electrical Resistivity Measurements

5.1 Abstract

Ultrasonic P-wave and S-wave as well as electric resistivity measurements were taken in a water-wetting and NAPL-wetting unconsolidated saturated sand. For our laboratory experiments the samples were initally saturated with one liquid, either water or n-dodecane, which was then displaced by the second liquid while measurements were made as a function of the volume of displaced liquid. The value of the residual saturation at the endpoints is mainly a function of the wettability. As expected, in hydrophilic media, lower residual NAPL saturations can be reached than in hydrophobic media. Normalized amplitude and velocity of seismic P-wave measurments show no signficant differences for water-wetting or n-dodecane-wetting sand, which could not be explained within the error of the measurements. But we hypothesized that since a change in

wettability is accompanied by a change in the amplitude of transmitted waves, the intergranular contact is a function of wettability. This idea is also supported by the observation that S-waves can be observed for n-dodecane-wet sand but not for water-wet sand.

Since the electric current prefers to flow within the conductor, which is water, the electric resistivity measurements as a function of NAPL-saturation showed some dependence on wettability. For initally water saturated samples no high resistivity values could be measured in the water-wet sample, since the grains were preferentally water wetting, whereas high resistivity measurements could be measured for the n-dodecane wetting sand. For the case were NAPL was displaced by water, the same behaviour could be observed in the hydrophilic and hydrophopic media; as soon as the water extended over the entire length of the sample the resistivity decreased instantly.

5.2 Introduction

Understanding and being able to measure the wettability of a polluted site is critical for remediation predictions. Wettability describes the tendency of a fluid to spread on a solid surface in the presence of another immiscible fluid. In general natural aquifer sands are water wetting, but they can change their wettability if exposed to certain NAPLs (nonaqueous phase liquid). Therefore a wide range of wetting conditions can be expected following spills of complex NAPL mixtures

to the subsurface (Powers et al., 1997). Since the wettability affects the capillary pressure at which the organic phase is displaced, it will impact the efficiency of many in situ remediation technologies. The more NAPL-wetting a polluted site is, the lower is the potential recovery of NAPL from the subsurface; hence it is critical to know as much as possible about the wettability of a site before its remediation.

To date, seismic wave propagation experiments have been performed only in water-wetting sand or it was assumed that the media was hydrophilic. Given that contaminated sites have mixed wettability, it is of interest if the wettability has an effect on the detection of NAPL by ultrasonic wave propagation.

5.3 Laboratory Experiments

Measurements of P-wave and S-wave transmission and electrical resistivity were made in quartz sand samples fully saturated with varying fractions of water and NAPL. These measurements were made in water-wetting and NAPL-wetting sand to determine if the type of wettability could affect the response. The NAPL used for our experiments was n-dodecane, which is an analog for the common groundwater contaminant, diesel fuel.

5.3.1 Wettability

Water-wet porous media have the potential of altering their wettability when exposed to NAPLs. We obtained hydrophobic media by adding coarse quartz sand to n-dodecane and letting is sit for 2 days, after which the sand was air or oven dried. Even though it was exposed to room temperature for two weeks, the air dried sand never really dried and kept its oily consistency, whereas the sand dried in the oven showed no sign of n-dodecane residue.

Since the wettability is a function of the adhesive forces existing between a fluid and a solid surface, the height (h) to which a fluid rises in a glass capillary tube is a function of its wettability. If the contact angle θ measured between the solid surface (s) and the tangent to the fluid (f) is smaller than 90°, the fluid is called wetting. The contact angle can be related to the interfacial energy between two media (γ) through the equation

$$\gamma_{cs} - \gamma_{fs} = \gamma_{fc} cos(\theta), \tag{5.1}$$

where, (c) stands for a second fluid or gas. The measured height of capillary rise is then given by

$$h = \frac{2\gamma_{fc} cos(\theta)}{\rho g R}, \tag{5.2}$$

where ρ is fluid density, g is acceleration due to gravity and R is the radius of

[1]Granusil #4075, North Kato Supply, Mankato, Minesota, U.S.A.

the capillary tube.

Equation 5.2 implies that the height of the capillary rise will decrease if the conditions change to reduce the wettability of the solid to the imbibed liquid. An easy way to compare the wettability of two porous media with the same pore radius and similar densities (Table 5.1) is therefore to measure their capillary rise. The experimental setup consisted of a plexiglas tube filled with sand and sealed on the bottom by an steel mesh. The bottom of this tube was immersed appoximately 5mm into a reservoir of blue dyed water. The sand sample was elevated from the bottom of the water container on a plastic rack to provide a good contact between the sand and the water. The porous medium was a sub-rounded quartz sand sieved between 18 and 20 mesh (840- and 1000 μm openings, respectively). For each experiment 200 gm of sand were used, and the diameter of the plexiglas tube was 44 mm; therefore hundreds of grains were in direct contact with the water, which allows the assumption that the average pore size for two compared samples was the same.

In a first experiment we compared the wettability of the oven dired and air dried NAPL-wetting sand, by placing the two samples into the same water reservoir (Figure 5.1). No spontaneous imbibition of the aqueous phase into the porous media took place; even after waiting for 4 and 5 days, no change in the water level could be observed. This implies that the wettability is not sensitive to the way the sand was dried.

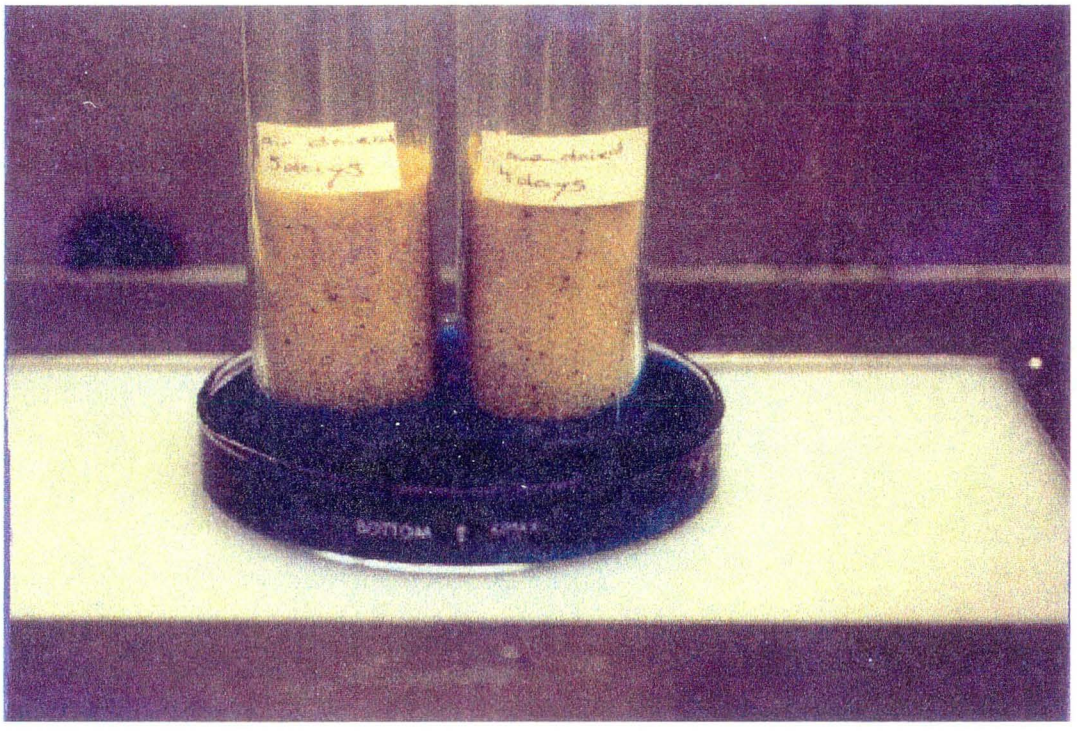

Figure 5.1: Plexiglas tubes filled with sand which were exposed to n-dodecane for a few of days. Sample at the right was air-dried where the sample on the right was oven-dried. Even though the samples were dried in different ways, there was no imbibition of water (dyed blue fluid) in either case.

Table 5.1: Physical and chemical properties of NAPL contaminants

Parameters	Water	n-Dodecane
Density[a)] (kg m^{-3})	997	745
Viscosity[a)] (mPa s)	0.890	1.378
Vapor Pressure[b)] (kPa)	3.17	0.016
Reflection Coefficent[a]	—	0.19
Interfacial Tension[a)]	—	52.8
Dielectric Constant[a)]	78.3	2.014
Solubility in water[a)]	—	0.0037

a) Geller and Myer 1995 b) Lide 1995

In a second experiment we compared the oven dried (Figure 5.2 a) and air dried (Figure 5.2 b) samples with untreated (water-wetting) samples and observed differences in capillary rise. Figure 5.2 shows that water imbibes spontaneously into samples which were not treated with n-dodecane. This method gives us a qualitative means of assessing wettability and proof that we could prepare the sand to be non-water-wetting.

Following our seismic and resistivity measurements, where the NAPL-wet sand was fully water saturated for at least two days, we compared this sand again with water-wetting sand. Figure 5.3 shows that the water preferentially wants to coat the solid surface of the untreated sand and that n-dodecane-wetting sand did not change its wettability.

a)

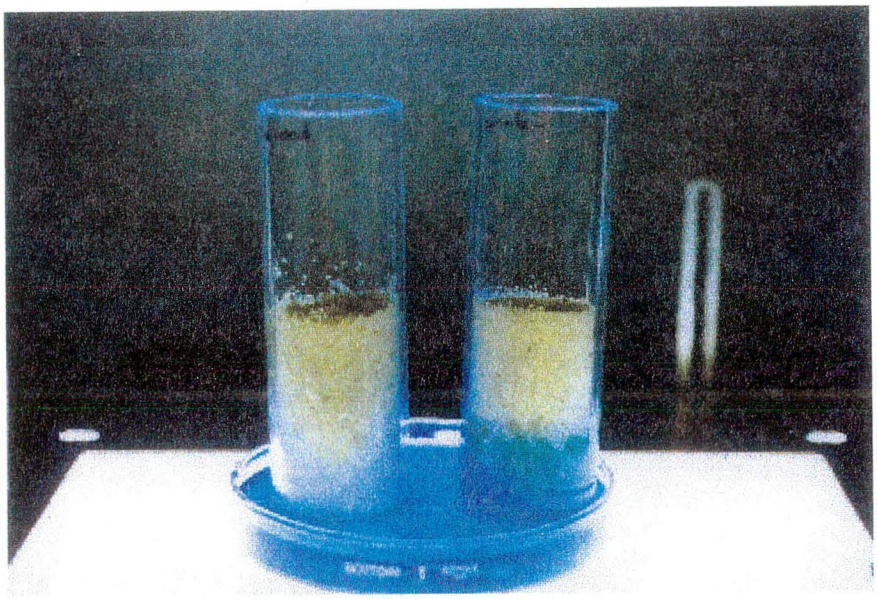

b)

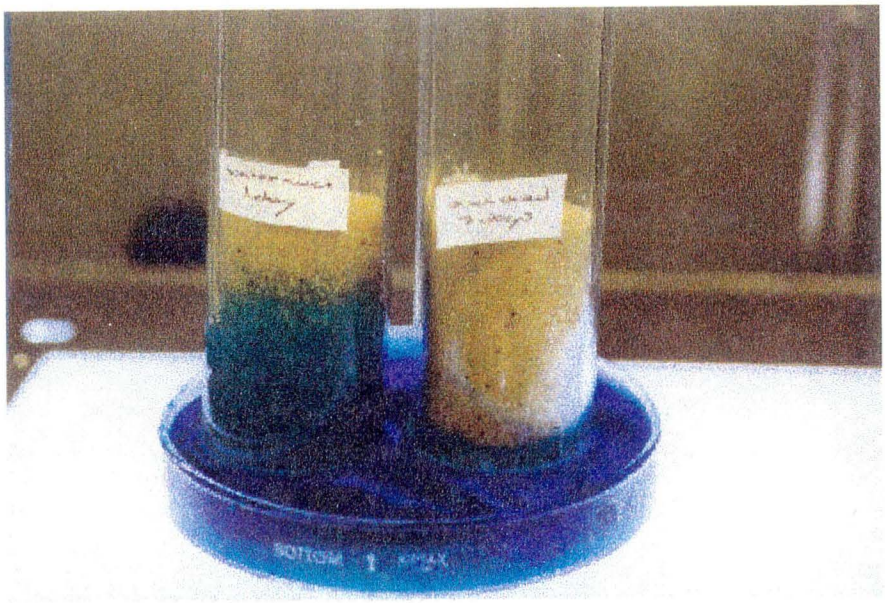

Figure 5.2: a) shows the air dried sand (left) and b) the oven dried sand (right) which were exposed to n-dodecane in comparison with the untreated sand. The untreated sand is highly water-wetting.

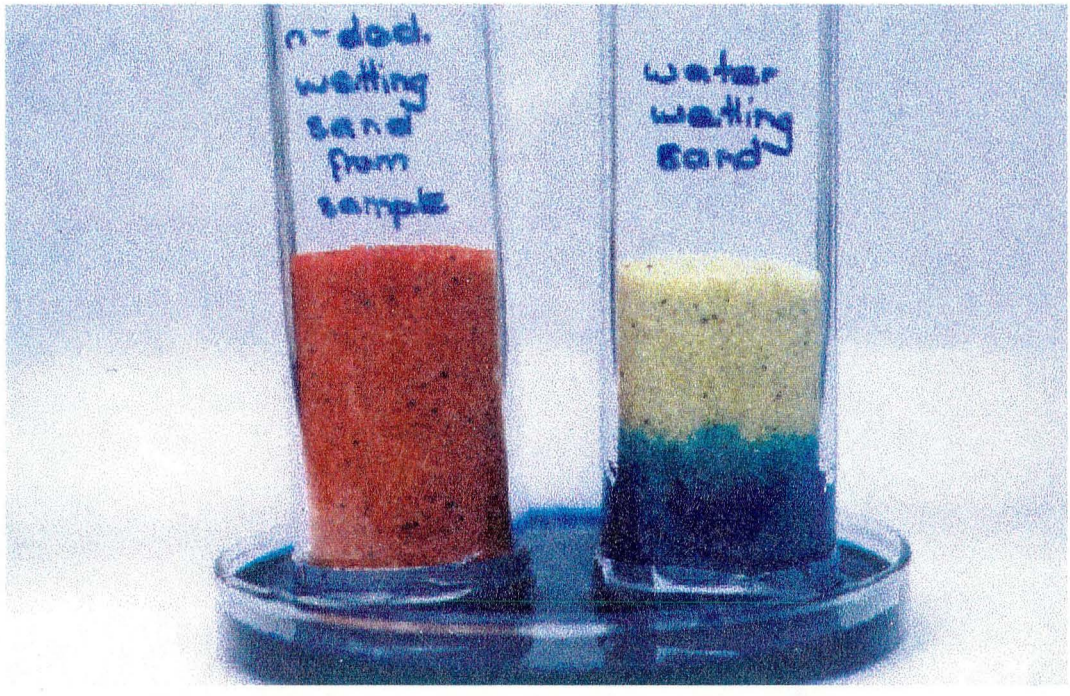

Figure 5.3: The sand on the left side had been used for our seismic and electric resistivity measurement, during which the sample was fully saturated with water for at least two days. As can be seen, this did not affect the wettability of the sand. The sand was dyed red by the coloured NAPL which we injected into the initally fully water saturated sample, to take measurements as a function of NAPL-saturation. On the right side for comparison is a sample of untreated sand.

5.3.2 Seismic and Electric Resistivity Measurments

P-wave and S-wave as well as electrical resistivity measurement were made simultaneously on 7 cm diameter by 4 cm long samples in a triaxial cell. Low axial and confining stresses, characteristic of the shallow subsurface (tenths of MPa), were applied. Experiments were conducted with media that were initially saturated with water and initially saturated with NAPL. The measurements were made in fully saturated samples while the ratio of NAPL to water in the saturating fluid was slowly changed.

Ultrasonic wave propagation was measured with the pulse-transmission technique in sand columns saturated with water and NAPL. Pulses were generated from a high-voltage source operating at 800 V with a pulse width of 600 ns. The transmitting and receiving elements were identical and had a central frequency of 500 kHz. The received traces were digitally recorded by a 20 MHz data acquisition system and stacked 100 times to reduce the noise. (For further details on instrumentation and set-up see Geller and Myer, 1995). We measured the change in travel time (from which velocity was computed) and zero-to-peak amplitude normalized by the amplitude for the initally water-saturated sample of the arriving wave as a function of NAPL saturation. Liquid saturation was changed by injecting incremental volumes of the displacing liquid with a syringe pump, and computed by mass balance on the displaced and displacing liquids. Electrical resistivity at 90 Hz was measured with the four-electrode technique,

using stainless-steel disks at the sample ends for current drivers; the potential electrodes were stainless steel rings embedded in the sand one third the total sample length from the sample ends.

Two series of measurements were made on each sample. Initally the sample was saturated with water and then n-dodecane was slowly injected from the top to displace water which was extracted from the bottom. This process continued until the injected n-dodecane began to appear at the bottom of the sample, indicating that n-dodecane was flowing through the sample without displacing water. The amount of water left in the sample at this point was called the residual water saturation. Once this saturation was attained, water was injected into the sample to displace n-dodecane. Most of the data indicate a hysteretic behavior, which may be due to the different liquid distribution during drainage compared to imbibition. The second series of measurements was similar to the first except that water was injected into a sample initially saturated with n-dodecane.

5.4 Interpretation

Let us first compare the seismic measurements of the NAPL-wet and the untreated sand which was strongly water wet. Figure 5.4 and Figure 5.5 show P-wave velocity and normalized amplitude as a function of n-dodecane saturation, for water-wetting and n-dodecane-wetting sand, respectively. The most

obvious difference between the two figures is the residual saturation. The black lines represent initally water saturated samples, where the water was displaced by NAPL. The saturation at which the injection of more NAPL did not displace any more water represents a saturation endpoint. In the case of the water-wet sands this endpoint is at approximately 57% NAPL (43% water). (Figure 5.4), whereas for n-dodecane-wetting sand (Figure 5.5) the endpoint reaches 93% NAPL (7% water). Starting out with an initally NAPL-wet sand (red lines) and displacing the NAPL by water, the opposite holds true. 85% of the inital n-dodecane can be displaced by water (Figure 5.4), whereas for the water-wetting sand only 55% can be displaced (Figure 5.5). These results make sense in terms of the wettability and capillary rise discussed earlier. NAPL injected into an intially water saturated sample can not occupy the smaller pore spaces, leading to a higher residual saturation of the water. If the sample is initally n-dodecane saturated, the water reaches the small pores, resulting in a lower saturation of NAPL. In a NAPL-wet system the opposite happens, as the organic phase will wet the sand grains and occupy the smallest pore spaces. Figure 5.6 compares the seismic pulse in fully water saturated and n-dodecane saturated samples for water-wetting and n-dodecane-wetting sand. Independent of the pore filling fluid, we observe that the NAPL-wetting sand always shows higher absolute amplitudes. This could imply that the intergranular contact of the sand was somehow improved by the change from water-wetting to n-dodecane wetting,

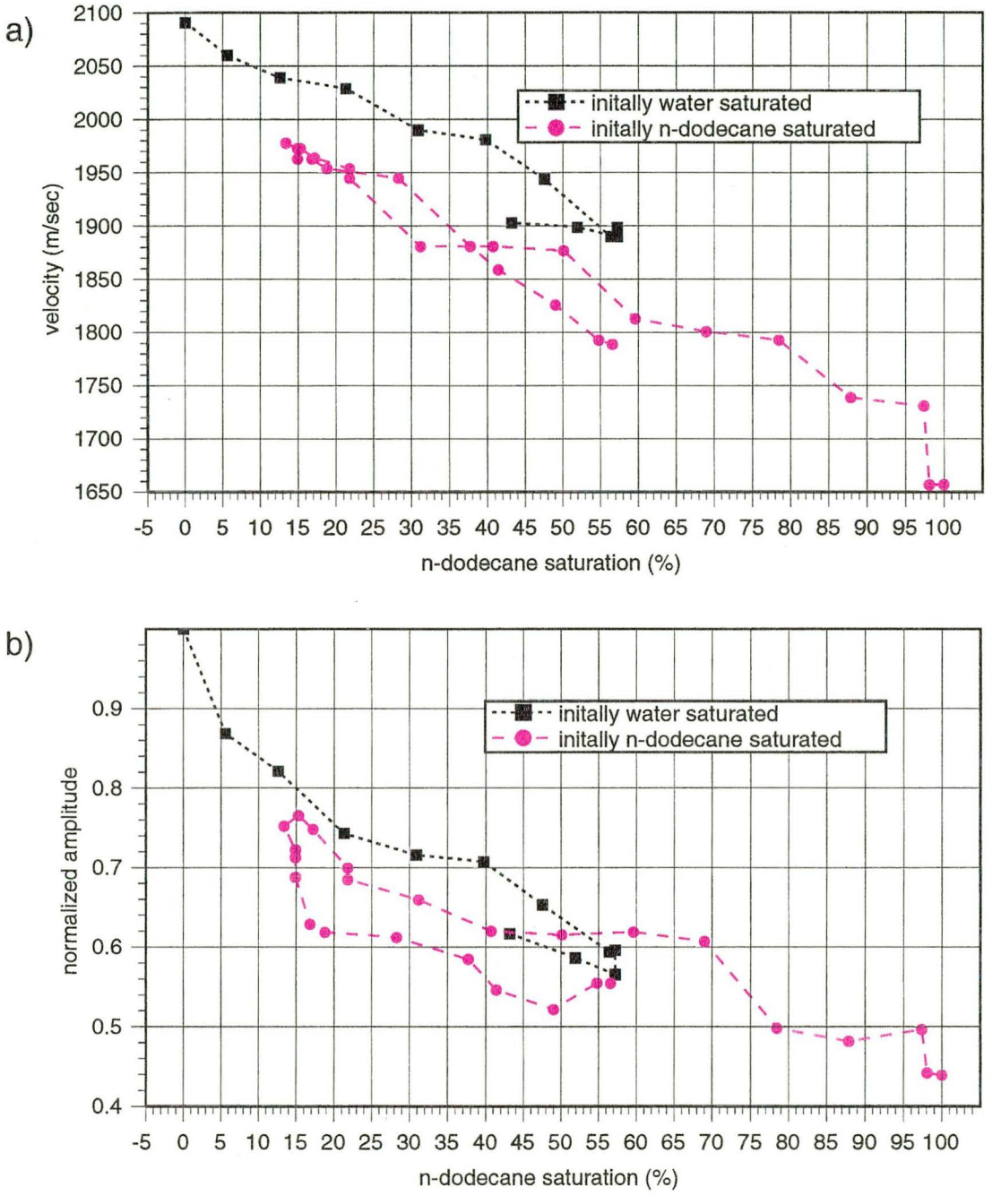

Figure 5.4: P-wave velocity a) and normalized amplitude b) as a function of n-dodecane saturation for water-wetting sand. Black line represents the initally water-saturated sample, where the water has been displaced by NAPL. The red line is the opposite, the sample was initally fully n-dodecane saturated and then displaced by water.

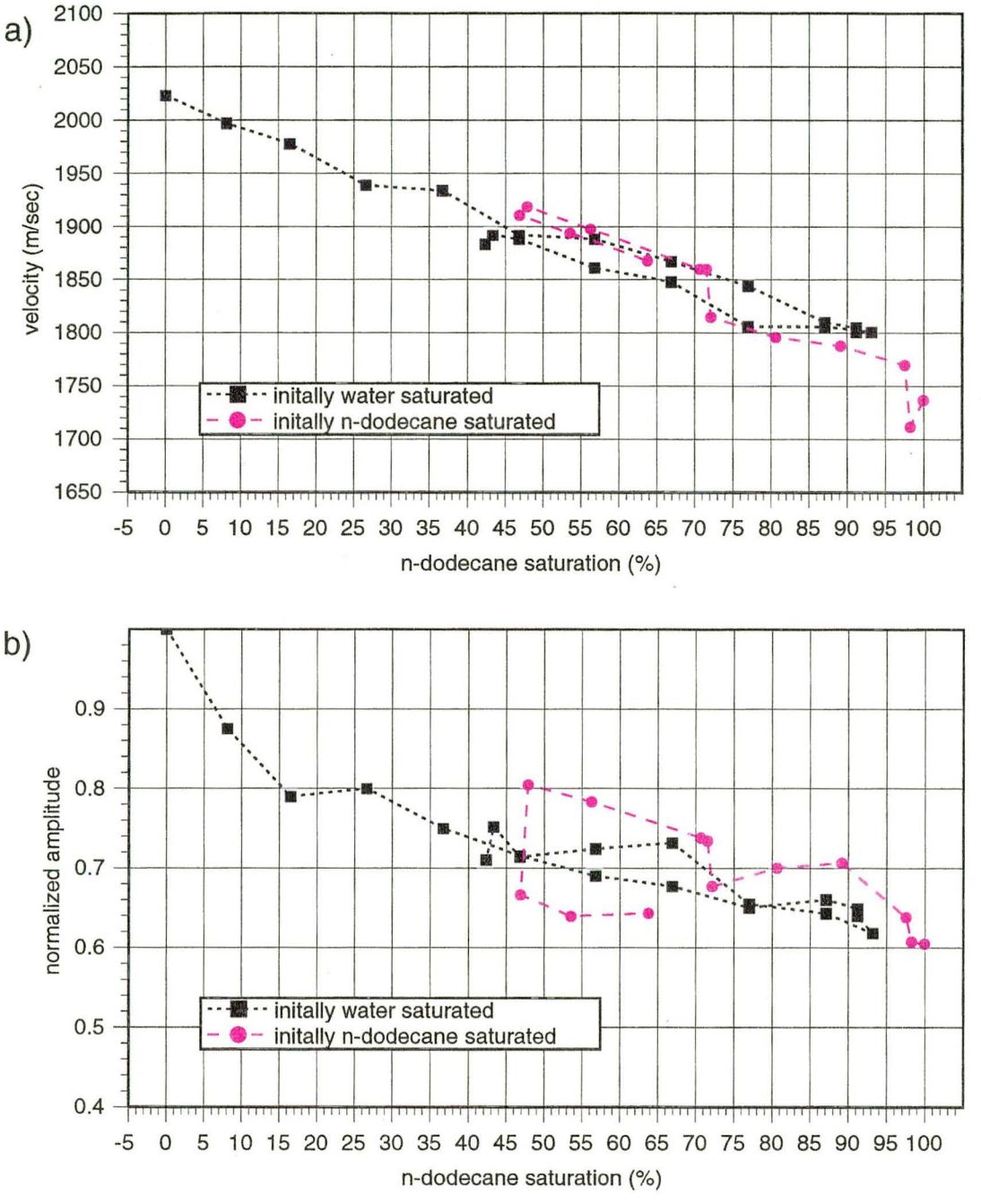

Figure 5.5: P-wave velocity a) and normalized amplitude b) as a function of n-dodecane saturation for n-dodecane-wetting sand. Black line represents the initally water-saturated sample, where the water has been displaced by NAPL. The red line is the opposite, the sample was initally fully n-dodecane saturated and then displaced by water.

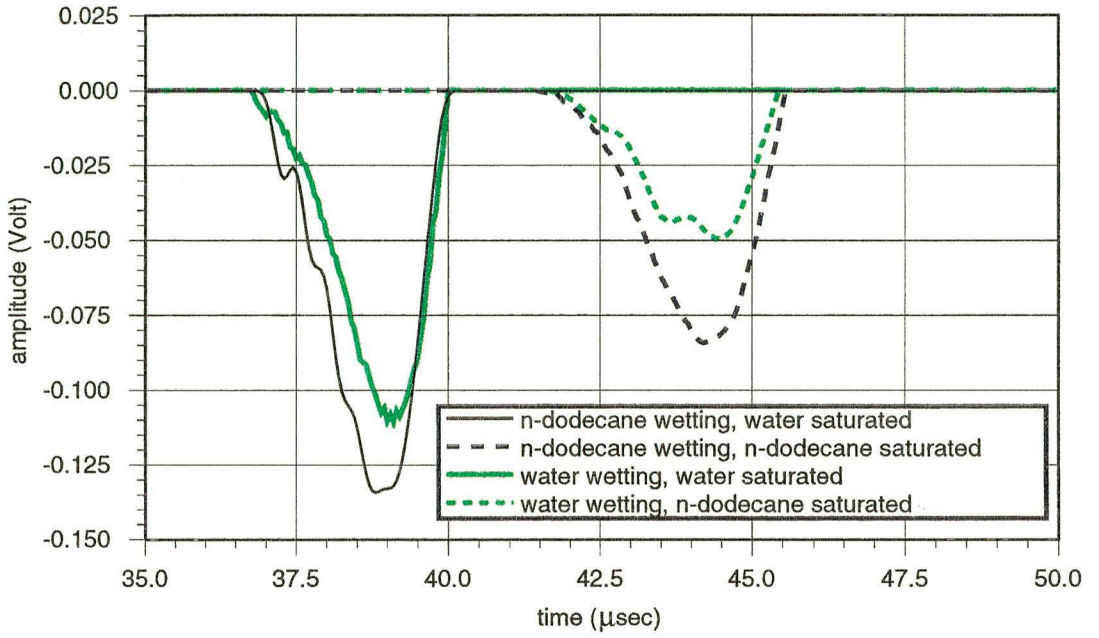

Figure 5.6: Measured first arrival of the P-waves for water-wetting sand (green lines) and n-dodecane-wetting sand (black lines). The amplitude for n-dodecane wetting sand is always larger than for water-wetting sand, independent of the pore-filling fluid, water (solid lines) or n-dodecane (dotted lines).

leading to less absolute attenuation. Another indication for this change, is that S-waves as a function of NAPL-saturation (Figure 5.7) can be observed and measured in the case of n-dodecane wetting sand, whereas S-waves could not be reliably measured for the water-wetting sample. S-waves are rather difficult to measure in unconsolidated material, since their amplitudes decrease much faster than those of P-waves. Furthermore, the converted S- to P-waves arrive before the main S-pulse, which can distort the first non-converted S-wave, making it hard to measure. Figure 5.8 shows the traces for a n-dodecane-wetting and water-wetting fully water saturated sample. The velocity was measured by extending the amplitude baseline until it intersected the trace of the first arriving

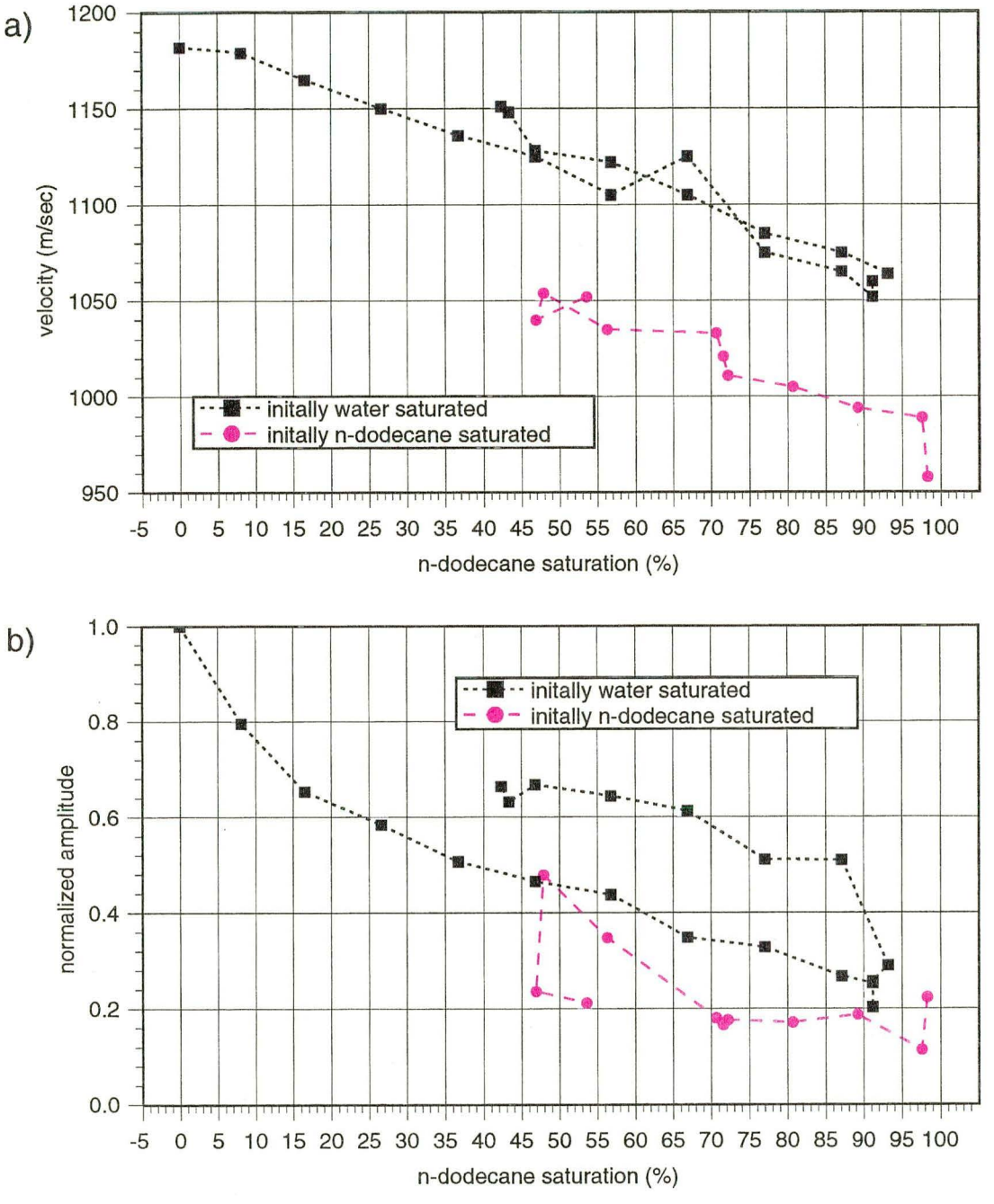

Figure 5.7: S-wave velocity a) and normalized amplitude b) as a function of n-dodecane saturation for n-dodecane-wetting sand.

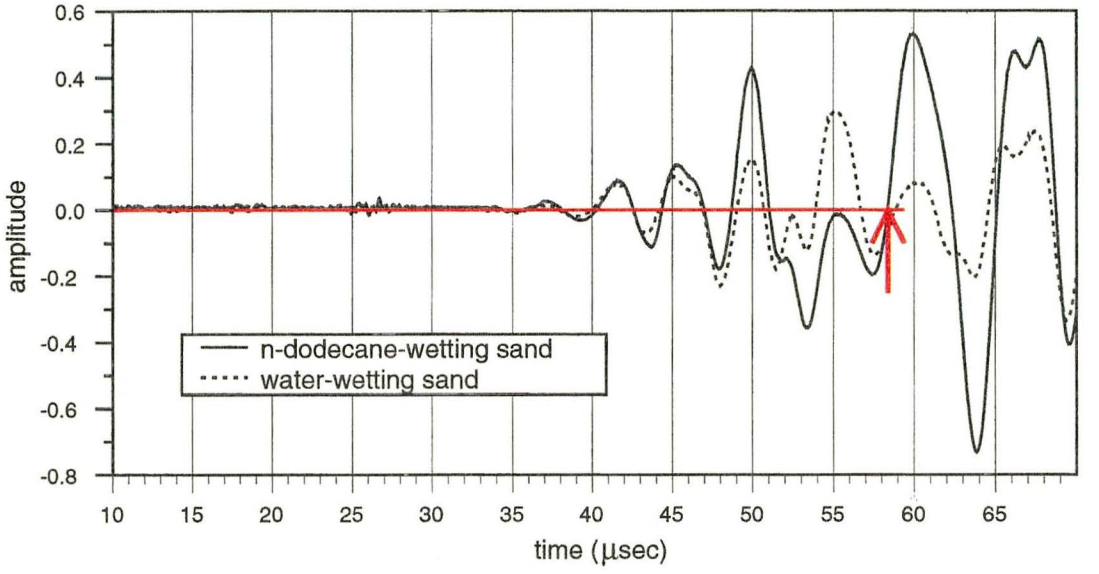

Figure 5.8: S-waves traces for a n-dodecane-wetting (solid line) and water-wetting (dotted line) sand, which was fully water saturated. In the case of the n-dodecane wetting sand the S-wave amplitude could be measure by extending the amplitude base line (red line) until it intersects with the first non-converted pulse. For the water-wetting sand samples the S-wave could not be reliably measured.

S-wave (red line in Figure 5.8) and the amplitude was taken from intersection point to the first peak.

The electric resistivity measurements as a function of NAPL-saturation are plotted in Figure 5.9a for water-wetting and in Figure 5.9b for n-dodecane wetting sand. Electric current flows through dissolved ions in the water and therefore water acts as a conductor. Since resistivity increases in the presence of a nonpolar organic liquids, electric resistivity is sensitive to the fraction of n-dodecane present. The initally fully water saturated hydrophilic sand shows only a small increase in resistivity with increasing NAPL-saturation (Figure 5.9a, black line). The electric current can flow through the water clinging to the

water-wetting grains in the NAPL-saturated part of the sample and hence the resistivity increases only slightly. When displacing the NAPL by water, a point is reached where the resistivity drops rapidly from 20 kΩ to 1 kΩ, suggesting that the electric current has found a fast path and water extends over the entire length of the sample (Figure 5.9a), red line).

In case of the NAPL-wetting sand the water can not travel along the layer of water attached to the grains. Because the grains are hydrophobic, an increase in NAPL-saturation leads to higher resistivity measurements (Figure 5.9b, black line). For the initally n-dodecane saturated sample, behavior similar to the water-wet sand can be observed, as the resistivity drops as soon as water extends over the entire length of the sample (Figure 5.9b), red line).

5.5 Conclusion

An experiment with n-dodecane and water saturated sands has shown that quartz grains change irreversibly from water-wetting to n-dodecane-wetting if the grains are exposed to n-dodecane for several days. Phase velocity and attenuation of ultrasonic waves are functions of NAPL concentration, whereas S-waves can be observed only if the sand grains are n-dodecane-wetting. Changing the wettability of a NAPL-water-mineral system is also accompanied with a change of the effective P-wave amplitude, with the NAPL-wet sand showing higher amplitudes than the water-wet sand. Hence, the wettability seems to

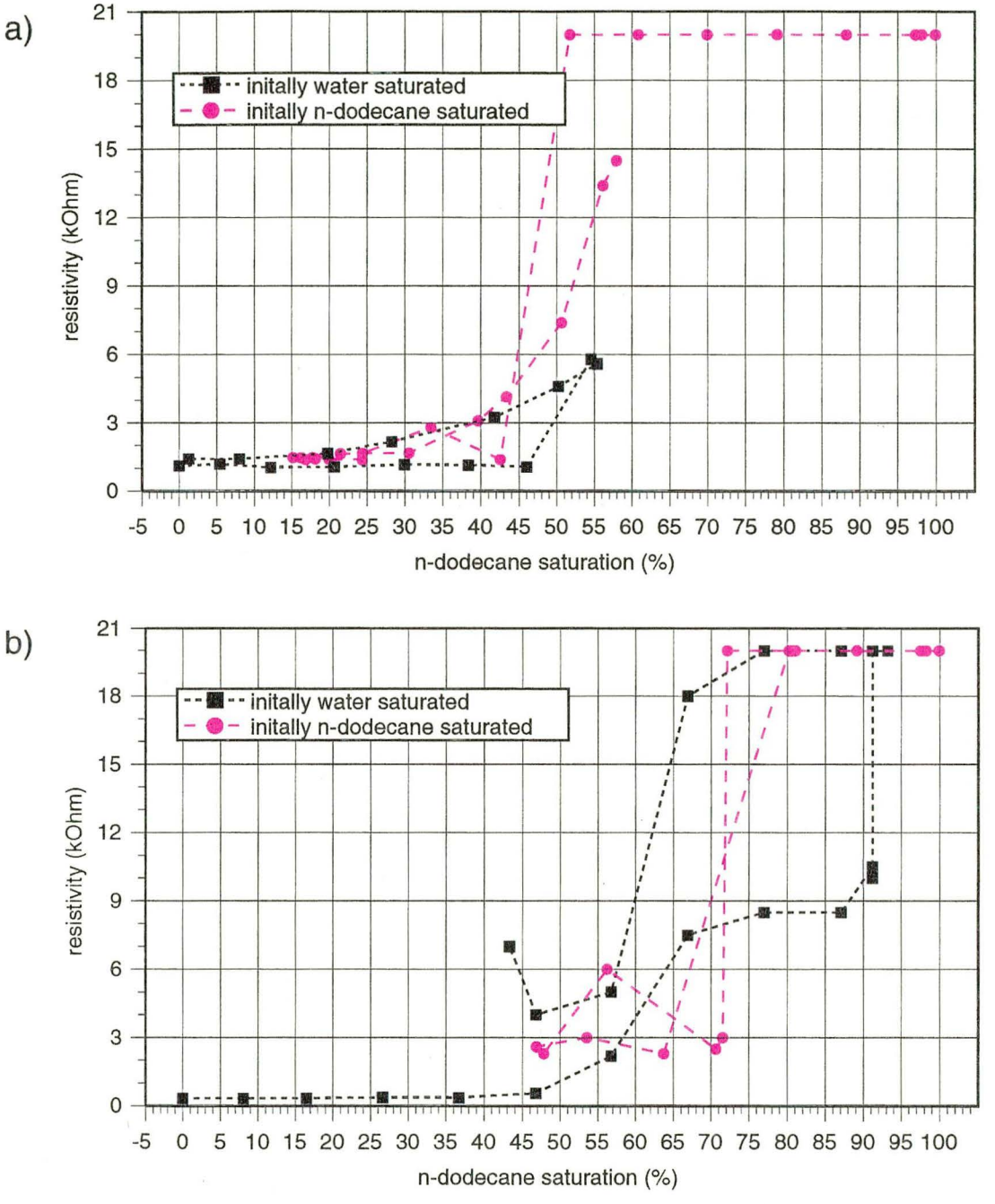

Figure 5.9: Resistivity measurements as a function of n-dodecane saturation for a) water-wetting sand and b) n-dodecane wetting sand.

affect the elastic properties of the grain contacts.

Resistivity measurements were also affected by the wettability of the sand-grains. An initially water saturated sample showed high resistivity only if the sand was n-dodecane wetting. Small resistivity can be observed if the grains are hydrophilic, because the grains are always covered by a thin film of water, which serves as an electric conductor that can not be displaced by n-dodecane. If n-dodecane was displaced by water, the sand sample showed high resistivity until water extended over the entire sample length and resistivity instantly decreased.

We conclude that in contaminated sites with mixed wettabilities, the observed behavior of S-waves and electric resistivity can help to distinguish between regions of different wettabilities.

Chapter 6

Outlook

This study shows that the attenuation and velocity in ultrasonic elastic wave propagation can mainly be explained by scattering. The agreement found in this study between laboratory measurements and numerical calculations suggests several topics for additional research. The results presented in this study focus on clean quartz sand sieved within certain meshsizes, which is a good representation of beaches, but has to be generalized for practical use.

Thus, to do justice to the real earth, it is important to look at heterogeneous grain-size distribution as well as varying clay and silt fractions mixed with sands. Poorly sorted sands and silts are going to affect wave propagation as well as liquid distributions. NAPL fraction and media characteristics will indicate the sensitivity of amplitude and velocity and maybe show how they can be jointly used to constrain their response to the presence of NAPL in heterogeneous media.

Further investigation should also concentrate on the extrapolation of lab-

oratory data to field scale. An experiment is currently beeing conducted at the Lawrence Berkeley National Laboratory to test the effect of scale on the response of seismic signals to the presence of NAPL contaminants in a 0.6 m-scale tank of sand. This will provide an upscaling of approximately one order of magnitude over the column experiments. The tomograms from this study might indicate how well the geophysical signals resolve the presence of NAPLs in a three-dimensional setting, which is also more representative of field conditions.

References

Adam, N. K., 1941, The physics and chemistry of surfaces: Lowe & Brydone, Printers, Ltd., London.

Akbar, N., Mavko, G., Amos, N., and Dvorkin, J., 1994, Seismic signatures of reservoir transport properties and pore fluid distribution: J. Acoust. Soc. Am., **59**, 1222–1236.

Berryman, J. G., 1980a, Confirmation of Biot's theory: Appl. Phys. Lett., **12**, 382–384.

——— 1980b, Long-wavelength propagation in composite elastic media I. spherical inclusions: J. Acoust. Soc. Am., **68**, no. 6, 1809 –1819.

Biot, M. A., 1956a, Theory of propagation of elastic waves in a fluid-saturated porous solid I. lower frequency range: J. Acoust. Soc. Am., **28**, 168–178.

——— 1956b, Theory of propagation of elastic waves in a fluid-saturated porous solid; II. higher frequency range: J. Acoust. Soc. Am., **28**, 179–191.

Biot, M. A., 1962, Mechanics of deformation and acoustic propagation in porous media: J. Appl. Phys., **33**, 1482–1498.

Bryant, S., and Raikes, S., 1995, Prediction of elastic-wave velocities in sandstones using structural models: Geophysics, **60**, 437–446.

Burridge, R., and Keller, J., 1981, Poroelasticity equations derived from microstructure: J. Acoust. Soc. Am., **70**, no. 4, 1140–1146.

Carmichael, R. S. N., 1989, Practical handbook of physical properties of rocks and minerals: CRC Press, Inc.

Childs, E. C., and Collis-George, N., 1950, The permeability of porous materials: Proc., Roy. Soc. London, Ser. A, **201**, 392–405.

Clark, V. A., 1992, The effect of oil under in-situ conditions on the seismic properties of rocks: Geophysics, **57**, 894–901.

de Hulst, H. C. V., 1957, Light scattering by small particles: Wiley Interscience.

Dvorkin, J., and Nur, A., 1993, Dynamic poroelasticity: A unified model with the squirt and the Biot mechansisms: Geophysics, **58**, no. 4, 525–533.

Dvorkin, J., and Nur, A., 1996, Elasticity of high-porosity sandstones: Theory for two north sea data sets: Geophysics, **61**, 1363–1370.

Endres, A. L., and Knight, R., 1989, The effect of microscopic fluid distribution on elastic wave velocities: The Log Analyst, pages 437–445.

Feather, N., and Shoenberg, D., 1949, Surface tension and the spreading of liquids: University Press, Cambridge.

Feustel, A. J., and Young, R. P., 1994, q_β estimates from spectral ratios and multiple lapse time window analysis: Results from an underground research laboratory in granite: Geophys. Res. Lett., **21**, 1503–1506.

Gassmann, F., 1951, Über die elastizität elastischer medien: Vierteljahresschrift der Naturforschenden Gesellschaft Zürich, **96**, 1–21.

Geller, J. T., and Myer, L. R., 1995, Ultrasonic imaging of organic contaminants in unconsolidated porous media: Journal of Contaminant Hydrology, **19**, no. 2, 85–104.

Gist, G. A., 1997, Fluid effects on velocity and attenuation in sandstones: J. Acoust. Soc. Am., **96**, no. 2, 1158–1173.

Greenhouse, J., Brewster, M., Schneider, G., Redman, D., Annan, P., Olhoeft, G., Lucius, J., Sander, K., and Mazzella, A., 1993, Geophysics and solvents: The borden experiment: The Leading Edge, **12**, 261–267.

Guard, U. S. C., 1984, Chemical hazard response information system (chris),2., hazardous chemical data: U.S. Departement of transport, Washington, D.C.

Harr, J., 1995, A civil action: Vintage Books, A Division of Random House, Inc., New York.

Homsey, G. M., 1987, Viscous fingering in porous media, annual review of fluid mechanics: Annual Review of Fluid Mechanics, **19**, 271–311.

Johnston, B. I., and Toksöz, M. N., 1979, Attenuation of seismic waves in dry and saturated rocks, ii, mechanisms: Geophysics, **44**, 691–710.

Kaelin, B., and Johnson, L. R., 1998, Dynamic composite elastic medium theory. part II. three dimensional media: Applied Physics, submitted.

Kaelin, B., 1998, Seismic imaging of the shallow subsurface: Ph.D. thesis, University of California, Berkeley.

Kennett, B. L. N., 1983, Seismic wave propagation in stratified media: Cambridge Univ. Press.

Knight, R., and Nolen-Hoeksema, R., 1990, A laboratory study of dependence of elastic wave velocities on pore scale fluid distribution: Geophys. Res. Lett., **17**, 1529–1532.

Kuster, G., and Toksöz, M., 1974, Velocity and attenuation of seismic waves in two-phase media: Part I. theoretical formulations: Geophysics, **39**, 587–606.

Lide, D. R., 1995, Handbook of chemistry and physics, 1913-1995: CRC Press, Inc.

Majer, E. L., Peterson, J. E., Daley, T. M., Kaelin, B., Myer, L. R., Queen, J., D'Onfro, J., and Rizer, P. S., 1997, Fracture detection using crosswell and single well surveys: Geophysics, **62**, 495–504.

Marion, D., Mukerji, T., and Mavko, G., 1994, Scale effects on velocity dispersion: From ray to effective medium theories in stratified media: Geophysics, **59**, 1613–1619.

Mavko, G. M., 1979, Frictional attenuation: an inherent amplitude dependence: J. Geophys. Res., **84**, 4769–4775.

McKee, J. E., Laverty, F. B., and Hertel, R. M., 1972, Gasoline in groundwater: J. Water Pollut. Control Fed., **44**, no. 2, 293–302.

Mercer, J. W., and Cohen, R. M., 1990, A review of immiscible fluids in the subsurface: Properties, models characterization and remediation: J. Contam. Hydrol., **6**, 107–163.

Murphy, W. F., Winkler, K. W., and Kleinberg, R. L., 1986, Acoustic relaxation in sedimentary rocks: Dependence on grain contacts and fluid saturation: Geophysics, **51**, 757–766.

Nihei, K. T., Myer, L. R., and Cook, N. G., 1995, Numerical simulation of elastic wave propagation in granular rock with the boundary integral equation method: Journal Acoust. Soc. Am., **95**, 1423–1434.

O'Connell, R. J., and Budiansky, B., 1974, Seismic velocities in dry and saturated cracked solids: J. Geophys. Res., **79**, no. 35, 5412–5426.

O'Connell, R. J., and Budiansky, B., 1977, Viscoelastic properties of fluid-saturated cracked solids: J. Geophys. Res., **82**, no. 36, 5719–5735.

Powers, S. E., Anckner, W. H., and Seacord, T. F., 1997, The wettability of napl-contaminated sands: Journal of Environmental Engineering, **122**, 889–896.

Press, W. H., Teukolsky, S. A., Vetterling, W. T., and Flannery, B. P., 1992, Numerical recipes in fortran: Cambridge Univ. Press.

Remi, J., Bellanger, M., and Homand-Etienne, F., 1994, Laboratory velocity and attenuation of p-waves in limestones during freeze-thaw cycles: Geophysics, **59**, 245–251.

Riddick, J. A., and Bunger, W. B., 1970, Organic solvents: Physical properties and methods of purification: Wiley Interscience.

Schwille, F., 1967, The joint problems of the oil and water industries: Institute of Petroleum, London.

Schwille, F., 1981, Groundwater pollution in porous media by fluids immiscible with water: Sci. Total Environ., **21**, 173–185.

Schwille, F., 1984, Migration of organic fluids immiscible with water:, *in* Pollutants in porous media: The unsaturated zone between soil surface and groundwater Springer-Verlag, New York, Ecological Studies, 47, 27–48.

Seifert, P. K., Geller, J. T., and Johnson, L. R., 1998, Effect of p-wave scattering on velocity and attenuation in unconsolidated sand saturated with immiscible liquids: Geophysics, pages 161–170.

Selfridge, A. R., 1985, Approximate material properties in isotropic material: IEEE transaction on sonics and ultrasonics, **SU-32**, no. 3, 381–394.

Shapiro, S. A., and Zien, H., 1993, The o'doherty-anstey formula and localization of seismic waves: Geophysics, **58**, 736–740.

Shapiro, S. A., Zien, H., and Hubral, P., 1994, A generalized o'doherty-anstey formula for waves in finely-layered media: Geophysics, **59**, 1750–1762.

Tang, X. M., Toksöz, M. N., Tarif, P., and Wilkens, R. H., 1988, A method for measuring acoustic wave attenuation in the laboratory: J. Acoust. Soc. Am., **83**, 453–462.

Toksöz, M. N., and Johnston, D. H., 1981, Seismic wave attenuation: Soc. Expl. Geophys.

Toksöz, M. N., Johnston, D. H., and Timur, A., 1979, Attenuation of seismic waves in dry and saturated rocks: I. laboratory measurements: Geophysics, **44**, 681–690.

Tutuncu, A. N., and Sharma, M. M., 1992, The influence of fluids on grain contact stiffness and frame moduli in sedimentary rocks: Geophysics, **57**, 1571–1582.

Vo-Thanh, D., 1991, Effects of fluid viscosity on shear wave attenuation in partially saturated sandstones: Geophysics, **56**, no. 8, 1252–1258.

Wang, Z., and Nur, A., 1991, Ultrasonic velocities in pure hydrocarbons and mixtures: J. Acoust. Soc. Am., **89**, no. 6, 2725–2730.

White, J. E., 1965, Seismic waves: radiation transmission and attenuation: McGraw-Hill, New York.

Winkler, K. W., and Murphy III, W. F., 1995, Acoustic velocity and attenuation in porous rocks:, *in* Rock Physics and Phase Relations American Geophysical Union, AGU reference shelf, 3, 20–34.

Yamamoto, T., Nye, T., and Kuru, M., 1994, Porosity, permeability, shear strength: Crosswell tomography below an iron foundry: Geophysics, **59**, 1530–1541.

Ernest Orlando Lawrence Berkeley National Laboratory
One Cyclotron Road | Berkeley, California 94720

Prepared for the U.S. Department of Energy under Contract No. DE-AC03-76SF00098